Master's thesis

Cold air outbreaks from Fram Strait into the Nordic Seas: characteristics and dynamical processes

presented by

Emmanuel Rouges

Msc Atmospheric and Climate sciences, ETH Zurich

Supervisors:
Dr. Lukas Papritz
Prof. Dr. Heini Wernli
Dr. Franziska Aemisegger

Zürich, March 15 2018

Abstract

Marine cold air outbreaks (CAOs) are defined by the advection of cold polar air masses from the sea ice onto the relatively warmer ocean towards lower latitudes. This meteorological phenomena is very common in the Nordic Seas and often crosses Fram Strait (between North-East Greenland and Svalbard), leading to extreme weather events like polar lows.

The research around CAOs has focused primarily on their development after the transport from the ice edge and their impact in the formation of polar lows. However, few is known about the driving processes and the characteristics of CAO air masses prior to their advection over the ocean. In this study, we use backward trajectories of CAO air masses from Fram Strait with the ERA-interim dataset to analyse the period 10 days prior to the CAO.

A first look at the climatology revealed a decreasing trend in CAO occurrence probably linked to Global Warming and that the number of CAOs happening in December is greater than in January or February. Looking at sample of the top 20 strongest CAOs of the ERA-interim period, we identified first similarities. In particular, CAO air masses originate mostly from the Arctic and Siberia, and stay for most of their evolution shallow. A brief analysis of the thermodynamic evolution showed a clear diabatic cooling.

As we analysed three case studies (typical and atypical cases), we identified the importance of a sea level pressure gradient through Fram Strait formed by a cyclone near Svalbard and an anti-cyclone over Greenland to transport the air masses from Fram Strait to lower latitudes. We also determined the presence of an anomaly of θ at 900hPa over most of the Arctic and especially around the CAO air masses, prior to the advection. The anomaly above CAO air masses is coupled to a tropopause level disturbance reaching into the mid-tropopause. The diabatic cooling identified earlier is probably linked to longwave outgoing radiation.

In the last part we could confirm on a climatological scale the importance of both the sea level pressure gradient and the θ anomaly for CAO formation and therefore, potential prediction.

Acknowledgements

I would like to express my sincere gratitude to my supervisors Dr. Lukas Papritz, Prof. Dr. Heini Wernli and Dr. Franziska Aemisegger for their support, many helpful comments and revisions. First to Lukas Papritz who proposed this very interesting topic and enriched my knowledge through his expertise. Heini Wernli helped me in many ways and in particular in this thesis by bringing insightful point of views. Franziska Aemisegger was ever present to give me both helpful insights and technical support.
Many thanks to the Atmospheric Dynamics group for giving me the opportunity to work in a great work environment.

A special thanks to my parents, friends and girlfriend Kim Weber who had to deal with me during those last six month and supported me anyways.

Contents

1

Introduction

Marine cold air outbreaks (CAOs) are a meteorological phenomena at the interface between the ocean and the atmosphere. They are characterized by the transport of cold air masses from polar regions towards lower latitudes. This cold air is advected from the sea ice margin over the relatively warmer ocean.

CAOs are an important topic of research because of their impact on the weather at high latitudes. They are specifically responsible for the formation of polar lows [Kolstad, 2011]. Kolstad [2011] underline that the low static stability of CAOs is a key component of the formation of polar lows. Bracegirdle and Gray [2008] defined polar lows as a subset of particularly intense polar mesocyclones. In fact they can lead to very damaging winds and large amounts of precipitation. Therefore, a climatology of CAOs is helpful to define both the locations and time periods where and when polar lows can happen most frequently.

In Figure 1.1, polar lows are clearly visible as small cyclones with cloud formations that are characteristic of CAOs.

Beside this very obvious impact, CAOs have also an important impact on the heat budget of the upper ocean. Wacker et al. [2005] simulated a CAO and its associated heat fluxes. Those heat fluxes can develop a very strong convective boundary layer with a thickness of 1500m.

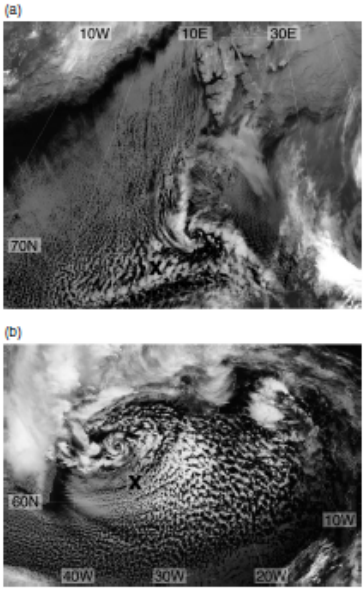

Figure 1.1: Representation of characteristic cloud patterns in the vicinity of CAOs. (a) Polar low forming in the Nordic Seas (rotating feature) . (b) Polar low forming at the south east tip of Greenland [Kolstad, 2011]. Crosses locate the position where the CAO is strongest.

The heat fluxes in the Nordic Seas are strongly cooling the ocean at the northern part of the Overturning Circulation. This cooling, increases the deep water formation necessary for the Overturning Circulation [Dickson et al., 1996] making it a key driver of the ocean deep water formation. It is thus important to study CAO formation and development in this region.

The region of the Nordic Seas has become a region of great interest because of the high frequency of CAOs and therefore polar lows.

Figure 1.2 shows clearly how the regions of high polar low frequency agree with regions of high CAO frequency. In particular, we already observe the high frequency of particularly strong CAOs near Svalbard. Papritz and Spengler [2017] also points out that not only is the Fram Strait region (between east of Greenland and Svalbard) a region of high CAO frequency but also that most CAOs that get to the Nordic Seas out of the Arctic come through Fram Strait.

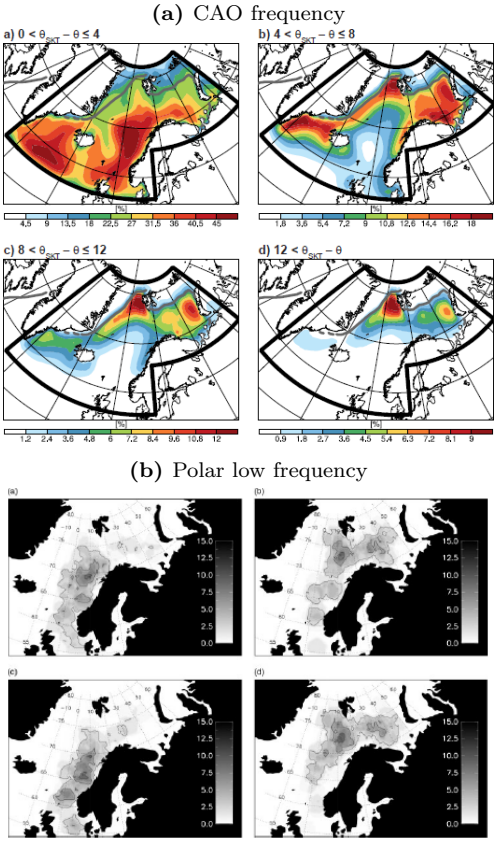

Figure 1.2: Representation of the frequency of both polar lows and CAOs in the Nordic Seas. (a) CAO frequency based on strength categories [Papritz and Spengler, 2017]. (b) Polar low frequency based on categories of different thermal advection [Bracegirdle and Gray, 2008].

We see how important this region is for CAOs and this explains why we will focus our work on this region.
The development of CAOs in this region has been studied because of their impact on polar low formation. Therefore, most studies (e.g.: Wacker et al. [2005], Papritz and Spengler [2017]) analyse the evolution of CAOs after the transport from the ice pack to the open ocean. However, there is a lack of knowledge about the driving processes and characteristics of CAOs prior to their formation over the open ocean. A Lagrangian, trajectory orientated, study in Papritz and Spengler [2017] has already revealed some of the history

of the air masses in a climatological sense but still little is known about the processes driving the preconditioning of the air masses..

This leads us to the main objective of this master thesis.

1.1 Goals

The goal of this master thesis is to extend our knowledge of CAOs to the formation period prior to their outbreak. In continuation of the work of Papritz and Spengler [2017], we will mainly focus on looking at CAO air masses and follow their evolution from 10 days before until the CAO event. This Lagrangian perspective allows for a clear investigation of the evolution of any parameter of the CAO air masses.

This will allow us to identify the characteristics of CAO air masses and determine both the underlying thermodynamic and dynamic processes, driving the formation of CAOs. These are the main research questions:

— What are the pathways of CAO air masses in the Arctic?

— What are the dynamical mechanisms of CAO formation?

— Do specific weather systems play a role for CAO formation?

— Are the air masses especially cold before reaching Fram Strait, even for Arctic conditions?

— Do large-scale pressure patterns, e.g., Iceland-Lofotes pressure difference or the NAO, influence CAO frequency or occurrence?

To reach our goals, the analysis is split into three main parts. The first one focuses on identifying the variability of the CAO frequency from year to year and also the seasonality (Chapter 3). Together with the correlation to large atmospheric patterns we will get a first insight into CAO properties.

The next part has the objective to identify, with the help of case studies, the key characteristics of CAO air masses and the underlying driving processes (Chapter 4).

Lastly, we will verify the validity of our findings on a climatological scale (Chapter 5). The aim is to certify that the key processes we identified are not specific to our cases but are valid for most or all CAOs.

Before going through our results, we first need to clearly define CAOs and describe our method of analysis.

2

Data and methods

This master thesis focuses on evolution of air masses and therefore adopts a Lagrangian perspective. This means that we will be looking at trajectories of air masses specifically computed for this thesis. The study period is the winters (December, January, February) from December 1979 to December 2016. Here is an overview of the observational data we will be using and how the analysis has been conducted.

2.1 Observational datasets

2.1.1 ERA-interim

The main data set used is the ERA-interim reanalysis dataset " from 1979, continuously updated in real time " [Dee et al., 2011]. This dataset is issued by the European Center for Medium-Range Weather Forecast (ECMWF) and is available at 6 hours intervals and 60 vertical levels. In the horizontal the data is interpolated from the original spectral resolution of T225.

2.1.2 CAO identification

CAOs can be defined by a positive difference in potential temperature between the airmass and the surface [Papritz and Spengler, 2017]. This definition enables to establish the following CAO index (CAOI):

$$CAOI = \theta_{SST} - \theta_p \tag{2.1}$$

θ_{SST}: potential temperature at sea surface. The potential skin temperature (θ_{SKT}) can also be used. The θ_{SKT} is the potential temperature of the layer of atmosphere just above the surface.
θ_p: potential temperature at specific pressure level (typically between 900

hPa and 700 hPa)
The temperature difference can vary between 2K and more then 12K for very intense CAOs. This index can help identify CAOs and differenciate between strength levels of CAOs. For instance, weak ($0<\theta_{SKT} - \theta<4$K), moderate ($4K<\theta_{SKT} - \theta <8$K) to strong ($8K<\theta_{SKT} - \theta <12$K) CAOs.

The index is summed over the violet box visible in fig 2.2 and every maximum is considered a CAO event. To avoid counting a CAO event twice, a declustering is used by removing all CAOs in a two day window. This calculation identifies CAOs during the ERA-interim period, and gives us a list with date and strength of each one.
The backward trajectories are then computed using the Lagrangian tool LAGRANTO (section 2.1.3) at t=-12h from the maximum in CAOI at the location of the blue line in fig 2.2 and at a starting level of 900hPa. Only the trajectories of the air masses with a southward motion are computed.

2.1.3 Trajectories

A major part of this thesis focuses on backward trajectories of CAO air masses. The principle is to compute backward trajectories from Fram Strait and keep the ones contributing to CAOs. To achieve that, the trajectories have been calculated using LAGRANTO version 2.0 which is a Lagrangian analysis tool developed in Wernli and Davies [1997] and improved in Sprenger and Wernli [2015].
The trajectories are calculated based on this equation:

$$\frac{D\mathbf{x}}{Dt} = \mathbf{u}(\mathbf{x}) \tag{2.2}$$

$\mathbf{x} = (\lambda, \phi, p)$: vector of position in geographical coordinates
$\mathbf{u} = (u, v, w)$: 3-D wind vector
Starting from a time t, the next position at a time $t + \Delta t$, Δt being the time interval, is calculated with this first iteration:

$$\mathbf{x}^* = \mathbf{x} + \mathbf{u}(\mathbf{x}, t) * \Delta t \tag{2.3}$$

The first iteration uses the wind speed at the starting point, which means that the first iteration gives only a first estimate of the position that does not take into account changes during this time interval. To get a better estimate, a second iteration is made using an average of the wind speed at the starting position and at the first estimated point of arrival:

$$\mathbf{u}^* = 0.5 * (\mathbf{u}(\mathbf{x}, t) + \mathbf{u}(\mathbf{x}^*, t + \Delta t)) \tag{2.4}$$

The new wind speed is plugged in equation 2.3. Per default, LAGRANTO uses three iterations [Sprenger and Wernli, 2015]. An example of the scheme is visible in this figure:

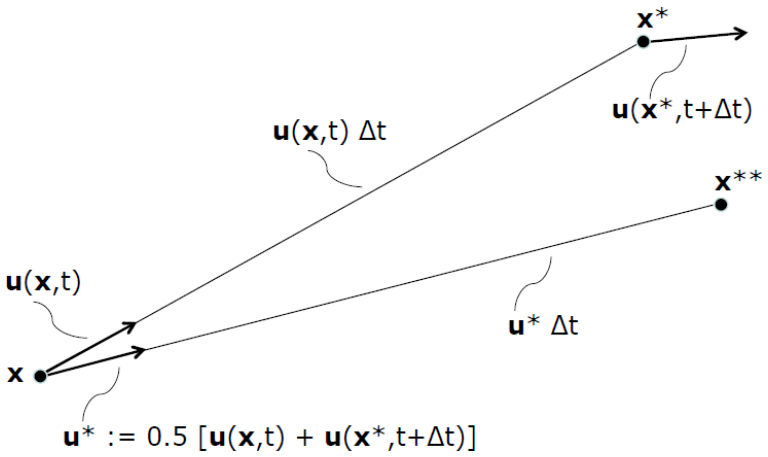

Figure 2.1: Schematic of the two iterations explained [Sprenger and Wernli, 2015]

This tool allows us to get forward and backward trajectories which will be essential for us. Besides, it give us the possibility to trace all meteorological variables needed at each time step:

Variable	Variable name
Pressure of air parcel (hPa)	p
Surface pressure (hPa)	ps
Temperature of air parcel (K)	T
Potential temperature of air parcel (K)	TH
CAO index	DTH
Skin temperature (K)	SKT
Surface sensible heat flux (W m^{-2})	SSHF
Surface latent heat flux (W m^{-2})	SLHF
Humidity (g/kg)	q
Zonal wind (m s^{-1})	u
Meridional wind (m s^{-1})	v
Tropopause pressure (hPa)	TROPO
Total water column	TWC
Top of the atmosphere net longwave radiation (W m^{-2})	TTR
Liquid water content	LWC
Ice water content	IWC

Table 2.1: Table of the variables traced along trajectories

2.2 Analysis methods

We now have defined our data sets we will rely on. The next step consists in looking for the appropriate way of analysing these data sets.

2.2.1 Use of trajectories/Lagrangian methodology

Trajectories represent the evolution of specific air parcels. This allows us to observe the meteorological characteristics of each air parcel and their evolution at each time step together with their path. In our study we look at the evolution of the variables listed in Table 2.1 beginning at -12h relative to the start of the event and finishing 10 days before the starting point at 6h time intervals.
At first we will analyse the evolution of the variables of the case study events using stereographic plots, similar to Figure 2.2. For all plots, we will use a polar view of the region. The starting points of the backward trajectories are specified by the blue line. The shading of the colours represents the temporal evolution in a given variable, here the pressure of the air parcel i.e. marker for their altitude. The value chosen for each section of the trajectories is the average between the value at time step "t+1" and "t".
This should provide first observations and some hints at the processes that these air masses are undergoing.

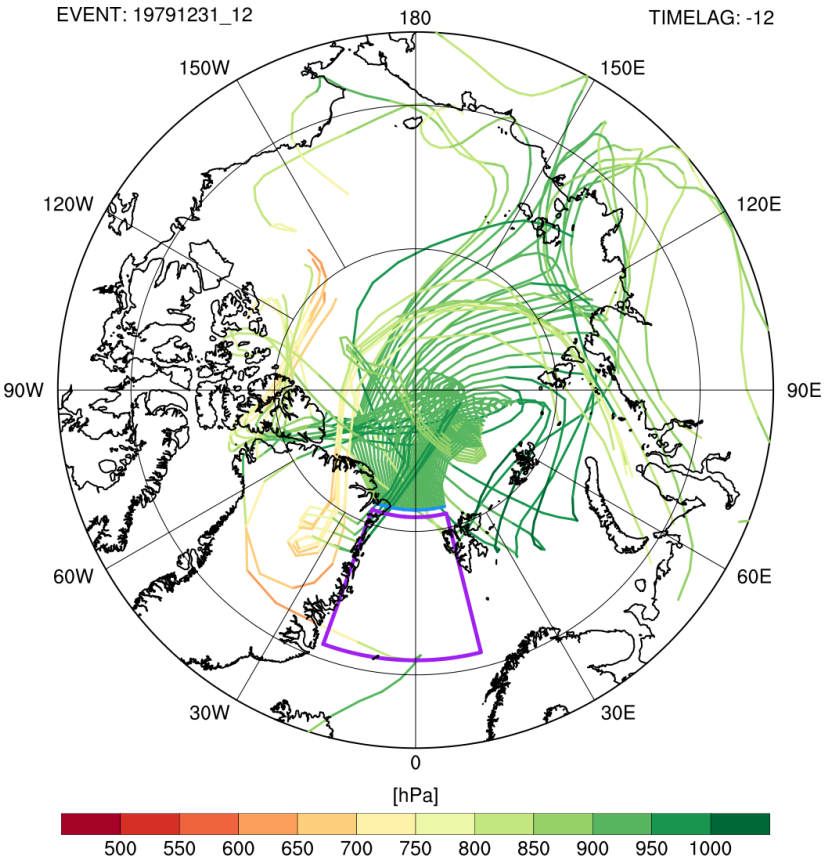

Figure 2.2: Example of trajectory plots used for the analysis of an event at 12h the 31/12/1979. The violet box represents the region used to identify the CAOs. In blue the starting line of all backward trajectories . The colorshading shows the pressure along the trajectories

2.2.2 Coupling of Lagrangian and Eulerian perspective

The first observations will be linked to potential impacting field variables at specifically chosen times. In fact, comparing the evolution of a variable along trajectories with environmental fields at each time steps allows us to make first deductions regarding the processes leading the evolution of the meteorological parameters.
This will be done through combining the Lagrangian and Eulerian perspective in the plots. This means that for each time step we plot the entire trajectories

with crosses of the exact position of each air mass together with the state of the chosen field at the same time. Figure 2.3:

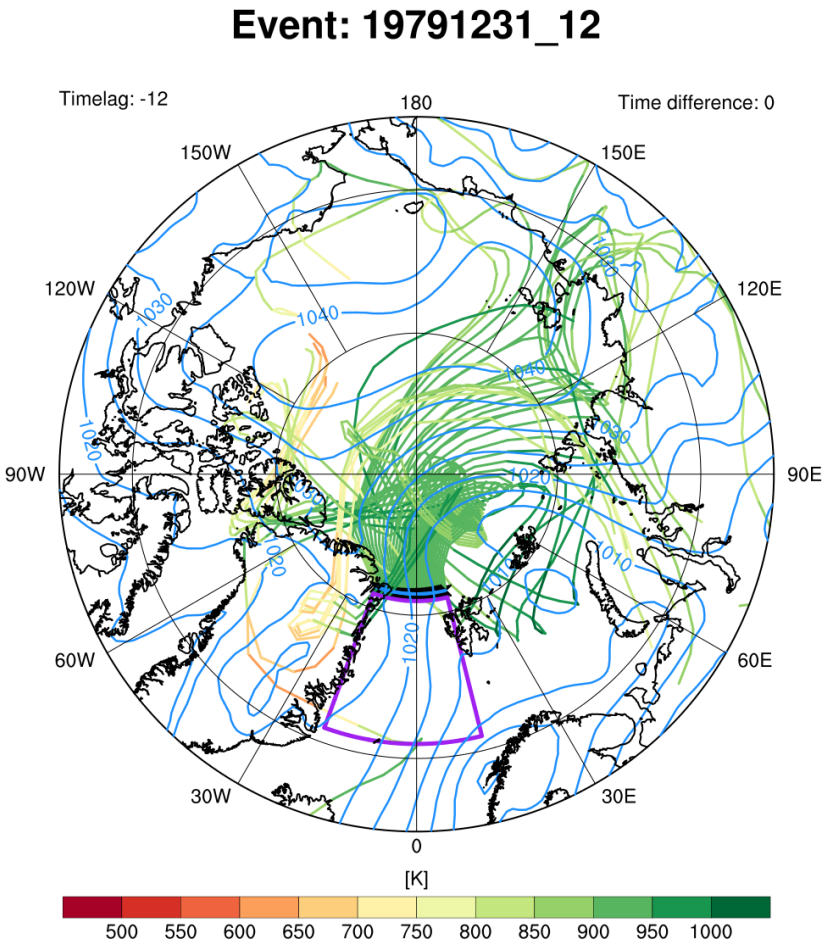

Figure 2.3: Example of trajectory plots together with eulerian field used for the analysis from the event at 12h the 31/12/1979. Same as in the previous figure but with isobars at sea level represented by the blue lines.

We can see the black crosses marking the positions, the shading representing the pressure of the air parcel and the contours of sea level pressure (SLP). This combination of Lagrangian and Eulerian perspectives allow to link the air masses to location and conditions to the environmental fields.

2.2.3 θ climatology

To assess if the potential temperature of the air parcel is anomalously low compared to the climatology we first calculated the climatology of potential temperature at 900hPa over the region for the ERA-interim period.
To do that we first calculated a running mean over 10 days to only account for anomalies to normal conditions over this 10 day period. Afterwards a yearly mean of the entire ERA-interim period, using the previously computed 10-day running mean, was computed.
The calculation of the anomaly then follows this equation:

$$\theta_{anomaly} = \theta_{900hPa} - \theta_{mean} \tag{2.5}$$

$\theta_{anomaly}$: potential temperature anomaly at 900hPa (K)
θ_{900hPa}: current potential temperature at 900hPa (K)
θ_{mean}: mean potential temperature at 900hPa over the ERA-interim period (K)
Both mean and current potential temperature being in Kelvin, a negative value will indicate a temperature lower than normal.

2.2.4 Theoretical background to potential vorticity

During this master thesis we will look both at dynamic and thermodynamic relationships. A very interesting relationship is the coupling between potential vorticity (PV) anomalies and isentropic surfaces.

A major characteristic of PV is its material conservation on isentropic surfaces in adiabatic and frictionless conditions. Hoskins [2015] defines PV with the following equation:

$$P = \frac{1}{\rho}\zeta\nabla\theta \tag{2.6}$$

P: potential vorticity
ρ: density
ζ: absolute vorticity
$\nabla\theta$: gradient of potential temperature
This quantity is materially conserved on isentropic surfaces, meaning:

$$\frac{dP}{dt} = 0 \tag{2.7}$$

Based on both equation 2.6 and 2.7, if the absolute vorticity increases the $\nabla\theta$ must decrease to keep the balance.
The invertibility principle is a key property of PV that enables to obtain from PV the wind and temperature fields. In the case of positive PV anomaly, this leads to an increase in the $\nabla\theta$. We can see the effect on the isentropes in the next figure.

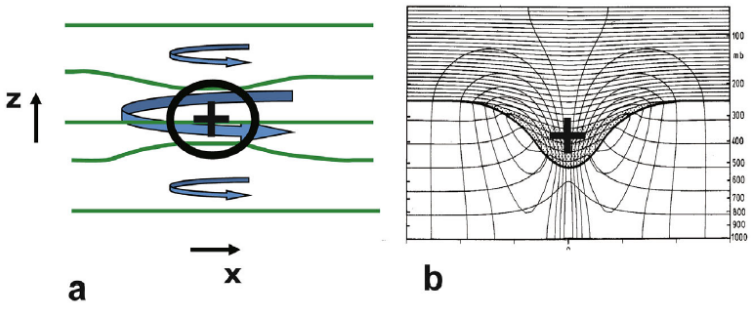

Figure 2.4: Schematic of a positive PV anomaly (a) local positive PV anomaly in uniform atmosphere. In blue the cyclonic rotation and in green the isentropes. (b) Positive PV anomaly at the level of the tropopause with horizontal lines being the isentropes and the bold black line the dynamical tropopause (2PVU) [Hoskins, 2015].

In Figure 2.4, we can clearly observe the effect of the increase of the $\nabla\theta$. The isentropic surfaces have an upward bend underneath the tropopause and a downward bend above the tropopause. The upward bend, is representative of a negative anomaly in θ. It is also important to see that the tropopause is lowered at the location of the positive PV anomaly.

These key principles are of use for our analysis.

2.2.5 Iceland Lofoten Pressure Difference (ILD)

In the section 1.1 we briefly mentioned the possible importance of the Iceland Lofoten Pressure Difference (ILD).
In Jahnke-Bornemann and Brümmer [2009], the ILD impacts prominent Northern Hemispheric pressure centres and especially the transport of ice through Fram Strait. As we are studying CAOs in precisely this region, it is interesting to see if this pressure pattern can influence CAO formation.
To identify any correlation we first have to create a data set representing the ILD during our period.
The ILD is representing the low pressure distribution over the region of Iceland. The paper from Jahnke-Bornemann and Brümmer [2009] demonstrates

that this region of low pressure has two centres that vary in strength with time. One centre is near Iceland and the second near the Lofoten.

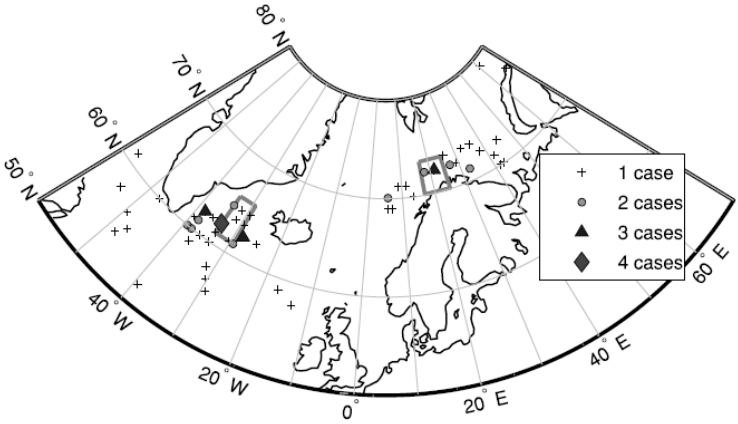

Figure 2.5: Defined regions for the ILD by Jahnke-Bornemann and Brümmer [2009].

The ILD is defined as a difference between the sea level pressure (SLP) anomaly over the Lofoten and Iceland.

$$ILD = \Delta p_L - \Delta p_I \tag{2.8}$$

$$\Delta p_L = \frac{p_{L(i)} - p_{L_{mean}}}{\sigma_L} \tag{2.9}$$

$$\Delta p_I = \frac{p_{I(i)} - p_{I_{mean}}}{\sigma_I} \tag{2.10}$$

Δp_L: SLP anomaly over the Lofoten region (hPa)
Δp_I: SLP anomaly over the Iceland region (hPa)
$p_{I(i)}$: mean SLP over the Iceland region at a specific time (i) (hPa)
$p_{L(i)}$: mean SLP over the Lofoten region at specific time (i) (hPa)
$p_{L_{mean}}$: mean SLP over the Lofoten region averaged over the entire period (hPa)
$p_{I_{mean}}$:mean SLP over the Iceland region averaged over the entire period (hPa)
σ_L: standard deviation of the SLP over the Lofoten region (hPa)
σ_I: standard deviation of the SLP over the Iceland region (hPa)

The equation 2.8 shows the definition of the ILD. Based on this equation we can now see that a positive ILD leads to a higher Δp_L than Δp_I which means that the atmospheric situation is more cyclonic over Iceland than the Lofoten region, and the opposite for a negative ILD.
For our purpose we calculated the ILD from December 1979 until December 2016 over the regions shown in Figure 2.6.

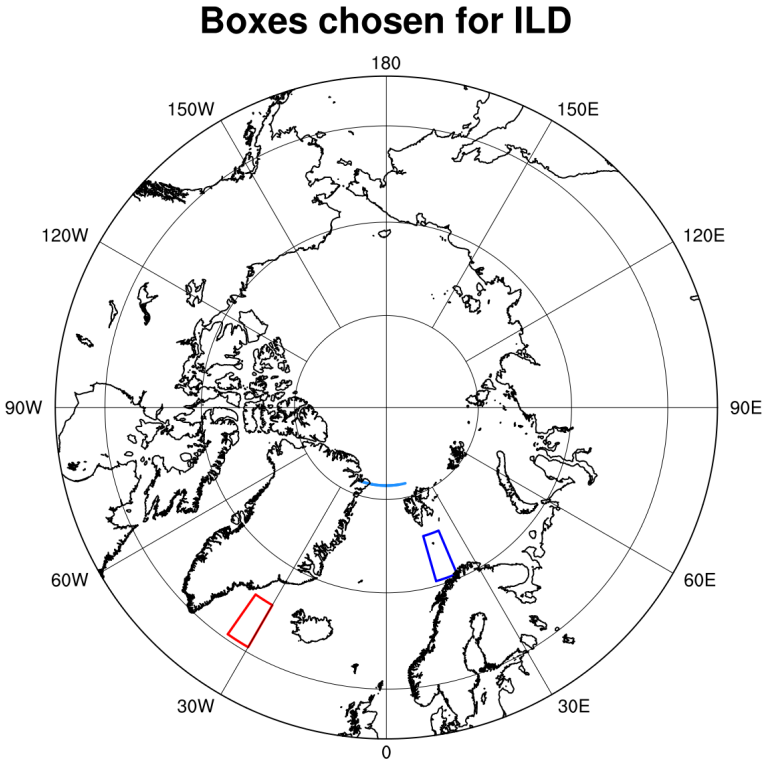

Figure 2.6: Areas chosen for the Iceland region (red) and the Lofoten region (blue).

We represented the regions we used in Figure 2.6. The regions are slightly different to avoid regions above sea level and slightly bigger to take into account larger pressure systems and their influence.

3

Inter-annual variability

The analysis of the inter-annual variability allows us to take a first look at the frequency of CAOs during the ERA-interim period. This variability, if linked to large atmospheric pressure patterns, might give us some informations on the processes that impact CAO formation and their frequency.

3.1 CAOI climatology and CAO frequency

We have defined in section 2.1.2 the CAOI and now have the CAOI for the entire ERA-interim period for winter months (December to February). A first step is to look at the trend of the CAOI. A linear trend as shown in Figure 3.1 provides a first impression. In this figure we represented the mean CAOI within the violet box (Figure 2.2) to have a clear representation of CAOs, very close to the definition of section 2.1.2. The trend is clearly negative with a slope of -9.8·10^{-5}K per 6 hourly time-steps which leads to a cumulative decrease of 1.315K over the 37 year period. This trend shows a decrease in CAO frequency.

The analysis of the CAO frequency is easier if we use the definition of CAOs as explained in section 2.1.2 and use as data the number of events. We filtered the results to only keep the moderate and strong CAOs. We then also computed the trend of CAOs during the ERA-interim period.

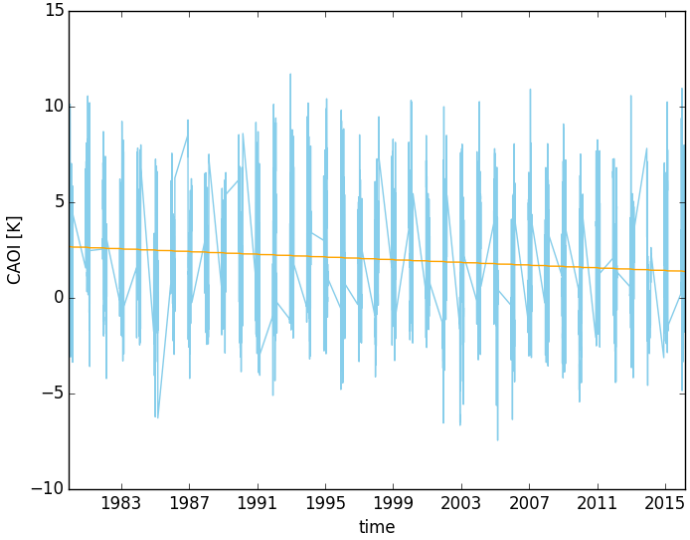

Figure 3.1: CAOI during the ERA-interim winter period with linear trend.

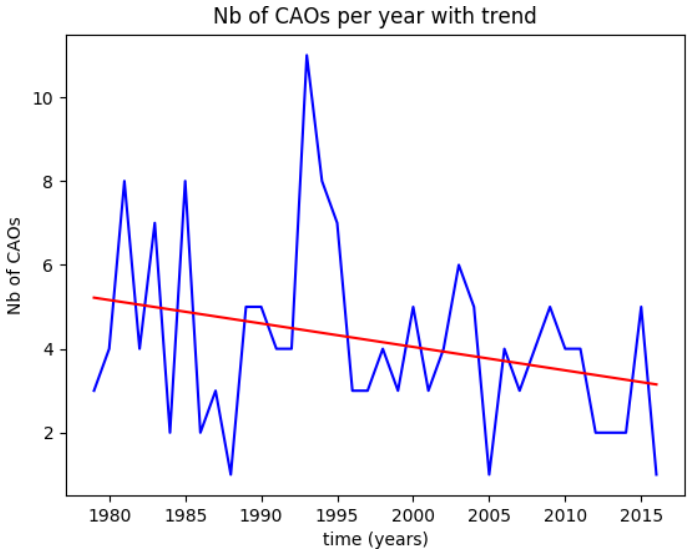

Figure 3.2: CAO frequency per year with linear trend.

Figure 3.2 shows first how the number of CAOs varied between years with for example only 1 CAO in the winter 2004/2005 and 11 in 1992/1993. On average we observe 4 CAOs per year but as we already saw for the CAOI, the CAO frequency decreases. The cumulative decrease amounts to 2 CAOs in 37 years. However, a linear trend is very simplistic and might not take into account possible periodicities in the CAO frequency that could be linked to atmospheric modes of variability.
We analysed the seasonality of the CAO frequency by considering the frequency of CAOs for each winter month.

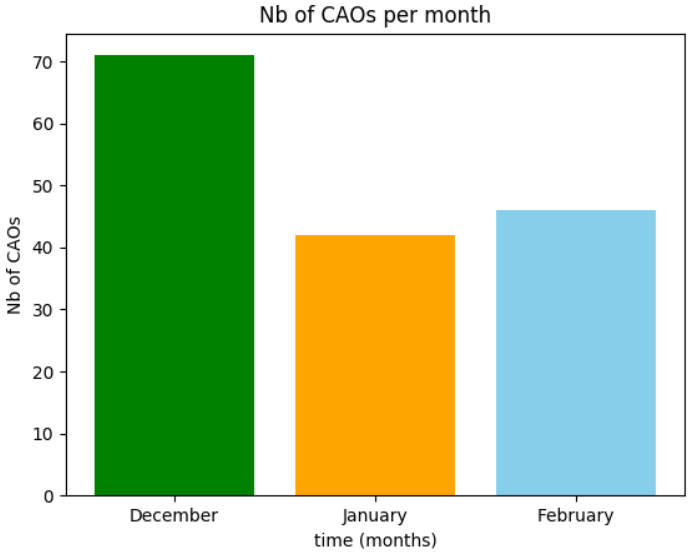

Figure 3.3: Total number of CAOs per month during the ERA-interim period.

Figure 3.3 shows very interesting results with a clear difference between December and the other winter months. December had 71 events during the 37 year period while January and February both had around 40 events during the same period. This large discrepancy could be explained by looking at the definition of CAOs. They are defined by a large θ difference between the ocean and the atmosphere. It is well known that the ocean has a greater thermal inertia. During the early winter, the atmosphere cools at a higher rate while the ocean is still warm from the summer. This leads to a larger θ difference that could explain the higher number of CAOs during December compared to the other months.

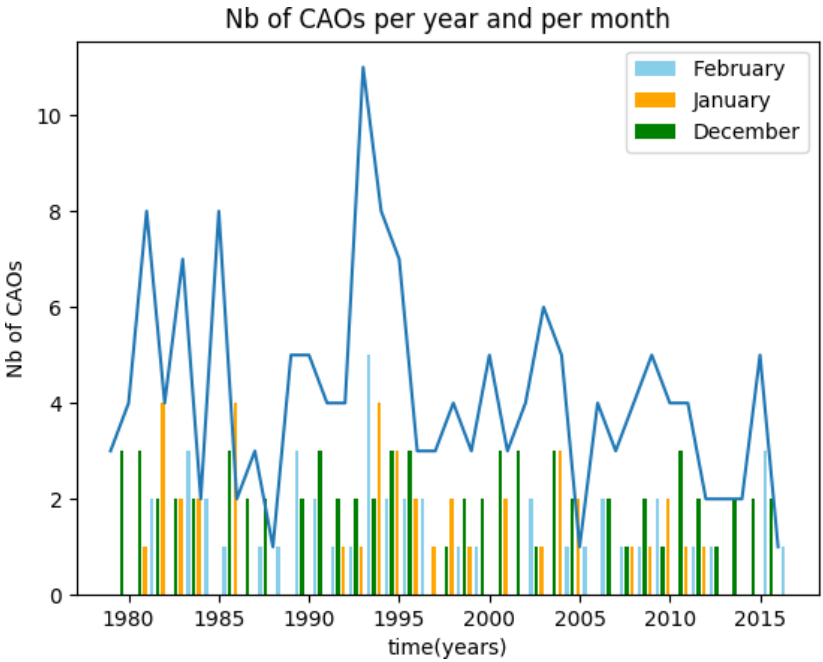

Figure 3.4: Number of CAOs per month (bars) and year (blue line) during the ERA-interim period.

Figure 3.4 shows that the CAO frequency per month each year is quite regular when looking at December but very irregular for January and February. Therefore, the yearly variability is determined mostly by the CAOs happening during January and February.

After looking at the CAO frequency per month, we will explore the frequency based on the strength level of CAOs. In our sample we have only the moderate (4K<CAOI<8K) and strong CAOs (CAOI>8K).

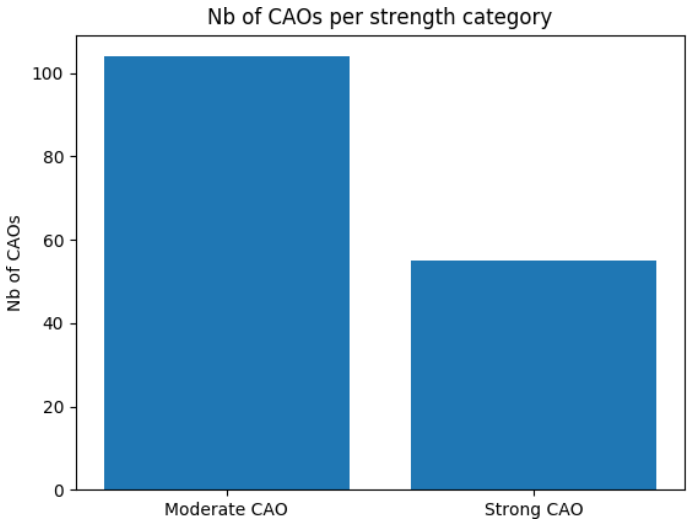

Figure 3.5: Number of CAOs per strength categories during the ERA-interim period.

Figure 3.5 shows a repartition as expected. There is a higher number of moderate CAOs than strong CAOs.

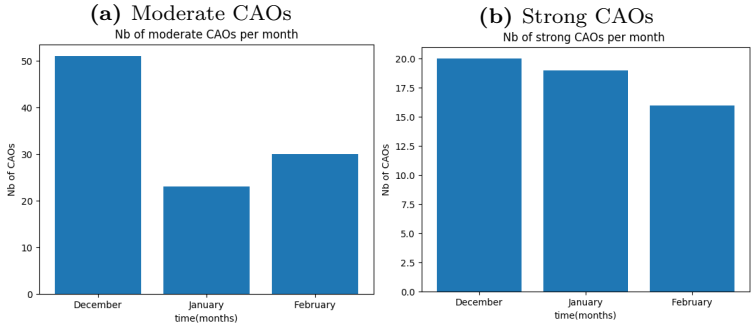

Figure 3.6: Number of CAOs per strength category for the ERA-interim period. (a) Moderate CAOs and (b) Strong CAOs.

Figure 3.6 shows how the CAO categories are spread between the winter months. While the moderate CAOs show the same pattern as the total CAO frequency per month, the strong CAOs show a more even pattern. The number of CAOs is still higher in December but the difference is less striking

and February has not more CAOs than January. Also, we have to keep in mind that there are only around 50 strong CAOs for 100 moderate ones. This sample is therefore quite small which means that the patterns are not very significant and should be handled with caution.
Similarly to Figure 3.4, Figure 3.7 depicts the frequency of CAOs of each category per year.

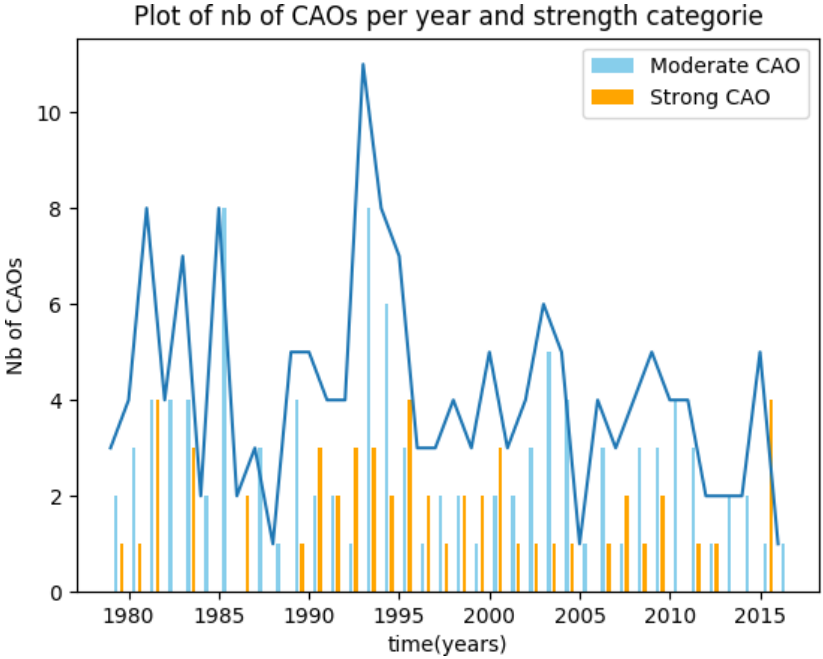

Figure 3.7: Yearly number, of moderate and strong CAOs (blue and orange bars repsectively) and total number of CAOs (blue line).

Compared to Figure 3.4, where the months with less CAOs explain most of the variability, the variability in Figure 3.7 is not clearly defined by strong CAOs. In fact, the moderate CAOs are not only predominant in number but also explain most of the inter-annual variability.

This first analysis showed us a high variability between years that can be explained by the variability in later winter months. During the ERA-interim period we witness a decreasing trend both in the CAOI and the CAO frequency. It is unclear whether this trend is significant and we will further investigate its possible causes in section 5.

Before going into a more detailed look at the processes driving CAOs, we will first verify if links between CAOs and large-scale pressure patterns can be found.

3.2 Large-scale atmospheric patterns

The pressure pattern that is controlling a large part of the weather in the North Atlantic is the North Atlantic Oscillation (NAO). To quantify this oscillation, an index has been developed using the normalized sea level pressure difference between Lisboa (Portugal) and Stykkisholmur (Island). A larger pressure difference (positive NAO index) representing a situation of strong westerly flow while a smaller pressure difference (negative NAO index) represents a situation with weaker westerlies.

However, the NAO is mostly impacting the weather at mid-latitudes and might therefore not impact CAOs which occur at high latitudes. To verify this hypothesis we will correlate the daily NAO index (NAOI) calculated according to Barnston and Livezey [1987] with the daily CAOI. To be thorough we computed both Pearson and Spearman Rank correlation.

Index	Pearson correlation	Spearman Rank correlation
CAOI-NAOI	-0.08	-0.11

Table 3.1: Correlations between daily NAOI and daily CAOI.

The Table 3.1 corroborates our first hypothesis that there is no obvious relation between the CAOI and the NAOI, since the correlation is very weak. This shows that the NAOI has probably no direct impact on CAO occurrence.

The NAO is defined with two poles, a pole of low pressure over Island and a pole of high pressure over the Azores. The pole of low pressure, as explained in section 2.2.5, can either be located over Island or the Lofoten region and is called the ILD. This dipole is located further north and could influence the CAO formation more directly than the NAO.
We calculated the correlation between the ILD and the CAOI.

Index	Pearson correlation	Spearman Rank correlation
CAOI-ILD	-0.53	-0.539

Table 3.2: Correlations between daily ILD and daily CAOI.

The correlation as seen in Table 3.2 is high, showing that this pressure

pattern could impact CAOs. The causality will be discussed in section 5.1.3.

As we mentioned in section 2.2.5, the ILD is the low pressure dipole of the NAO. In Jahnke-Bornemann and Brümmer [2009], the correlation between the ILD and NAO was very low. We also compute this correlation (Table 3.3)

Index	Pearson correlation	Spearman Rank correlation
NAO-CAOI	0.09	0.08

Table 3.3: Correlation factors between daily ILD and daily NAOI.

and find that the correlation is very low. This shows that the NAO has probably neither a direct nor an indirect impact on CAO formation and occurrence. The ILD, however shows high correlation and this will be investigated more thoroughly as me mentioned earlier.

This first analysis of both the CAO frequency and trend, together with the first look on impacting weather pattern, has already shown some interesting points. To better understand the behaviour of CAOs and the driving processes we will focus in the next section on shorter time-scales and smaller samples.

4

Case studies

The case studies presented in this chapter have the main goal to obtain a detailed understanding of the evolution of CAO air masses prior to their arrival over the ice-free ocean. This detailed look allows us to identify first characteristics and driving processes that apply on a climatological scale. To begin with, we will look at a sample of 20 events to have an overview of similarities and differences between CAOs.

4.1 Top 20 strongest events

We decided to use a sample of the 20 strongest events to be sure that we are looking at clearly defined CAOs and impact-full events in terms of, for example air-sea heat fluxes. In this first analysis we will study the pressure of the air parcels (P), the temperature (T) and the potential temperature (θ) of the air masses, the surface sensible heat fluxes (SSHF) and the surface latent heat fluxes (SLHF).
This first analysis will enable us to select subjectively, based on first observations, the most interesting cases to analyse and show.

4.1.1 Origins

The different parameters of the air masses are defined by their initial state, at the origin, and their temporal evolution . Here, we investigate if CAO air masses come from preferred regions. We distinguish the following regions of origin:

— The interior Arctic covering all the Arctic ocean bordered by Russia, Canada, Alaska, Greenland and Svalbard. For our study, we included the Canadian Arctic Archipelago to this region and all islands within the Arctic ocean (e.g. Yuhzny and Severny islands).

— The region of North America which includes both Canada and Alaska (obviously without the Canadian Arctic Archipelago that is part of the previous region).

— The Siberian region which includes all Russia without the Arctic islands of Russia.

To identify the origin, we used the trajectories and marked the position of each air mass at the time -240h (10 days prior to arrival to Fram Strait). By visual inspection we find that all air masses either originate from the Siberian region or the interior Arctic or a combination of both. More details in Table 4.1.

Regions	Number of events coming from this region	Percentage
Mostly interior Arctic	8	40 %
Siberia	4	20 %
Mostly Siberia	8	40 %

Table 4.1: Origin of air masses.

In the Table 4.1 we introduced three categories to take into account that we follow a large number of air masses per CAO and that not all come from the same region. To summarize, 40% come from the interior Arctic and the majority, 60%, mainly from Siberia. It is surprising to see, that from our sample, not one air mass was coming from the region of North America. The reason could be that Greenland is working as an orographic barrier for those air masses . Iwasaki et al. [2014] identified two main streams of polar cold air mass. One of them originating over North America and which is steered by both the Rocky Mountains and Greenland and ends over the west of the North-Atlantic ocean. This corroborates our theory that air masses from North America are blocked by Greenland, reducing their potential contribution to CAOs over Fram Strait.
This might change when considering all the CAOs from the ERA-interim period or maybe signal that this is specific to particularly strong CAOs.
After this qualitative analysis of the origin, we will investigate the evolution of the air masses.

4.1.2 Pressure of air parcels

The temporal evolution of the pressure of the air parcels shows us at which altitude they travel. Changes in altitude indicates whether compres-

sion warming and expansion cooling are important processes. A first observation is that most air parcels are moving at lower altitude. Most of them are between 850 and 1000hPa.

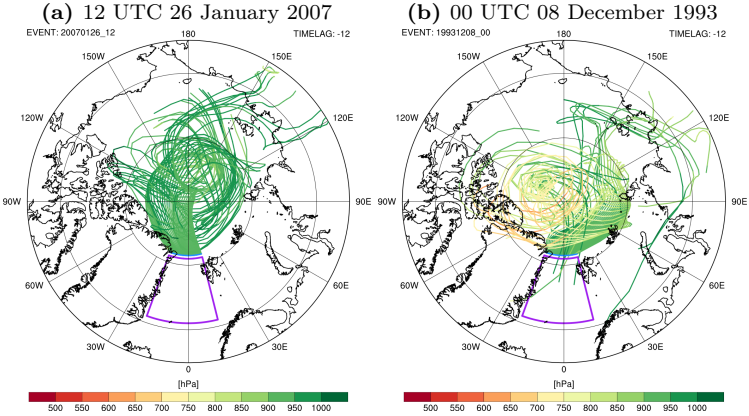

Figure 4.1: Trajectories of two events: shading representing the pressure of the air masses.

In the Figure 4.1, the events are named after the date at which the CAO peaks in the following way YYYYMMDD_HH (YYYY: year, MM:month, DD:day, HH:hours).

In most cases, as portrayed in Figure 4.1 (a), the air masses stay at high pressure levels. In some cases, the air masses are at higher altitude at their point of origin or get to higher altitudes during their evolution as shown in Figure 4.1 (b). Even in those cases, the air masses are at low altitude when arriving near Fram Strait, at the date of the CAO. This makes us deduce that air parcels undergo a compressional warming during a descent, at least in the last stages of their evolution. This is also due to the fact that the backward trajectories we use start at 900hPa, meaning that if they reach higher altitudes earlier on, they will have to descend to the 900hPa level.

This decrease in altitude is clearer in the following Figure 4.2 showing the mean pressure of all trajectories together with the standard deviation as dotted lines. We see a clear increase in pressure during both evolution of trajectories in the following figure.

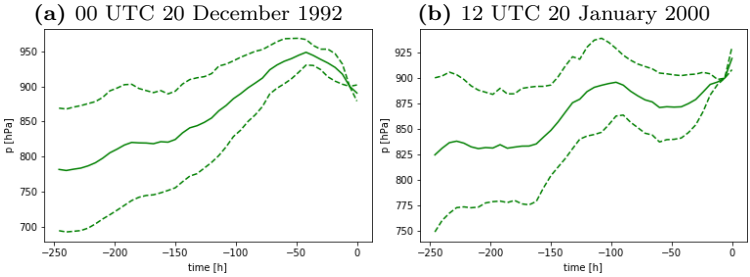

Figure 4.2: Mean pressure of trajectories between -240h and 0h of two CAOs.

Unrelated to the pressure, the trajectories also reveal an interesting feature. In 70% of cases we see a vortex-like feature. This feature is visible in both cases of Figure 4.1 as a region where the air parcels have a circular motion. This will be discussed in the following case studies.

4.1.3 Thermodynamic evolution of air parcels

The evolution of the temperature of an air mass is governed by the following equation [Holton, 2004]:

$$\frac{DT}{Dt} = \frac{\kappa T \omega}{p} + (\frac{p}{p_0})^{\kappa} \frac{D\theta}{Dt} \tag{4.1}$$

$\kappa = \frac{R}{c_p} = 0.286$: Poisson constant
R: gas constant
c_p: specific heat coefficient at constant pressure
p_0: reference pressure (1000hPa)
T: temperature
p: pressure
θ: potential temperature
ω: vertical motion

This equation links the thermodynamic evolution to vertical motion and diabatic heating.

The absolute temperature of an air mass is dependent on both diabatic and adiabatic processes. The evolution of the temperature along the trajectories could show the relative importance of both types of processes.
Within our sample, the temperature is continuously decreasing along the trajectories. In the few cases where the compression through a descent is very strong we see a significant adiabatic increase of temperature.

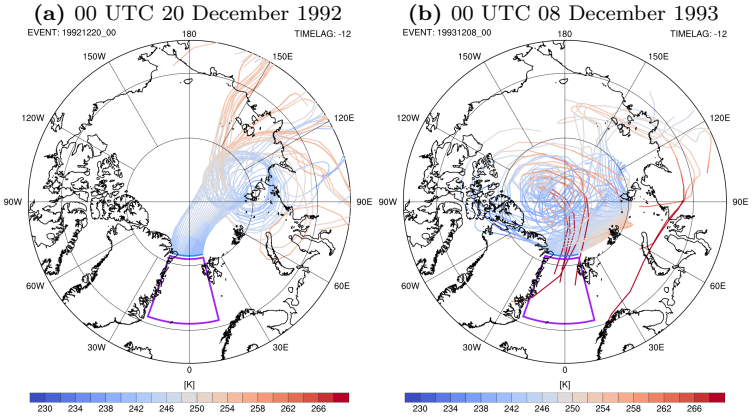

Figure 4.3: Temperature of trajectories between -240h and 0h of two CAOs.

In Figure 4.3 we can clearly see a continuous decrease in temperature along the air parcel's path through the interior Arctic. For the event 19921220_00, there is no distinct increase of temperature even though warming by compression is happening due to the increase in pressure as seen in Figure 4.2. On the other hand, for the CAO of 19931208_00 the compression seems to be sufficiently strong to see a significant increase in temperature on the eastern part of the trajectories, few hours before reaching Fram Strait.

The fact that most air parcels in all events have a decrease in temperature even during the compression phase, hints towards a strong and continuous diabatic cooling that will be discussed later in the case studies. Also, this suggests that warming by compression warming is not a limiting factor in the occurrence of CAOs.

It is important to mention this very curious event of 20150212_18 (see Figure 4.4) with a strong warming along the air masses paths through the Arctic. This particular event, proves that air masses which undergo strong warming can still be associated to CAOs. We have to observe that a cooling a few hours before the arrival at Fram Strait significantly decreases the absolute temperature of the air masses and probably has compensated the previous warming.

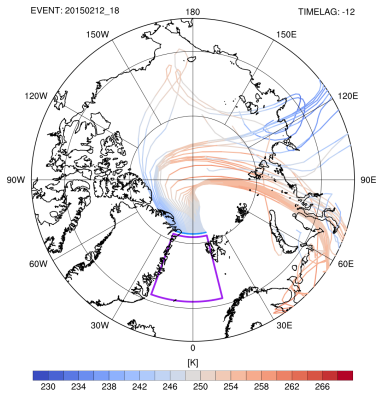

Figure 4.4: Atypical warming event during evolution of CAO air masses for the event 20150212_18.

Next we will be looking at potential temperature which, compared to the absolute temperature, will enable us to assess the influence of a diabatic processes since the potential temperature, by definition, is independent of any adiabatic processes such as compression and expansion.

The potential temperature follows for all cases a continuous decrease along the trajectories. The only exception is the case of 20150212_18 which shows an increase in the same period as for the absolute temperature.

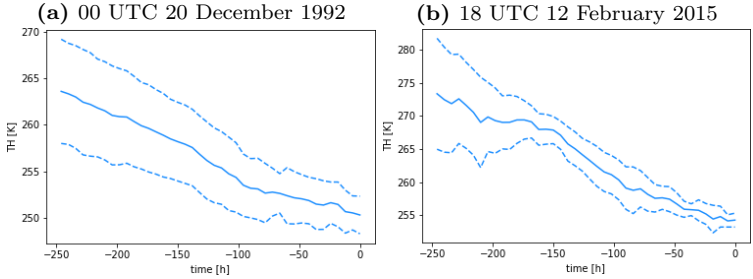

Figure 4.5: Mean potential temperature of trajectories between -240h and 0h of two CAOs

The continuous decrease is even clearer than for absolute temperature. In Figure 4.5, the decrease does not experience any particular jumps or rapid changes. This is interesting, and shows that the cooling process is mainly diabatic and occurring at a similar intensity during the entire evolution of

the trajectories. This would suggest that radiative cooling could play an important role.

The warming period of the 20150212_18 event is slightly dampened by the average over all trajectories, but still visible between -200h and -150h.

4.1.4 Surface sensible heat fluxes and latent heat fluxes

We have seen the evolution of both temperature and potential temperature. The first observations hint towards diabatic processes governing most of the changes of temperature. The surface sensible heat flux (SSHF) is a good candidate since the cold surface of the sea ice can cool the surface layer of the atmosphere by heat transfer from the atmosphere to the sea ice surface. We will also have a look at surface latent heat fluxes (SLHF) which, due to the very dry region, seems a less plausible candidate.

To begin we have to define our convention of sign for both heat fluxes. If the heat flux is positive, the atmosphere above the surface is giving up heat and therefore cools.

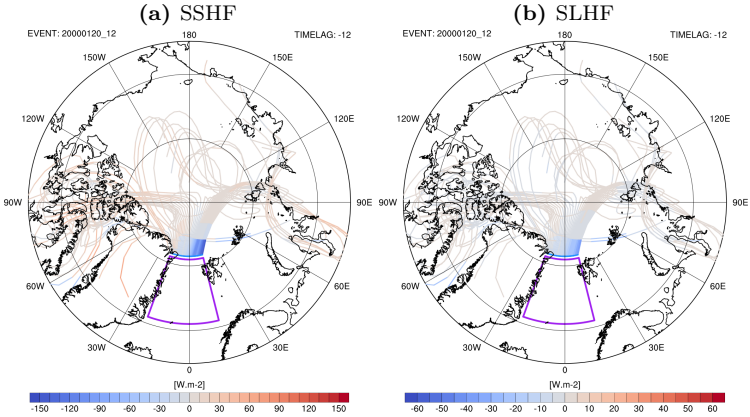

Figure 4.6: Trajectories of event 20000120_12 with colour-shading representing (a) SSHF and (b) SLHF.

In the Figure 4.6 we see that both heat fluxes tend to be positive most of the time but near Fram Strait. This points towards a cooling of the atmosphere during a large part of the evolution. Important to notice, is that both fluxes have a very low value with less than 50W m^{-2} for SSHF and around 10W m^{-2} SLHF. This is clearer to observe in Figure 4.7.

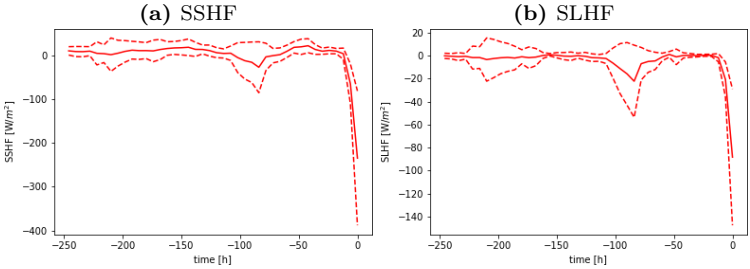

Figure 4.7: Mean (a) SSHF and (b) SLHF of trajectories between -240h and 0h of CAO 19921220_00.

The values are barely above 0W m^{-2} until just before Fram Strait. This tells us that SSHF could be responsible for some of the cooling but the magnitude is too small to be the only contribution. Furthermore, due to the sea ice, the boundary layer in this regions is very shallow cf. Chapter 2. The conditions at the surface are very likely to form an inversion which leads to very small turbulences or convection. This, and the relatively high altitude of the CAO air masses (above 900 geopotential height), renders heat exchanges very difficult and should lead to a very small impact of SSHF.

SLHF has an even smaller magnitude and can not cool the atmosphere, even if it is directed to the ocean. The clear jump to very negative values can be explained by the air masses moving over the open sea, which we will verify in the next section.

4.1.5 Sea ice

As stated previously, looking at the sea ice distribution could give information on the evolution of the heat fluxes.

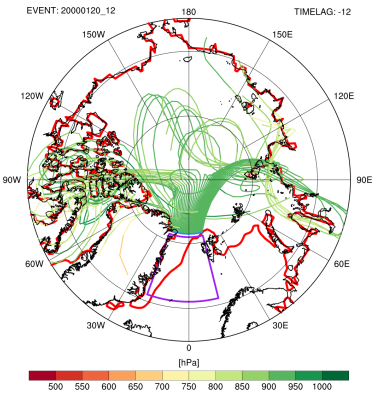

Figure 4.8: Sea ice distribution in red of the event 20000120_12.

In this case, air masses are very close to the ice margin and this could explain the sudden change of sign in heat fluxes. Another important remark is that CAO air masses either travel above continents or above ice and therefore are not impacted by the open sea before reaching Fram Strait.

A small observation that won't be discussed more in this thesis. When looking at the evolution of the sea ice distribution during the 10 days prior to a CAO, we either see no clear difference or a slight expansion of the sea ice margin towards lower latitudes in the Fram Strait region. The small expansion could be related to the cooling of the ocean by the CAO air masses, leading to more ice formation or transport of ice by the northerly winds. This is beyond the scope of this master thesis but could be interesting to study how sea ice distribution and sea ice transport is influenced by particular weather phenomena like CAOs.

4.1.6 Summary: table

In the following table we will summarize the specific characteristics of the top 20 events based on the previously identified features. This table has also the aim to better identify the CAOs that are most interesting to study further. For the following in depth case studies we will look at both very typical and atypical cases. To this end, we will have to identify what typical means based on the previous observations.

Event	Origin	Integrated CAOI	Vortex	θ
19791231_12	Mostly Arctic	3674.81	Present	Continuous decrease
19810115_06	Mostly Arctic	3831.70	Present	Overall decrease
19810222_12	Mostly Arctic	3704.62	Present	Overall decrease
19911222_06	Siberia	3673.98	Present	Overall decrease
19920205_18	Mostly Siberia	3413.67	Present	Continuous decrease
19921220_00	Siberia	4251.04	Present	Continuous decrease
19931208_00	Mostly Arctic	3437.59	Present	Continuous decrease
19940101_06	Siberia	3696.68	Present	Overall decrease
19950128_00	Mostly Siberia	3595.40	Absent	Continuous decrease
19950202_00	Mostly Siberia	3778.93	Present	Overall decrease
19951212_18	Mostly Siberia	3562.40	Absent	Overall decrease
19980228_00	Mostly Siberia	3436.86	Present	Overall decrease
20000120_12	Mostly Arctic	3748.06	Absent	Continuous decrease
20000128_18	Mostly Siberia	3718.08	Absent	Continuous decrease
20011225_12	Mostly Siberia	3628.68	Present	Overall decrease
20040126_12	Siberia	3724.58	Absent	Continuous decrease
20070126_12	Mostly Arctic	3961.30	Present	Continuous decrease
20121225_12	Mostly Arctic	3838.74	Present	Overall decrease
20150212_18	Mostly Siberia	3718.12	Absent	Warming period within overall decrease
20151226_06	Mostly Arctic	3976.65	Present	Overall decrease

A typical case is characterized by a continuous decrease in potential temperature, air masses mostly coming from Siberia, the presence of a vortex-like feature and shallow trajectories that tend to mostly descend.
Based on this description, that represents most of the sampled CAOs, the chosen event to represent the typical cases will be the on at 19921220_00. The event of 20150212_18 will be very interesting to study due to the strong warming period that is very specific to this event. Also, it does not have a vortex feature. The last event chosen is from 20000120_12 and has the particularity to show a split between two branches of air masses and no vortex feature. Besides these characteristics, the cooling is very typical which means that we might be able to isolate the effect of the absence of a vortex feature.

4.2 Typical case: 12 December 1992 at 00:00 UTC

To start the case study, we will have a quick look at the overall trajectory of the air masses.

The Figure 4.9 shows that the air masses are spread around a large part of Siberia at the beginning before getting gathered within a vortex over the coast. In this vortex the air masses ascend before being brought back down and converging together towards Fram Strait. The analysis now has the purpose to link the trajectories to the environmental conditions and see how they are influencing the air masses of CAOs. The procedure is, as stated in the section 2.2.2, a coupling of both the Lagrangian and Eulerian perspective. The first step will be to look at the synoptic situation.

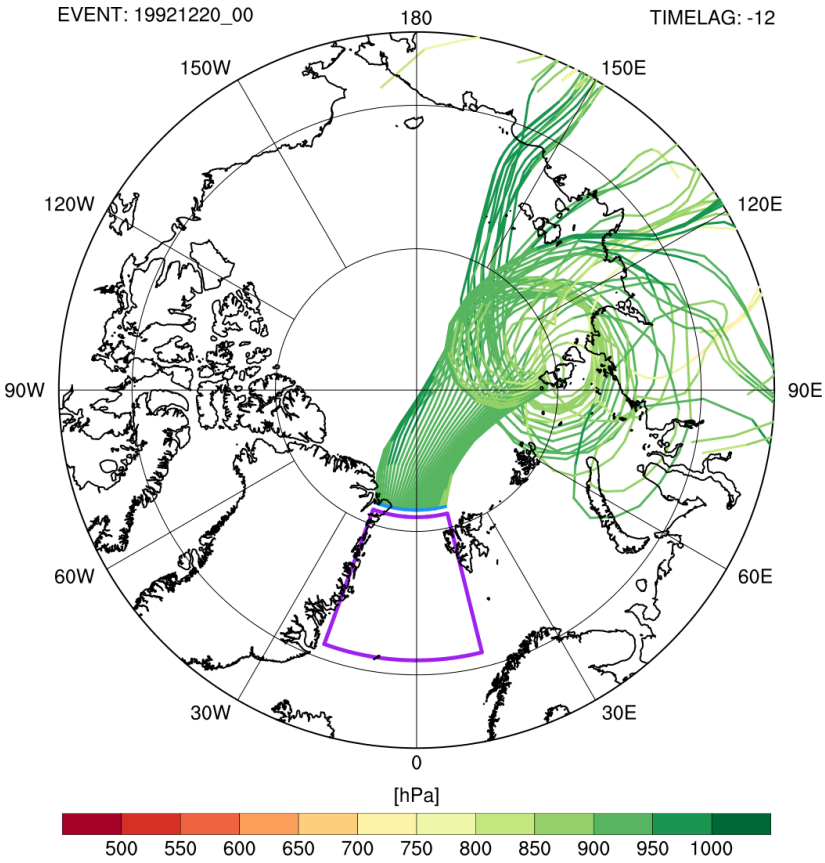

Figure 4.9: Trajectories of the 19921220_00 CAO with pressure as colour-shading.

4.2.1 Synoptic situation

Looking at the synoptic situation will help us to identify specific weather features that are directly and indirectly influencing the dynamics and therefore the paths of the air parcels. To do so, we will first look at both the sea level pressure (SLP) and the geopotential height at 500hPa (Z500). This should give enough information on the state of the troposphere surrounding these air parcels to explain their behaviour.

The motion of the air masses is driven by both low and high pressure systems at various heights. The air masses follow isobars as stated by the geostrophic approximation. We will focus on the motion related to the vortex feature and the advection towards Fram Strait.

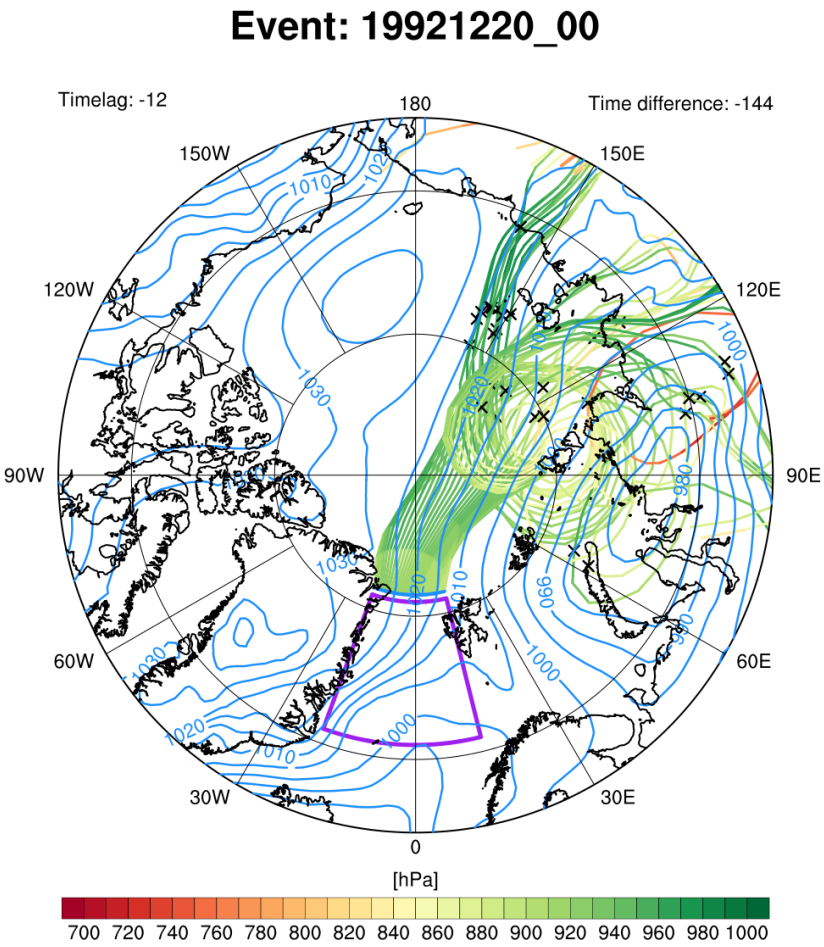

Figure 4.10: SLP field of event 19921220_00 with air masses at t=-144h. colouring represents the pressure along the backward trajectories and blue lines are isobars at sea level. Crosses represent the position of air masses.

The air masses begin to gather within this vortex at -144h. At this point a large surface depression is present over the north-western coast of Siberia as seen in Figure 4.10.

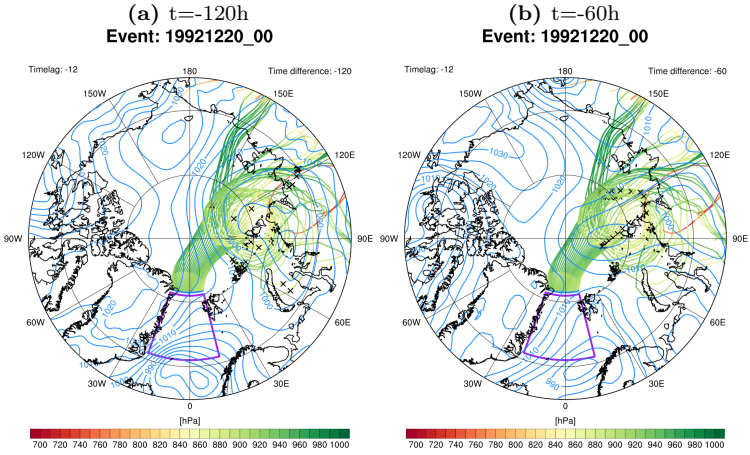

Figure 4.11: SLP field representing the evolution of a depression over north coast of Siberia from (a) -120h to (b) -60h.

This large depression moves over the location of the vortex feature and stays there from -120 to -60h clearly driving the motion of the air masses during the entire period. The following Figure 4.11 shows how the air masses are entrapped within the large depression which then circles approximatively midway between east and west Siberia. The stationary rotation of the cyclone during this period is apparently responsible for the vortex feature visible in the trajectories.

Is is important to notice that this cyclone also appears on the Z500 fields. This exhibits a stationary and barotropic cyclone responsible for the vortex and for the gathering of air masses prior to the advection towards Fram Strait.

The evolution thereafter shows a disappearance of the cyclone on lower levels while the low pressure system is still visible at higher levels.

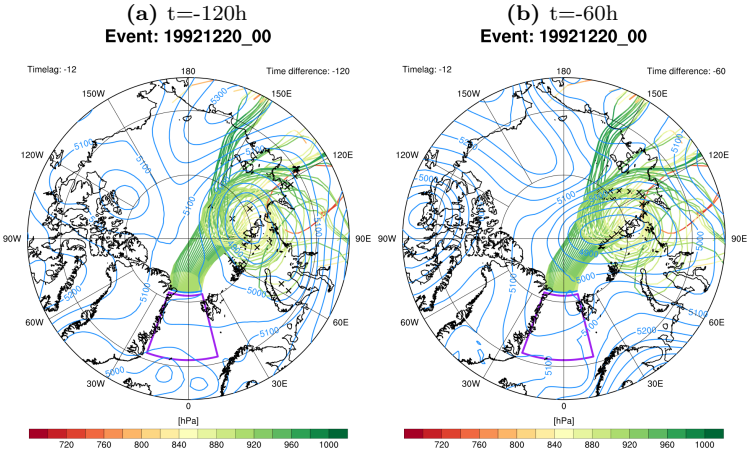

Figure 4.12: Z500 field representing the evolution of a depression over north coast of Siberia from (a) -120h to (b) -60h.

In Figure 4.13, at -48h the cyclone is not visible at sea level but still present at 500hPa.

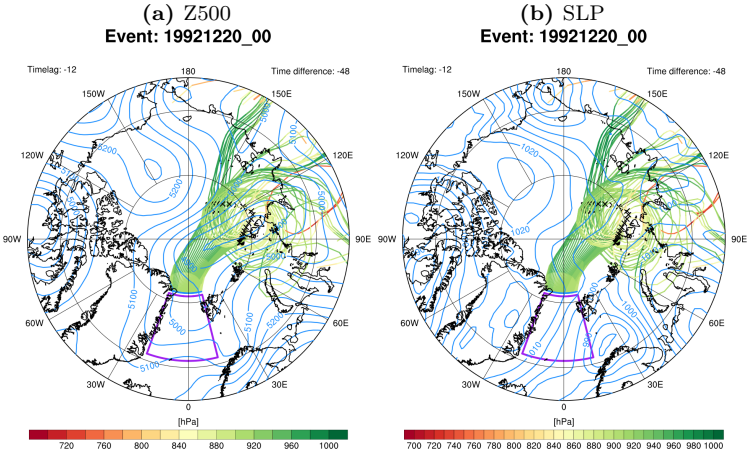

Figure 4.13: Depression at t=-48h on (a) Z500 and (b) SLP field.

Considering that for the next 48h the fields at different levels are quite different, we will split our analysis and first look at the Z500 pressure fields. In the following evolution, the low pressure system stretches from the Siberian coast towards Fram Strait until it splits with a centre over Fram Strait. During this time, the air masses always move beneath this mid tropospheric low pressure system.

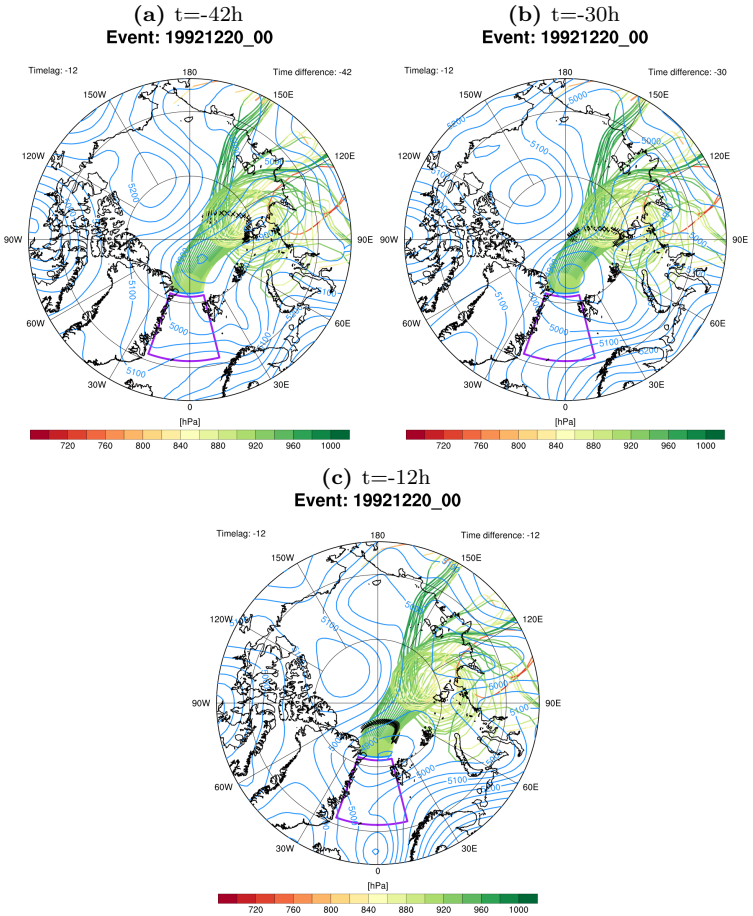

Figure 4.14: Evolution of depression on Z500 field from (a) -42h continuing(b) to -30h until (c) -12h.

The evolution is depicted in the three panels in Figure 4.14.

In the mean time at sea level, a pressure gradient develops over Fram Strait created by a stationary high pressure zone over Greenland and two low pressure systems moving from the coast of Norway towards the coast of Russia.

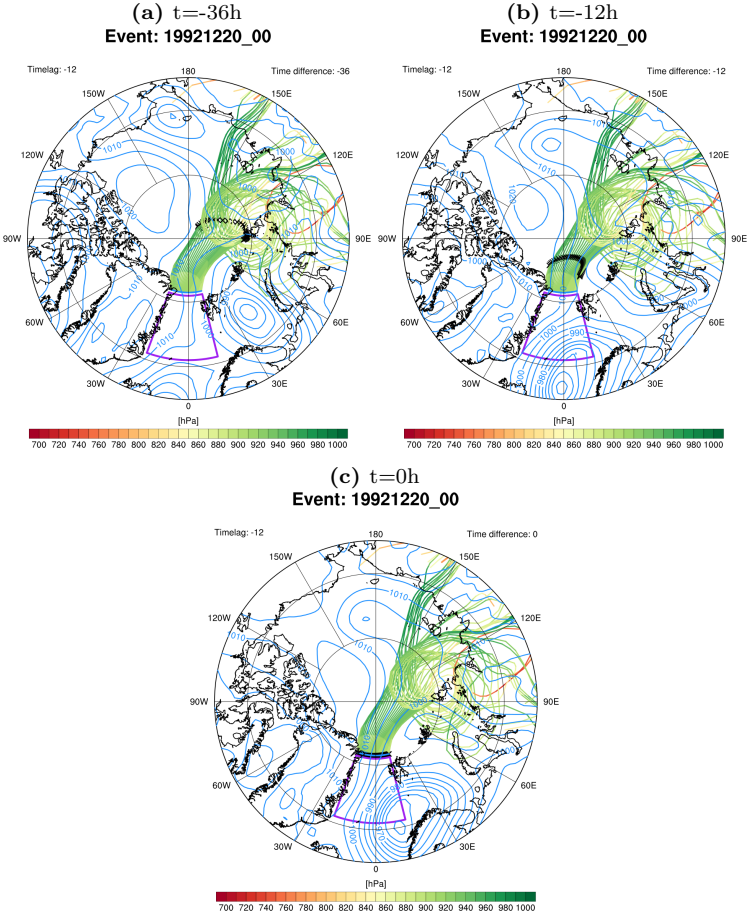

Figure 4.15: SLP field representing a pressure gradient through Fram Strait, from (a) -36h to (b) -12h until (c) 0h.

This pressure gradient formed by the combined flow of an anticyclone and cyclones is steering the air masses along a channel towards Fram Strait.

The markers in Figure 4.15 are moving together in this channel, proving that the CAO air masses are advected towards Fram Strait first and then to lower latitude after, because of this flow pattern.

In summary, a stationary and barotropic cyclone is responsible for the vortex feature and for gathering the air masses. This cyclone disappears at sea level while still present at 500hPa and moves towards Fram Strait with the air masses beneath. In the mean time, the combined flow of a high pressure system over Greenland and surface cyclones south and east of Fram Strait steer the air masses to Fram Strait and to lower latitudes.

4.2.2 Temperature evolution and temperature anomaly

CAOs are characterized by a positive temperature difference between the sea surface and the above atmosphere, it is therefore insightful to analyse the evolution of the temperature of the air masses to identify any specific patterns.

The air masses experience in this case a distinct cooling both in terms of the temperature and the potential temperature. The decrease in potential temperature is about 18K and continuous with no distinct jumps for the entire 10 days as shown in Figure 4.16 (c). The temperature follows a strong decrease at first before an increase between -150h and -70h. This increase is related to the descent of the air parcels that are leaving the direct influence of the depression discussed in the previous section. From -60h onwards, the temperature decreases until the air parcels reach Fram Strait. In total, the air masses experience a decrease in temperature of around 7K.
In Figure 4.16, we can see that the increase in temperature is correlated with a stronger increase in pressure after -150h.

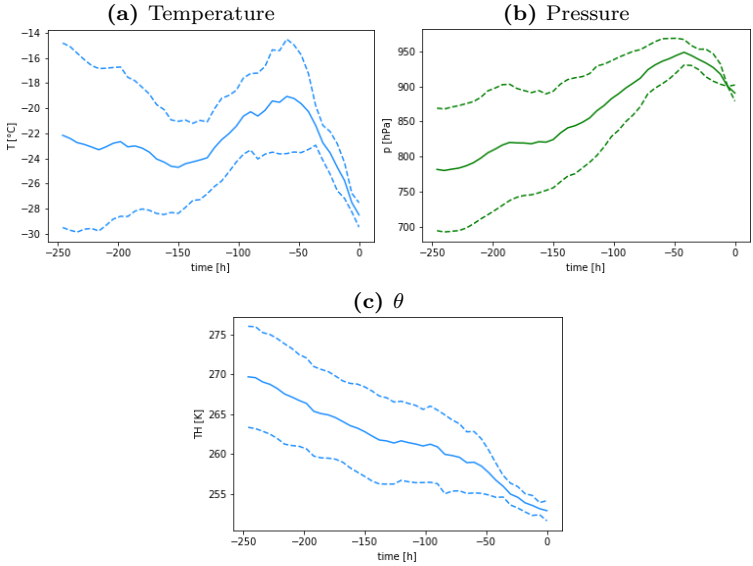

Figure 4.16: (a) Mean temperature, (b) pressure and (c) θ of trajectories between -240h and 0h of event 19921220_00.

In the section 4.1.3 we already discussed that the most important cooling processes are diabatic, therefore we will mostly focus on the evolution of potential temperature and the correlation with diabatic cooling processes. We already discussed in section 4.1.4 the influence of surface heat fluxes and deduced that even if they contribute to the cooling, the strength of the heat fluxes is too small to explain this strong cooling.

In the regions north of the Arctic circle, the main cooling process in winter is the radiative cooling due to the absence of the short wave radiation from the sun. The radiative cooling happens through the emission of longwave radiation (LWR) by the surface and the atmosphere. This process is happening all the time during the period of transport of air masses and can be considered a priori continuous. This is why, radiative cooling could be a reasonable candidate to explain the observed cooling of CAO air masses. To investigate this possibility, we looked at the LWR at the top of the atmosphere (LWR-TOA).

In this case the LWR-TOA along the trajectories is almost constant around -180W m^{-2} with only small variations. The mean increases slightly during the 10 days from slightly below -180 to around -170W m^{-2} as can be seen in Figure 4.17.

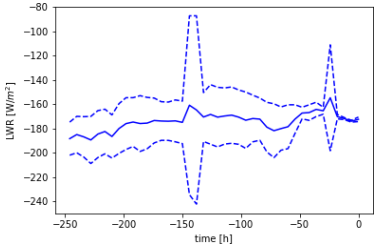

Figure 4.17: Mean LWR-TOA along the trajectories of event 19921220_00.

A striking feature can be seen when looking at the LWR-TOA distribution over the Arctic region. The air masses, at the beginning, do not follow particular regions of strong or weak LWR-TOA, but as they gather under the depression and then move towards Fram Strait, the LWR-TOA is particularly small in magnitude in the region of CAO air masses compared to nearby locations.

In Figure 4.18 we can see that around the green crosses representing the location of the CAO air parcels, the radiation is less important which is counter-intuitive at first. Considering our hypothesis that the driver of the cooling might be the LWR-TOA, we would have expected a larger amount of radiation explaining why these air masses are cooling this much. To explain this we first have to remember that LWR-TOA is the sum of all radiation from the surface and all atmospheric layers and is mostly dependent on two parameters: temperature and water content. The temperature is directly linked to radiation through the Stefan-Boltzmann Law.

$$L = \epsilon \sigma T^4 \tag{4.2}$$

L being the irradiance (W m^{-2}), σ the Stefan-Boltzmann constant ($5.67*10^{-8}$W $m^{-2}K^{-4}$), ϵ the emissivity and T the temperature (K). This means that the decrease in radiation is proportional to the decrease in temperature to the power of 4. This leads to the fact that at higher altitude the colder air emits less radiation.

The water content influences the LWR-TOA by absorbing some of this radiation. A layer of higher water vapor concentration or clouds will absorb the surface radiation leading to a decrease in LWR-TOA.
With this knowledge, we will try to identify the reason for this weak radiation. Looking at the total water content (TWC) we can correlate the regions with weak LWR-TOA with regions of low TWC.

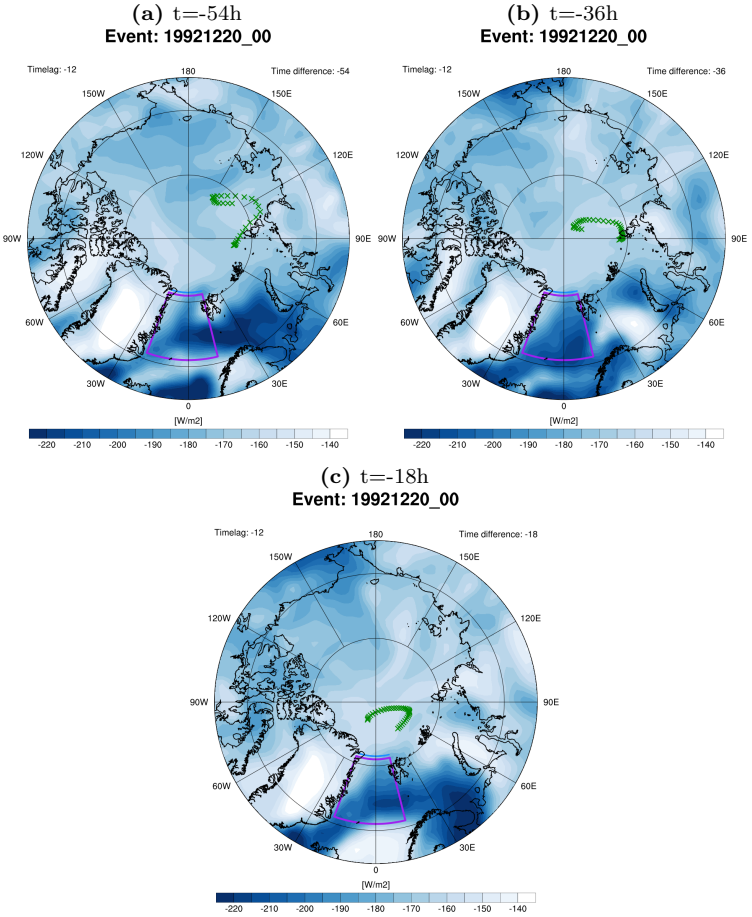

Figure 4.18: LWR-TOA distribution over the Arcticfrom (a) -54h to (b) -36h until (c) -18h.Green crosses represent the location of air masses.

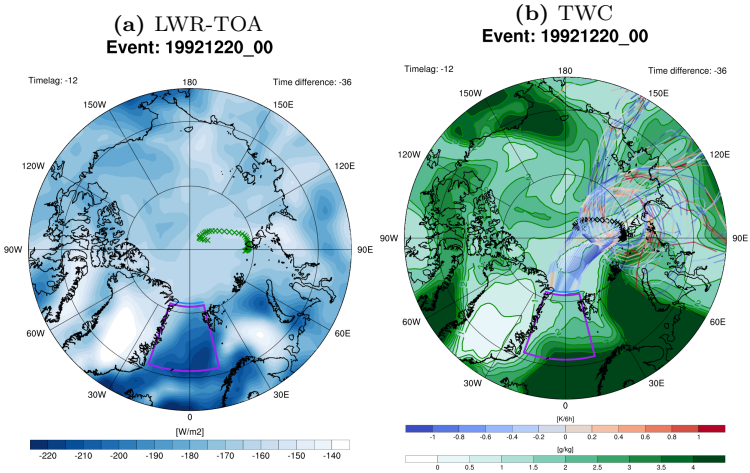

Figure 4.19: Distribution over the Arctic at -36h of (a) LWR-TOA and (b) TWC.

Figure 4.19 shows clearly that the less intense LWR-TOA is not due to a cloud layer or a particular important TWC. The weak radiation is therefore due to low emissivity of dry air. The reason however, of this dry air is the very cold temperature. As there is a discrepancy between the location of the CAO air parcels and the neighbouring regions, we can assume that the CAO air masses are colder. The weakening observed of LWR-TOA during the 10 day evolution might also be explained by the decrease in temperature.

The LWR, even if slightly counter-intuitive at first, is a reasonable candidate to explain the cooling. Also, LWR-TOA shows that CAO air masses have a specific imprint of less intense radiation compared to surroundings due to colder temperature. This leads us to one a of the major research questions of this master thesis: does this mean that CAO air masses are also cold relative to Arctic conditions? And if yes, why?

To identify any anomaly in potential temperature (θ) we used the dataset created as explained in section 2.2.3.

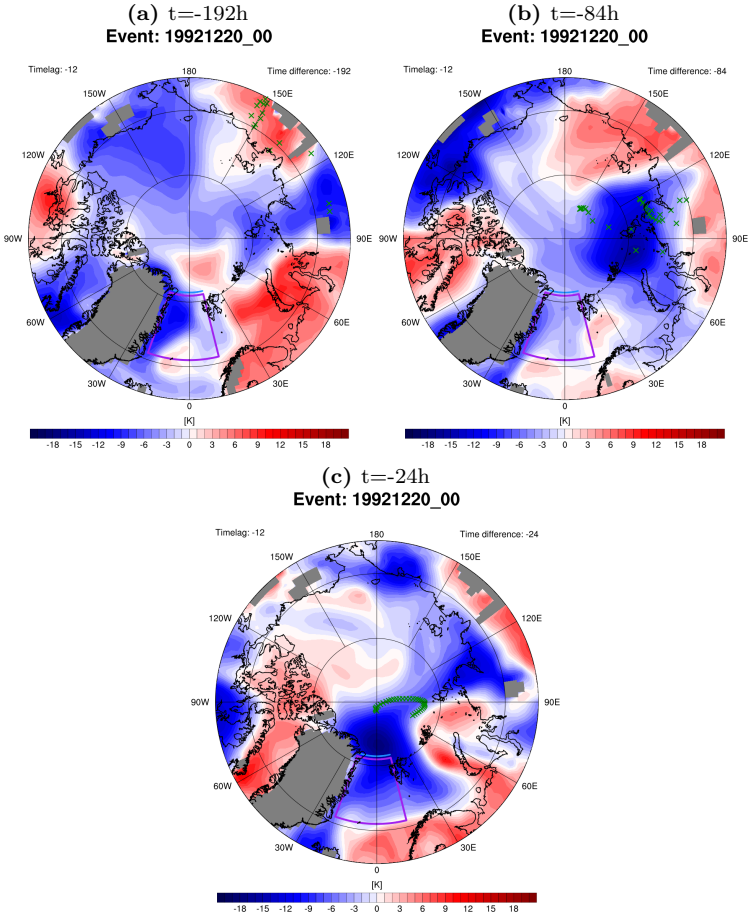

Figure 4.20: $\theta_{anomaly}$ over the Arctic represented by the colour-shading at (a) -192h, (b) -84h and (c) -24h. Green crosses marking the position at each timestep and the grey areas are location at higher altitude than 900hPa therefore without data.

In Figure 4.20 the anomaly is mostly negative at -192h over the Arctic with warmer regions over west and east Russia. At this point, the CAO air masses are mostly over regions of positive $\theta_{anomaly}$. In the next panel at -84h the convergence of all air parcels occurs in a region of very anomalously cold θ. From this point onward the air parcels move within this cold anomaly until they reach Fram Strait. It is very interesting to see that the air masses

not only follow a region of cold anomaly but the coldest region.

We would like to point out the fact that the cold anomaly seems to move ahead of the air masses. This can be related to the definition of CAOs that was taken. In fact, a CAO is defined by the point in time when the CAOI is at its highest point within the violet box. This means that cold air has already been advected before, explaining why the negative $\theta_{anomaly}$ is slightly ahead of CAO air masses we are following.

This figure not only shows us that a large part of the Arctic region is colder than average but more importantly that CAO air masses have an even stronger negative $\theta_{anomaly}$. This first example leads us to think that the CAO air masses are not only cold for lower latitudes but already cold for Arctic conditions. These cold air masses are cooled diabaticaly through LWR radiation in very dry regions. Their cold temperature also leads to a reduced outgoing radiation.

In the next section we would like to assess if a dynamic link to this cold anomaly is visible.

4.2.3 Dynamical link to thermodynamic evolution

To identify any link with the dynamic situation we will proceed by analysing first the surface layer then the middle troposphere and end by looking at the dynamical tropopause.
We will use as in section 4.2.1 the SLP fields but this time together with the $\theta_{anomaly}$ field.

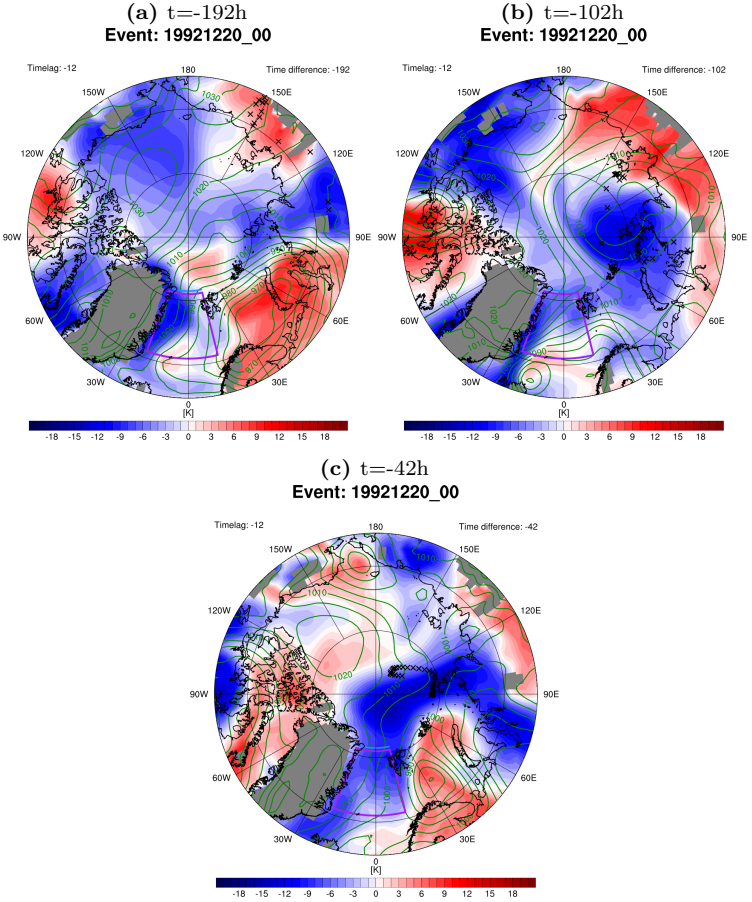

Figure 4.21: $\theta_{anomaly}$ as colour-shading and SLP as green at (a) -192h, (b) -102h and (c) -42h. Black crosses represent the position of air masses at specific timesteps.

The Figure 4.21 shows at first a surface cyclone over a large positive $\theta_{anomaly}$ at -192h. This same surface cyclones then moves over a cold $\theta_{anomaly}$ at -102h. We recognize this cyclone as the cyclone seen in Figure 4.11 which is responsible for the vortex feature and the gathering of the air masses. In the end, the cyclone disappears at low levels as already shown in section 4.2.1 and we see a strong pressure gradient forming between Greenland and Svalbard at -42h. This pressure gradient is steering the CAO air masses and the anomalously cold air towards Fram Strait.

This confirms the role of the surface layer of steering the flow in the later stages to advect the air towards Fram Strait.

If we look at the Z500 pressure fields we see a different pattern appear. In fact, in Figure 4.22 we can identify that all "pools" of negative $\theta_{anomaly}$ are directly linked to a low pressure system at 500hPa.

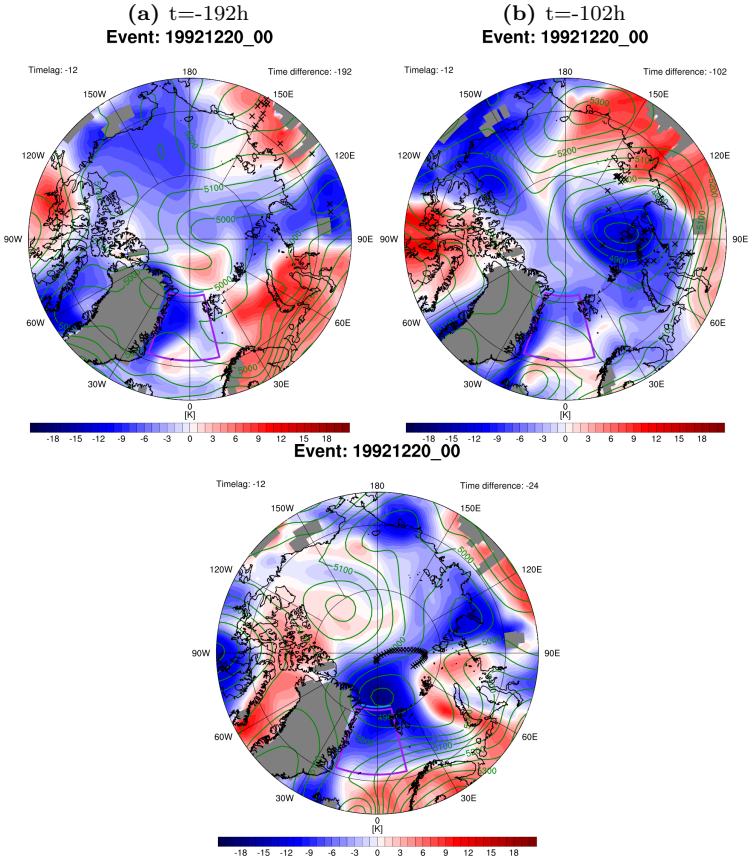

Figure 4.22: $\theta_{anomaly}$ as colour-shading and Z500 as green lines at (a) -192h, (b) -102h and (c) -24h. Black crosses represent the position of air masses at specific time-steps.

This is especially clear when looking at -102h where the large depression is located at the exact horizontal location of the largest negative $\theta_{anomaly}$.

This implies that the cyclone responsible for the convergence of CAO air masses is also responsible for gathering cold air in general. If we continue to follow the evolution we see that the split of this cyclone into two smaller cyclones identified in figure 4.14 also leads to the split of this cold "pool" into two cold "pools" with both a cyclone located just above.

The analysis of the Z500 pressure fields shows a distinct link between between low pressure system in the mid troposphere and cold anomalies. These cyclones are creating "pools" of negative $\theta_{anomaly}$ that can be brought to Fram Strait and create a CAO.

To further extend our analysis, we will take a look at the upper troposphere and more precisely at the tropopause (dynamical tropopause defined by the 2PVU boundary). The aim is to identify any specific features of the upper level flow and find some links to the low level flow together with the CAO air masses. To have the best overview of both dynamical and thermodynamical parameters, we decided to plot the pressure at tropopause level and the temperature at the same level. This representation allows to identify potential vorticity (PV) anomalies and their effect on the isentropes e.g. lifting of isentropes under positive PV anomaly. A positive PV anomaly will be determined by a lowered tropopause and therefore a higher pressure at tropopause level (cf. section 2.2.4).

In the following figure, the colour-shading represents the pressure at tropopause level and the contours the potential temperature at tropopause level.

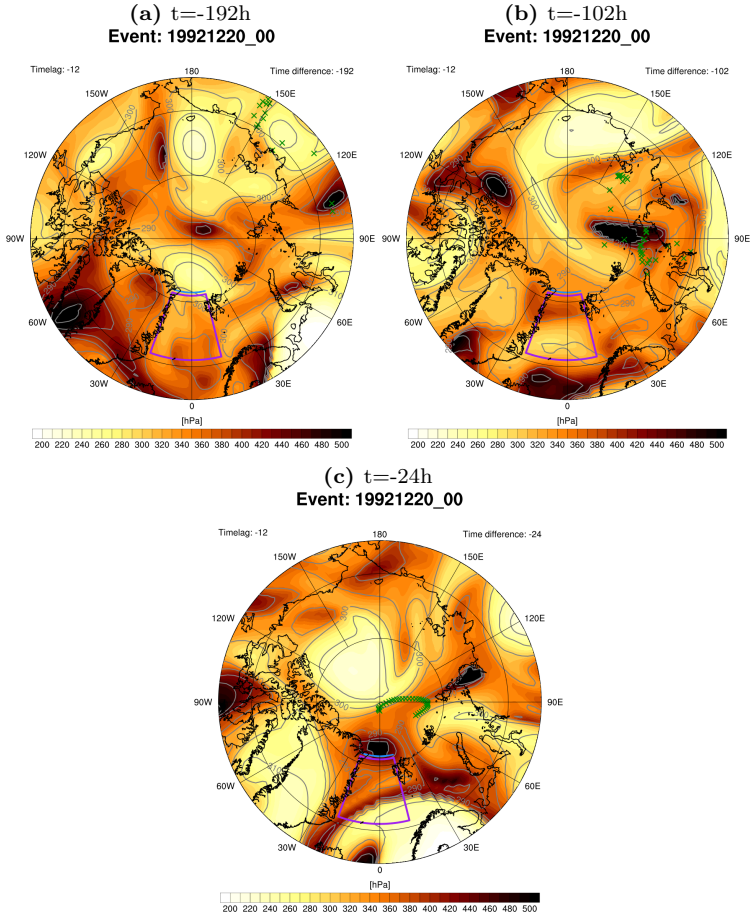

Figure 4.23: Pressure as colour shading and potential temperature as grey lines at tropopause level at (a) -192h, (b) -102h and (c) -24h. Green crosses representing the position at a specific time-step.

These last three panels in Figure 4.23 show how the previously identified cold "pools" are linked to an especially low tropopause and lifted isentropes. At -102h the large cyclone has a clear imprint of a lowered tropopause together with the lifted isentropes. At -24h we also see the same feature that corresponds to the mid-tropospheric cyclones seen in Figure 4.22. The lifting of the isentropes shows regions of negative anomaly in potential temperature below the positive PV anomaly. Those regions are also the locations of the

CAO air masses showing that they are most of the time within regions of negative anomaly in potential temperature.

The dynamical link to the $\theta_{anomaly}$ is defined through this analysis. The lower layers are mostly steering the flow with the CAO air masses in later stages of the evolution. The upper layer on the other hand is directly linked to the thermodynamic evolution with a strong positive PV anomaly resulting into a negative potential temperature anomaly underneath. This anomaly extends into the mid-troposphere into a mid-tropospheric cyclone which is linked to "pools" of cold air.

4.2.4 Small summary

Here we shortly summarize this first case study which is supposed to represent 70% of our sampled cases.

The CAO formation is characterised by a convergence of air masses into a large cyclone. This cyclone is present throughout the troposphere at first but loses strength at the surface until it is only present at 500hPa. It moves towards Fram Strait together with the air parcels. These air parcels are advected by the combined work of an anti-cyclone over Greenland and two cyclones over the coast of Norway. A clear and continuous decrease of potential temperature leads to the conclusion that the cooling is mostly diabatic. This cooling is probably due to the continuous LWR happening during the Arctic winter. CAO air masses have a distinct imprint of reduced LWR due to lower temperature and are dryer than the surrounding atmosphere.

Furthermore we see the influence of a strong positive PV anomaly creating a negative θ anomaly beneath, extending into the mid-troposphere, coupled to regions of negative $\theta_{anomaly}$.

4.3 Atypical case-No vortex: 20 January 2001 at 12:00 UTC

The same way we started the previous case, we will take a first look at the overall trajectories.

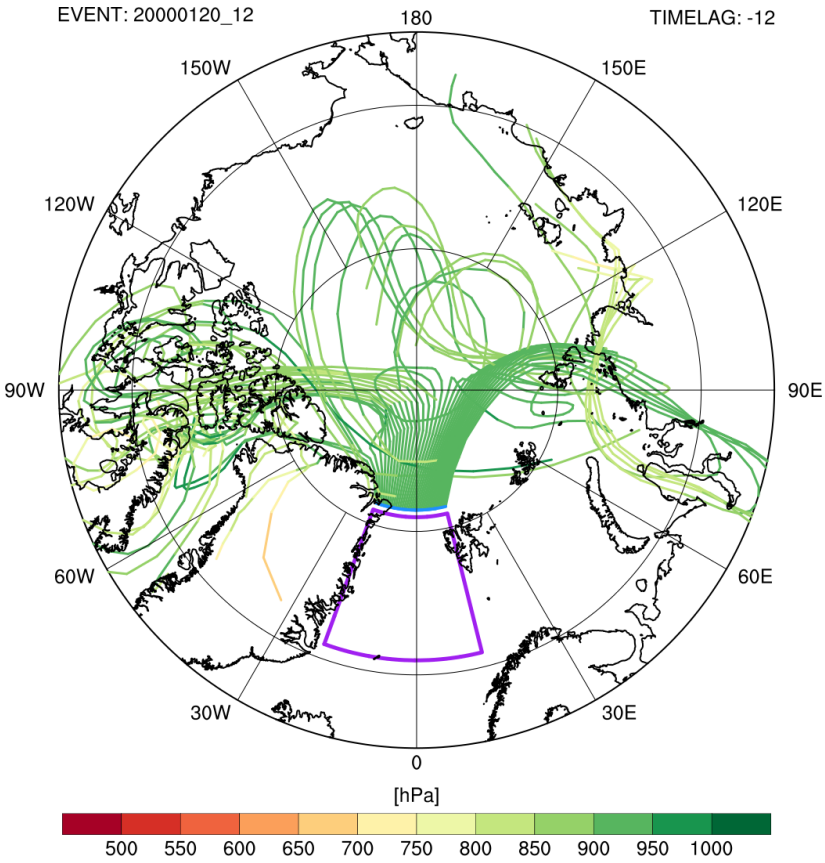

Figure 4.24: Trajectories of the 20000120_12 CAO with pressure as colour-shading.

In this case we have all air masses coming mostly from the interior Arctic with some originating from the Greenland Ice-Sheet. The air masses later on split going either towards Siberia or Canada. The air masses over Canada follow a rather complicated path but mostly over the same region while the others travel across the Arctic and parts of Siberia without staying within a specific region for a long time.

4.3.1 Synoptic situation

At a very early stage, the air masses are split by a large high pressure system located north coast of Siberia.

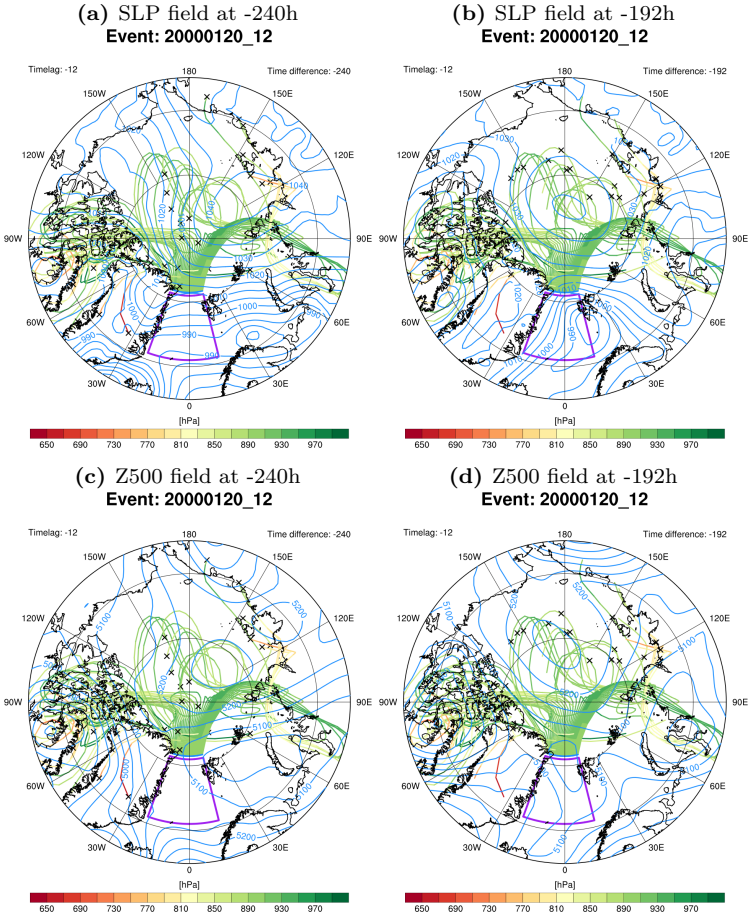

Figure 4.25: SLP field at (a) -240h and (b) -192h, and Z500 field (c) at -240h and (d) -192h. Black crosses representing the position at a specific timestep.

The Figure 4.25 shows the motion of the anti-cyclone from the north coast Siberia over the Arctic which is splitting the air masses. This anti-cyclone is visible distinctly at both levels. From now on, we can follow the evolution of these air masses in two separate blocks: Canadian and Siberian air masses.

First, the Siberian air masses are moving towards Siberian by the combined work of the previous anti-cyclone and a cyclone over north Siberia.

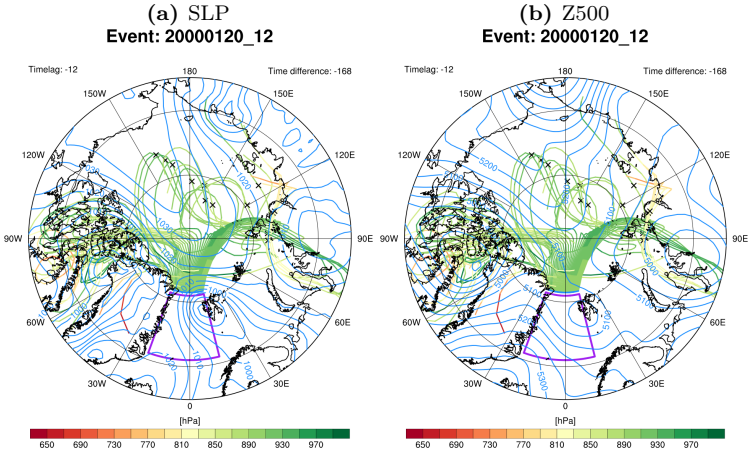

Figure 4.26: Motion towards Siberia showed at -168h (a) SLP field and (b) Z500.

In Figure 4.26, both fields show a pressure gradient between a high pressure system over the Bering Strait and a low pressure system over Siberia leading air masses towards the coast of Siberia.

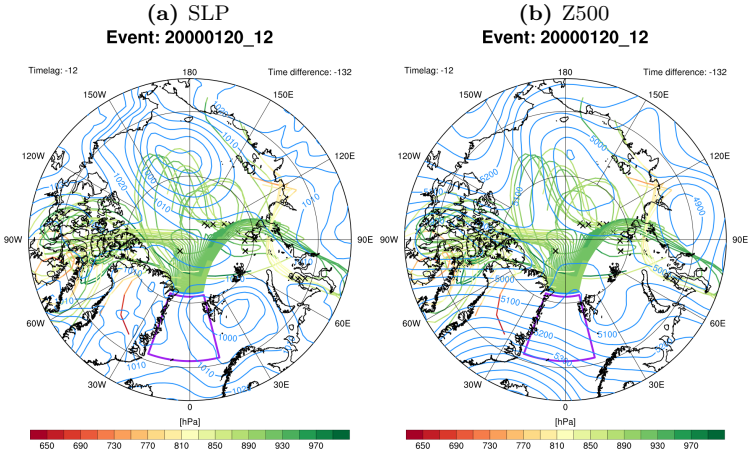

Figure 4.27: Mid-tropospheric cyclone over Canada seen at -132h on (a) SLP and (b) Z500 field.

This pressure gradient is better seen with the SLP field, confirming the role of the surface flow in steering the flow. Z500 only displays that the cyclone stretches from the surface to at least the mid Troposphere.

In the mean time, the Canadian air masses have been transported over Canada where a cyclone is stationary over the Canadian Arctic Archipelago. They stay there and rotate around this cyclone until -72h. This cyclone is particularly visible at Z500 and is behaving in a similar manner as the barotropic cyclone in the previous case which was responsible for the vortex feature.

In fact, the Canadian air masses follow a similar evolution as the case from 19921220_00 as they are gathered in a barotropic and stationary cyclone that slowly disappears in SLP level but is still visible in Z500. In figure 4.27 we can still see at -132h the cyclone at Z500 but not at SLP level any more.

In the following time, both blocks of air masses converge towards the North Pole where they will meet.

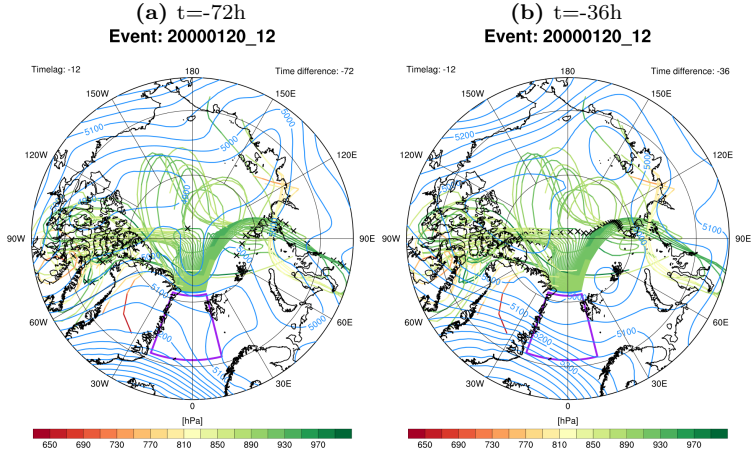

Figure 4.28: SLP fields showing the northward motion and a pressure gradient over Fram Strait at (a) -72h and (b) -36h.

The Figure 4.28 depicts how a cyclone over Scandinavia is moving Siberian air masses northward and a cyclone near the coast of Canada is pushing the Canadian air masses to the North Pole. At -36h, they meet over the North Pole while we recognize a familiar feature going through Fram Strait: a strong pressure gradient.

As in the previous case, this pressure gradient is due to a cyclone east of Svalbard and an anti-cyclone over Greenland. This demonstrates that even with a very different initial setting and a strong difference in the evolution

of the air masses the later stages of the evolution that lead to the CAO are almost identical to the previous very typical case.

4.3.2 Temperature evolution and temperature anomaly

We will now look at the thermodynamic evolution of this event as in the previous case.

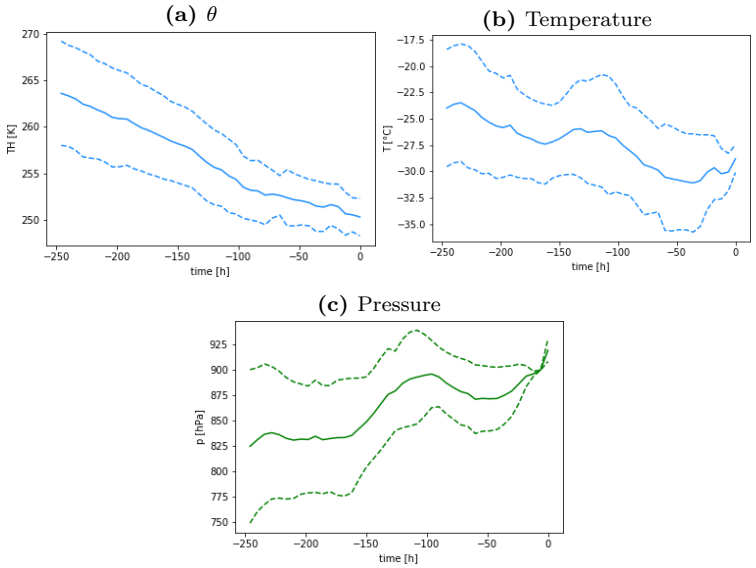

Figure 4.29: Evolution of (a) mean temperature, (b) pressure and (c) θ as continuous line with standard deviation as dotted lines.

The same way than for the previous case, we observe a clear and continuous decrease in θ without any jumps while the temperature decreases following variations in pressure. Both temperature and θ decrease, proving again that despite the warming through compression, the diabatic cooling is stronger. Interestingly, as both blocks of air masses merge, we still see a difference in θ until Fram Strait.

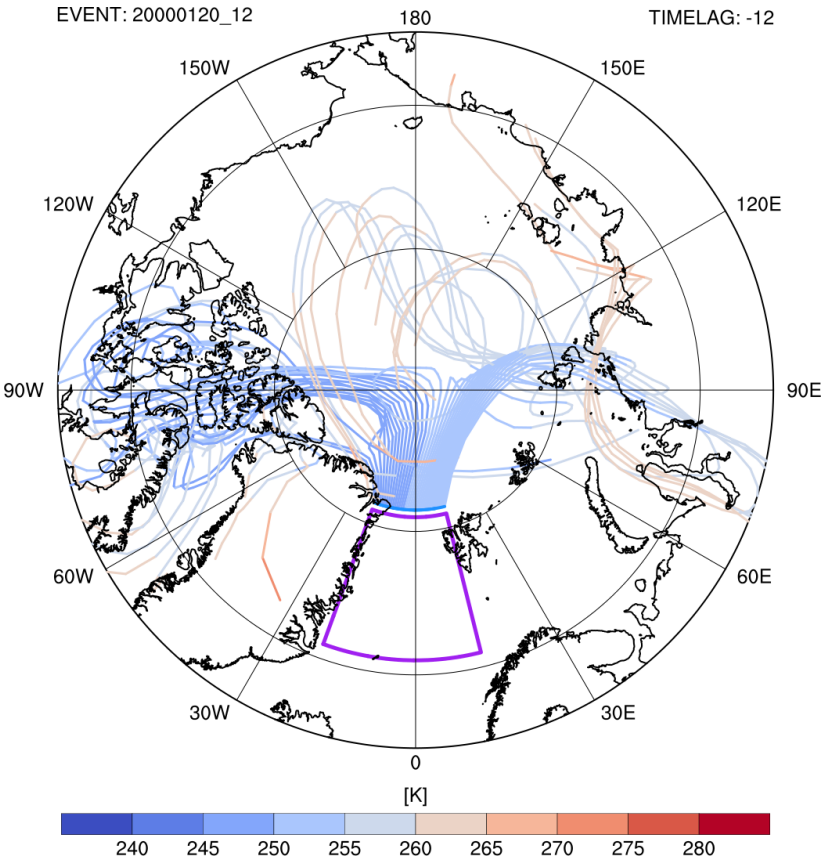

Figure 4.30: Trajectories of the 20000120_12 CAO with θ as colour-shading.

As the thermodynamic evolution is similar, LWR is expected to follow the same evolution than the typical case.

(a) LWR-TOA distribution at -90h.

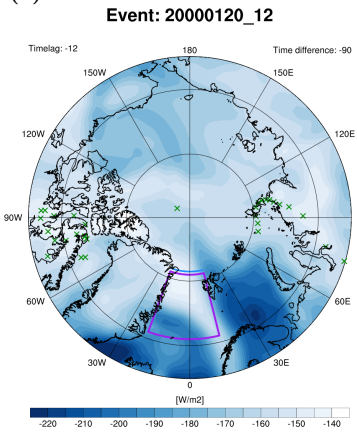

(b) LWR-TOA distribution at 0h.

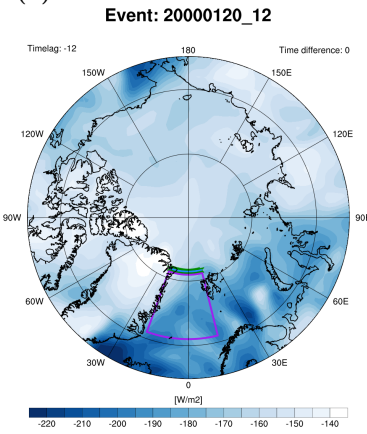

(c) Mean LWR-TOA and standard deviation.

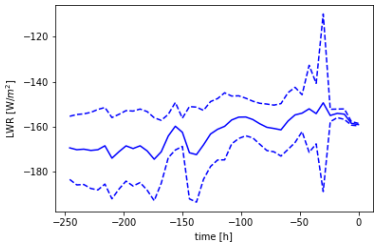

Figure 4.31: LWR-TOA distribution at (a) -90h and (b) 0h, and (c) mean LWR-TOA along trajectories.

In Figure 4.31 we can see that both blocks of CAO air masses are situated in regions of low outgoing radiation at -90h and also at 0h near Fram Strait. The CAO air masses still have this imprint of low outgoing radiation.

Looking at the mean LWR-TOA along the trajectories we observe that it behaves the same way than in the previous case, with similar magnitude and small increase in time.

The evolution of θ and the particular imprint in LWR points again toward particularly cold air even for Arctic conditions.

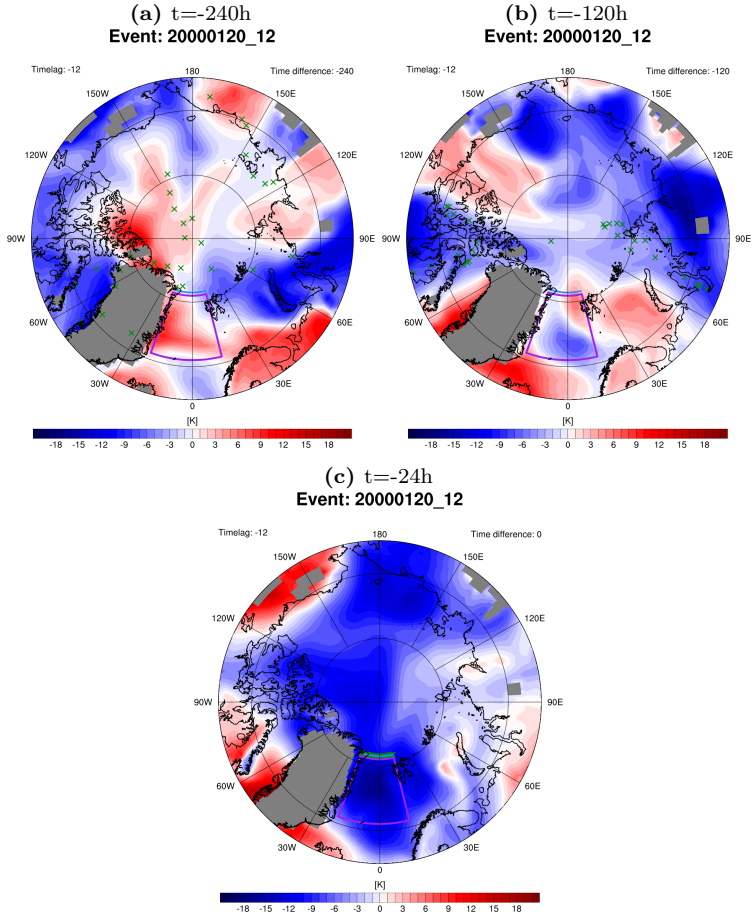

Figure 4.32: $\theta_{anomaly}$ as colour-shading and green crosses as position of air masses at specific time-steps (a) -240h (b) -120h (c) 0h.

Contrary to our first case, the Arctic is quite anomalously warm at first. However, in the following panels in Figure 4.32 we see cold pools developing mostly at the coasts to the Arctic and more specifically in both locations of the CAO air masses. At 0h, almost the entire Arctic is anomalously cold and especially over Fram Strait at the location of the CAO air masses. Also, we see that the air masses over Siberia were in a region of slightly less negative anomaly, maybe explaining the differential in temperature.

In the end, the thermodynamic evolution is very similar to our first case. The CAO air masses experience a distinct diabatic cooling due to outgoing radiation that led to an anomalously cold Arctic. Based, on our first cases we can continue to suggest that the CAO air masses are also cold relative to Arctic conditions. In the following section, we will continue and consider the link between the dynamic situation and the thermodynamic evolution of the air parcels.

4.3.3 Dynamical link to thermodynamic evolution

The dynamical situation at sea level is not very clear in this case. The only pattern we can distinctly identify with certainty is the steering effect in later stages of the surface layer flow.

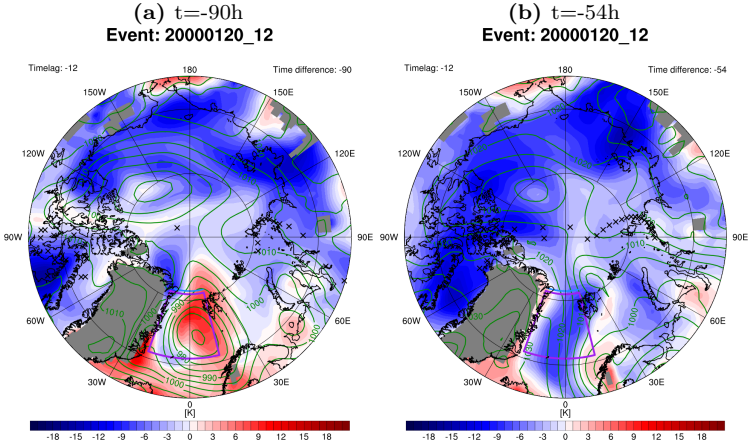

Figure 4.33: $\theta_{anomaly}$ as colour-shading and green lines represent the SLP at (a) -90h and (b) -54h.

Figure 4.33 shows how a cold "pool" in the east of Canada is steered towards the Canadian Arctic Archipelago where it meets another cold "pool" and then are moved northward. Greenland seems to play the role of an orographic barrier, forcing the cold air and the CAO air masses to go around Greenland through the north coast.
On the other hand, the impact of the mid level flow is much more evident. The pattern identified in the previous case in section 4.2.3 is also strongly visible: strong cyclones in the mid-troposphere are located in regions of cold "pools".

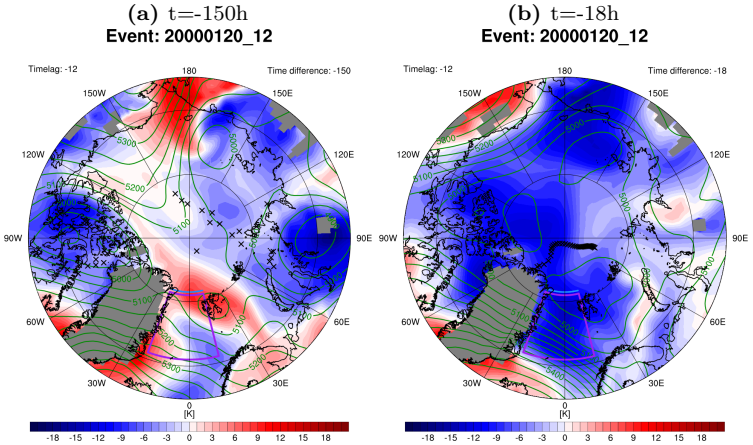

Figure 4.34: $\theta_{anomaly}$ as colour-shading and green lines represent Z500 at (a) -150h and (b) -18h.

We can identify two cyclones situated above regions of strong negative $\theta_{anomaly}$ at -150h in Figure 4.34 where the CAO air masses are located.

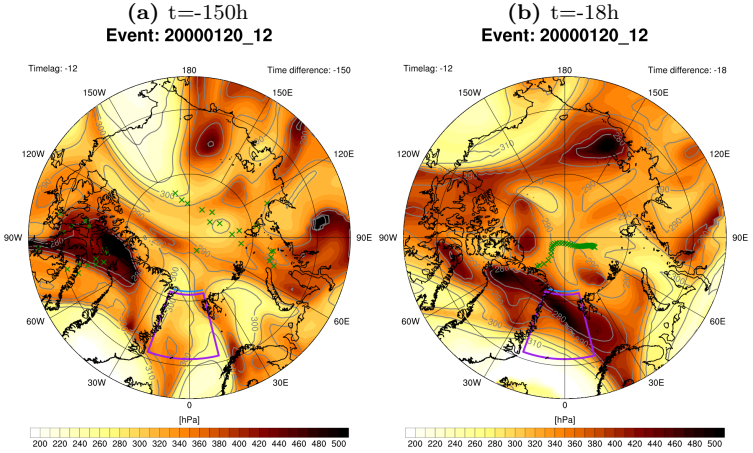

Figure 4.35: Pressure as colour-shading and grey lines represent θ at tropopause level at (a) -150h (b) -18h.

Furthermore, the overall anomalously cold Arctic at -18h is characterised by a cluster of three large cyclones creating a large region of low pressure

over the Arctic. The three centres of lower pressure are precisely localised over regions of stronger negative $\theta_{anomaly}$.
This observation is the same as in the previous case and shows the important role of these mid-tropospheric cyclones as they are dynamically coupled to these regions of cold anomaly.
In Figure 4.35 we are looking at the same time-steps as for Z500 and can see that the location of these cyclones are locations of a lowered tropopause. As in the previous case, the lowered tropopause goes together with lifted isentropes underneath and therefore with a negative θ anomaly.

This exhibits the influence of the high level flow on the mid- and lower Troposphere. These generated cold anomalies impact directly the CAO air masses that are located in these regions.

4.3.4 Small summary

To sum up, despite the different initial dynamic setting and evolution, this case behaves very similarly to our typical case. The air masses undergo a diabatic cooling, probably due to outgoing radiation. Even though the entire air parcels do not gather within a stationary cyclone, they still move over regions of strongly negative $\theta_{anomaly}$ generated by the upper level flow. Further, we see that even with a splitting of the air masses, they end up coming together over the North Pole and being advected through Fram Strait with the combined work of a low pressure system over Svalbard and a high pressure system over Greenland.

4.4 Atypical case-Strong warming event: 12 February 2015 at 18:00 UTC

This case is very interesting, especially regarding the thermodynamic evolution. Indeed, until now the previous cases have shown that CAOs might need an anomalously cold Arctic and especially that the CAO air masses should be anomalously cold. However, this case has been chosen because of the very strong warming that takes place for most air parcels.

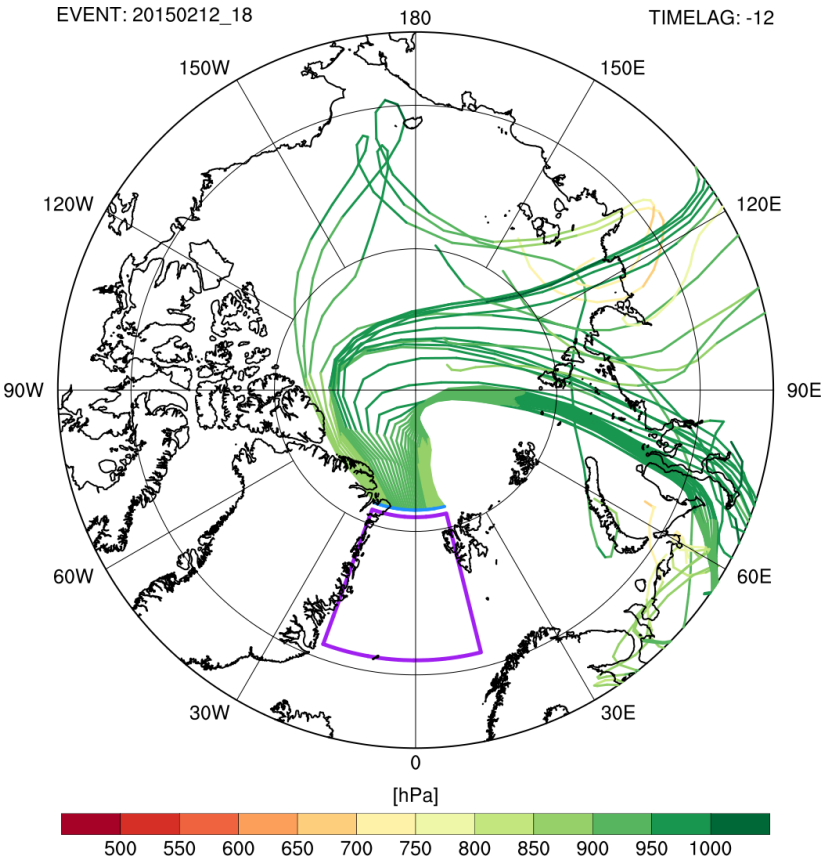

Figure 4.36: Trajectories of the 20150212_18 CAO with pressure as colour-shading.

In Figure 4.36 we observe that the air masses are spread out over a large part of Siberia and a few over the Arctic ocean. As mentioned in section 4.1.6, this case has no visible vortex feature and the trajectories seem mostly, after a certain point, to move towards the North Pole before changing direction towards Fram Strait. The synoptic situation leading to these trajectories will be discussed in the next section.

4.4.1 Synoptic situation

In this case we will be focusing on the synoptic situation starting at t=-120h. The reason being that all CAO air masses are moving in much lower

latitudes until this point and are not visible on our polar view before. The synoptic situation is rather the same for almost the entire 120h (5 days).

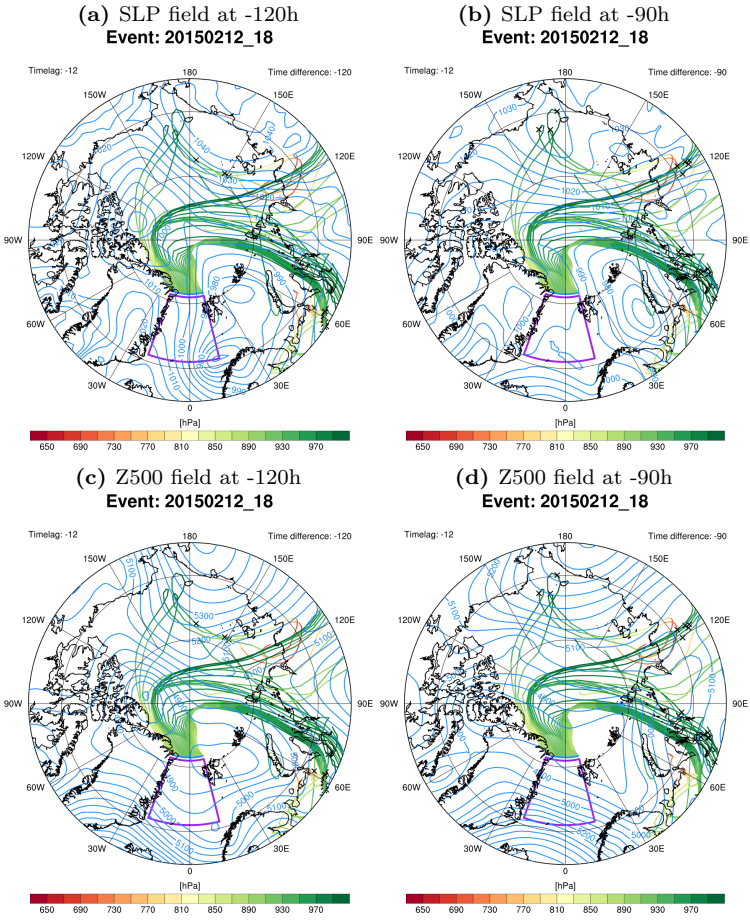

Figure 4.37: Pressure gradient forming towards North Pole on SLP field at (a) -120h and (b) -90h, and on Z500 field at (c) -120h and (d) -90h.

In Figure 4.37 we observe the configuration which will be responsible for the motion of the CAO air masses for most of the time. We see a low pressure system between the north coast of Scandinavia and the Severny Island and a high pressure system over the east of Siberia almost over Bering Strait, forming a pressure gradient going from the coast of Siberia to the North

Pole. This pressure gradient is like a channel for the air masses that move northward. At -90h, a smaller pack of CAO air masses appears in the east of Siberia. This pattern is also visible at 500hPa but the cyclone is more stretched out to the west.

We therefore have two packs of CAO air masses, one west of Siberia and one east which are moving in a similar way towards the North Pole with a slight time difference at first.

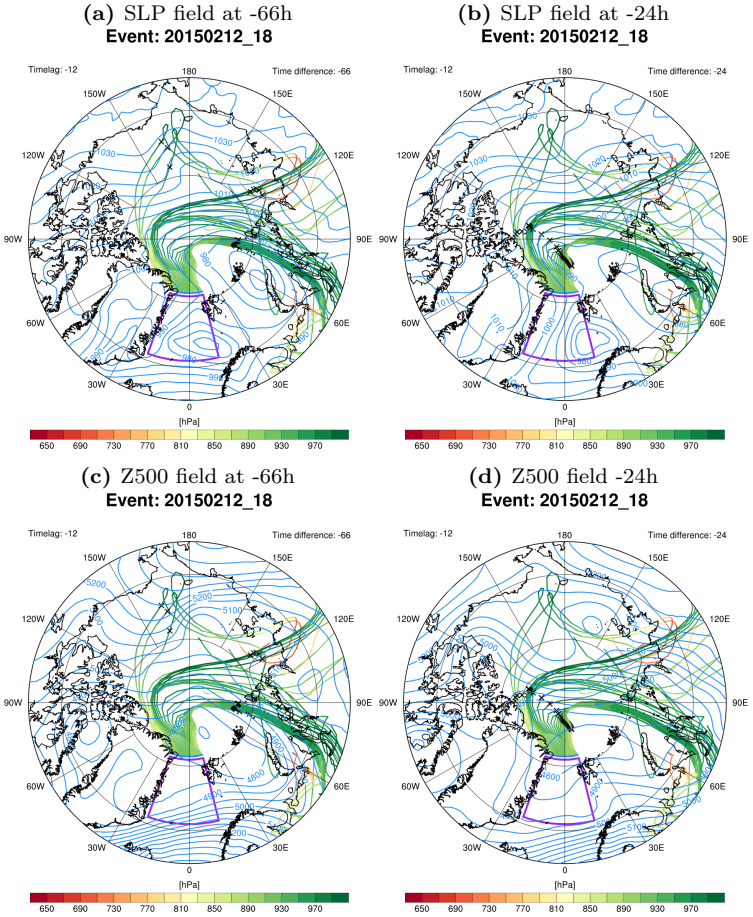

Figure 4.38: Pressure gradient extends to Fram Strait on SLP field at (a) -66h and (b) -24h, and on Z500 field at (c) -66h and (d) -24h.

In Figure 4.38, the configuration is maintained throughout due to the stationary anti-cyclone over Bering Strait and a continuous replacement of the cyclone over north Scandinavia by cyclones coming from Iceland. In the mean time, a high pressure system is located over Greenland, and the continuous arrival of cyclones from Iceland extends the pressure gradient from the North Pole to Fram Strait. Again, the same configuration appears and leads the CAO air masses that meet over the North Pole towards Fram Strait.
Very similar to our previous cases, the pressure gradient controls the motion in the later stages. Contrary to our previous cases, these air masses do not move within a cyclone.

4.4.2 Temperature evolution and anomaly

Onto the thermodynamic evolution of the air masses of this case, we will begin by remembering the Figure 4.4 which represented the evolution of θ along the trajectories. We observe a general warming event for most air masses as the air masses move from Siberia towards the North Pole.

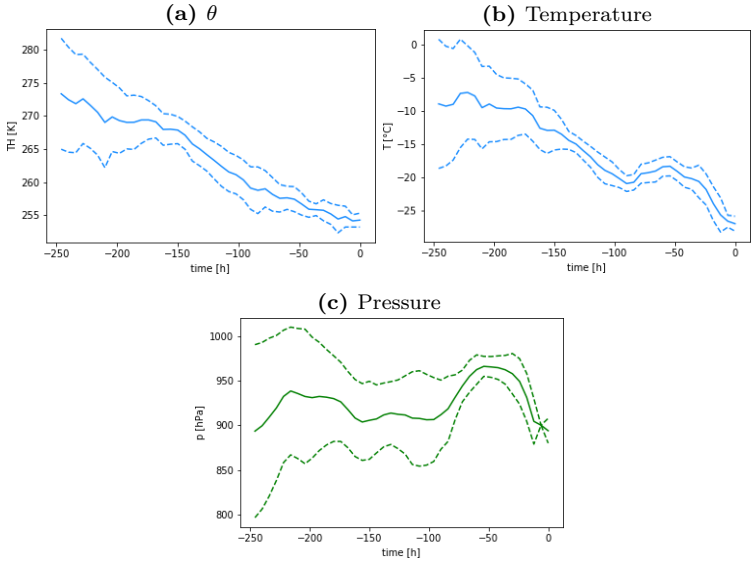

Figure 4.39: Mean (a) pressure, (b) temperature and (c) θ along the trajectories with standard deviation.

Looking at the mean θ and T in Figure 4.39 the increase is not as impressive but still between -90h and -60h the θ decreases less and T increases by

at least 2K. This increase could be due to an ascent of the air parcels in the warm sector of a cyclone which we will investigate when looking at $\theta_{anomaly}$ and the dynamical link.

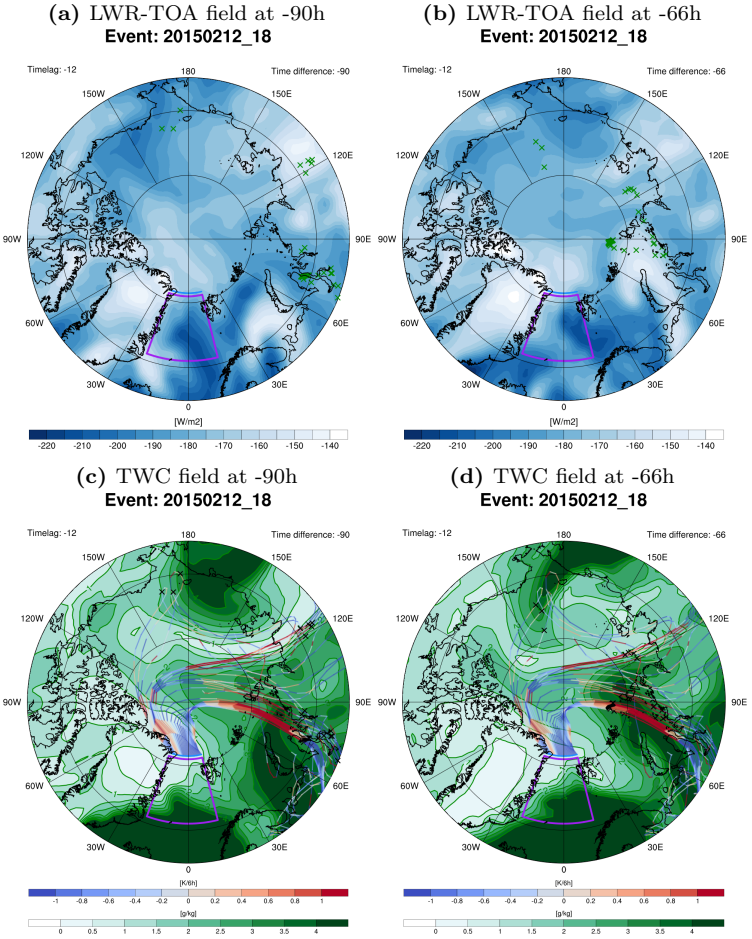

Figure 4.40: LWR-TOA as colour-shading at (a) -90h and (b) -66h, and TWC as colour-shading at (c) -90h and (d) -66h.

Besides this warming event, the evolution of both θ and T is very similar to our previous cases with a decrease of around 13k for θ and 15K for T.

We will now take a look at both LWR-TOA and also the total water content starting at -90h. We have also plotted the change in θ between each time-steps on the TWC plots.

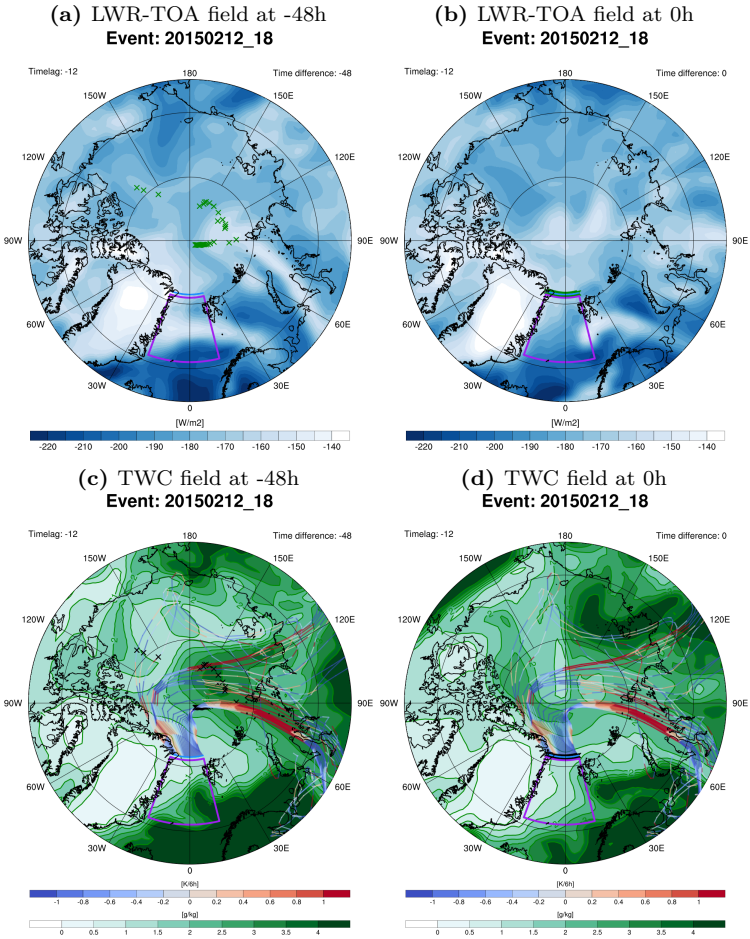

Figure 4.41: LWR-TOA as colour-shading at (a) -48h and (b) 0h, and TWC as colour-shading at (c) -48h and (d) 0h.

Contrary to the previous cases, the LWR-TOA is quite high at -90h around the CAO air masses until -72h when a region of less outgoing radiation moves over the CAO air masses. This coincides with a region of a higher TWC as seen in Figure 4.40.

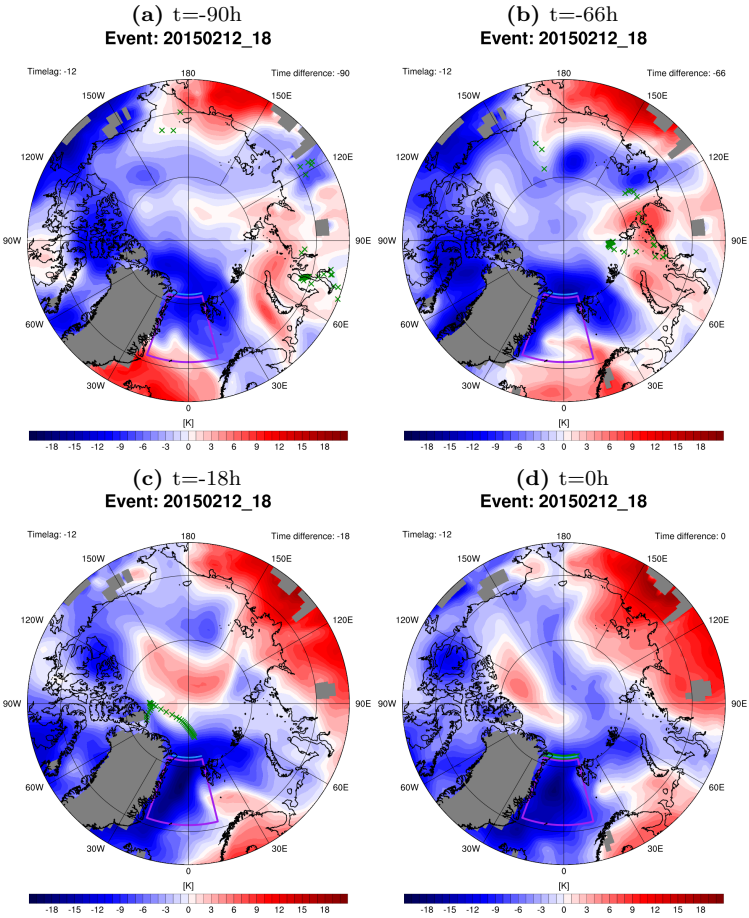

Figure 4.42: $\theta_{anomaly}$ as colour-shading at (a) -90h, (b) -66h, (c) -18h and (d) 0h.

In this case, the reduction of outgoing radiation is not due to a decrease of temperature but to the absorption of LWR by a higher concentration of water in the atmosphere.

The θ change, shows clearly the strong increase in θ from -90h until -60h.
In Figure 4.41, we observe how the region of low outgoing radiation moves over the Arctic which still corresponds to a region of higher TWC. At 0h, the CAO air masses reach another region of low outgoing radiation but this time in a dry region.
This case represents almost the opposite to our previous cases, with a warming in a region covered by a higher TWC which reduces radiative cooling. A similar pattern appears when looking at $\theta_{anomaly}$.

Figure 4.42 shows at the location of the reduced outgoing radiation a strong positive $\theta_{anomaly}$ where the CAO air masses move. After -66h, the CAO air masses move at the edge between positive and negative anomalies which correlates with the onset of a cooling period as can be seen in figure 4.41.
During the 90 hours before, Fram Strait stays in a cold anomaly which grows stronger as the air masses approach. It is possible, that despite the strong warming the CAO air parcels where still colder than the climatology in the region of Fram Strait.

This case shows that a CAO is still possible with a strong warming but the air parcels should still be cold relative to conditions near Fram Strait. The determining part seems to be the late cooling event that compensates the warming period

It is interesting to notice that, this event has the smallest CAOI from our three cases. This could tell us that $\theta_{anomaly}$ is perhaps not the most determining property for a CAO to occur but might have a role in determining the strength of the CAO.

4.4.3 Dynamical link to thermodynamic evolution

The dynamical link to the thermodynamic evolution is very straightforward regarding both sea level and the mid-troposphere.

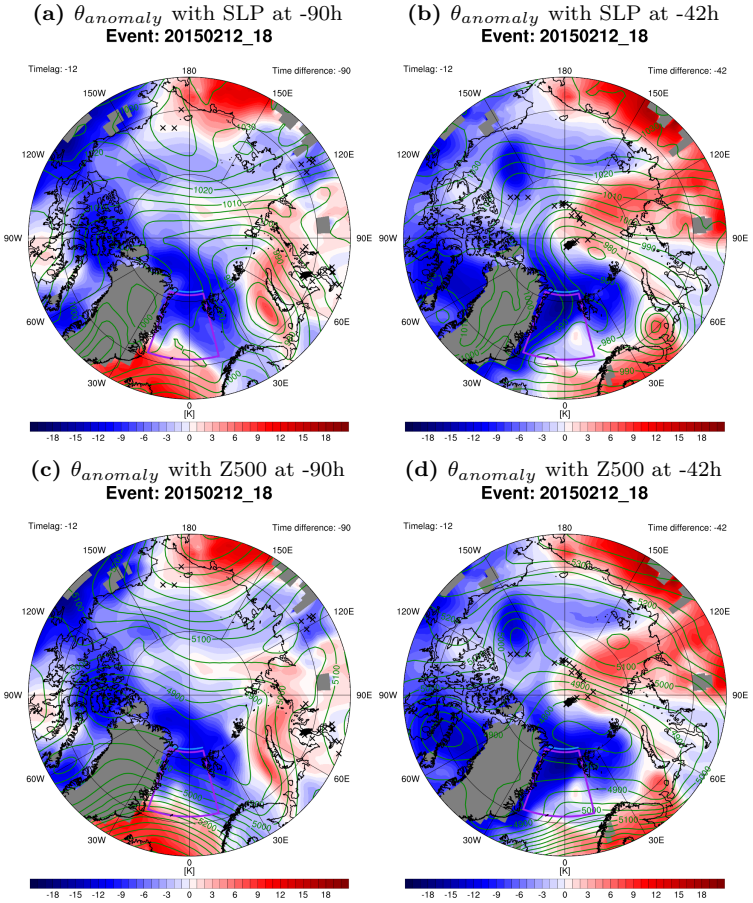

Figure 4.43: $\theta_{anomaly}$ as colour-shading and SLP as green line at (a) -90h and (b) -42h, and with Z500 (c) -90h and (d) -48h.

In Figure 4.43 we see on the SLP fields a cyclone over north Scandinavia bringing warm air from Europe while at 500hPa a stationary cyclone is located above a pool of cold air. Both cyclones are respectively linked to the warming and the negative $\theta_{anomaly}$ over Fram Strait.

At higher level, we see an interesting pattern emerge from the combination of warm anomaly and cold anomaly.

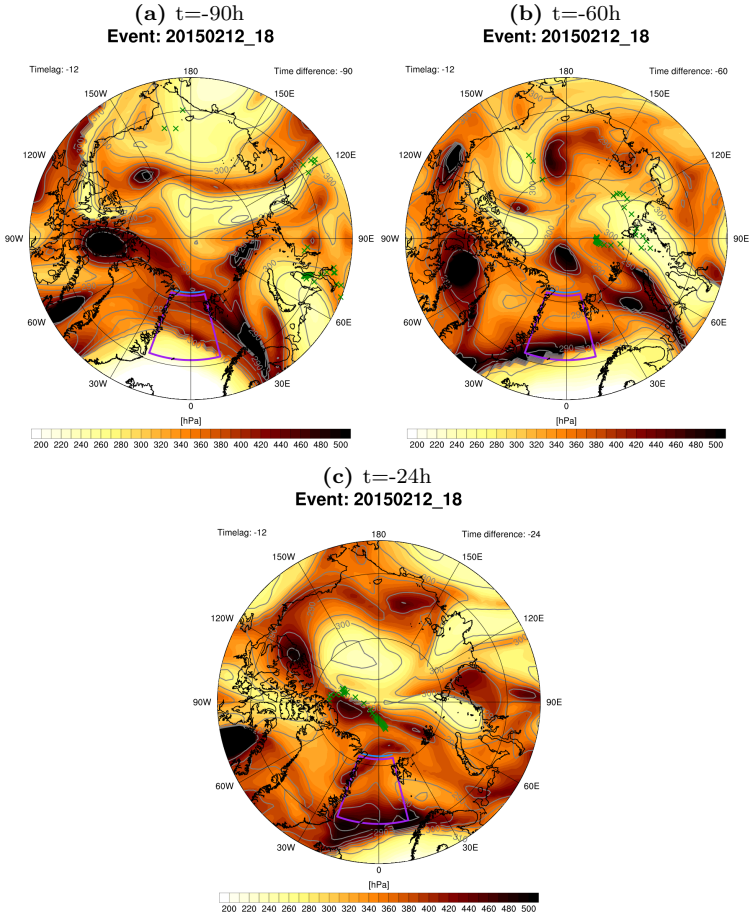

Figure 4.44: Pressure as colour-shading and isoterms as grey lines at tropopause level at (a) -90h, (b) -60h and (c) -24h.

Figure 4.44 underlines how the CAO air masses first follow a region of negative PV anomaly from -90h to -60h with a higher Tropopause and lowered isentropes and then switch to a region of positive PV anomaly. The CAO air masses, reach in the later stages a region of negative θ anomaly where they experienced a short cooling before reaching Fram Strait.
This still confirms the findings of the previous cases, but this time the cooling within a cold "pool" generated by an upper-level disturbance comes later after a warming period.

4.4.4 Small summary

This case showed an interesting thermodynamic behaviour due to a strong warming event. This warming period delayed the cooling to the last 60h before the event leading to a weaker negative $\theta_{anomaly}$ in the end.
This underlines the importance of the localised $\theta_{anomaly}$ around the CAO air masses and not for the entire Arctic but also that intermediate warming events can still lead to CAO events. The very last stages become even more important to ensure that the cooling is sufficient.

4.5 Conclusion

The three cases are at first sight very different but from the analysis we can take three main common features that are determining for the formation of CAOs. First of all, the Arctic is generally anomalously cold prior to the event and especially at the location of the CAO air parcels. At the very least only the region around the CAO air masses have a negative $\theta_{anomaly}$. The cold anomaly has an imprint of lower outgoing radiation and lower TWC due to the dryness. These cold $\theta_{anomaly}$ are formed in stationary and barotropic cyclones that are coupled to cold "pools" within their circulation. These cyclones originate from an upper level disturbance visible at tropopause level which are linked to negative θ anomaly. The last point concerns the advection of the CAO air masses towards lower latitude. The transport is carried out by the combined work of a high pressure system over Greenland and a low pressure system east of Svalbard creating a pressure gradient at sea level with a southward flow direction.

In the three case studies we have studied in the previous sections, we identified very specific cyclones. These cyclones are characterised by being barotropic and having a closed circulations. They are also upper-level disturbances that are coupled to negative θ anomalies within their circulation.
In Cavallo and Hakim [2010], very similar structures are defined as tropopause polar vortices (TPVs). TPVs are characterised by a frequent appearance within the polar vortex away from the jet with a cold core and closed material contours. In addition they are upper-level disturbances and generate negative θ anomalies in the troposphere through strong radiative cooling, especially within their centre.

Based on this description it is quite judicious to think that these TPVs could be our stationary and barotropic cyclones, and explaining therefore the formation of cold "pools" at their location. Unfortunately, we have not researched sufficiently in this direction to be categoric. We will only be able to say that these features could be a key to understanding the formation of strong negative $\theta_{anomaly}$ and the evolution of CAOs and need further re-

search.

The objective is now to verify if the previous findings are applicable on a climatological scale. The following analysis will focus on identifying a correlation between all the CAO events of the ERA-interim period, negative $\theta_{anomaly}$ and a pressure gradient.

5

Climatological correlation

This section is dedicated to verify the importance of key driving processes. In the following, we discuss the pressure patterns that lead to the advection of cold air masses to lower latitudes and the temperature patterns responsible for those cold air masses.

We will progressively increase the period of study from our three cases as a basis to the entire ERA-interim period.

5.1 Pressure patterns

The existence of a pressure gradient appeared first to us as being an essential driving process. Without the southward flow created by a cyclone east of Svalbard and an anti-cyclone over Greenland, the cold air masses could not possibly be advected from the sea-ice onto the ocean. We will continue to investigate this by looking at the pressure gradient between two defined regions at different time steps.

We defined two boxes at the same latitude, west and east from Fram Strait, where we averaged the SLP (see Figure 5.1).

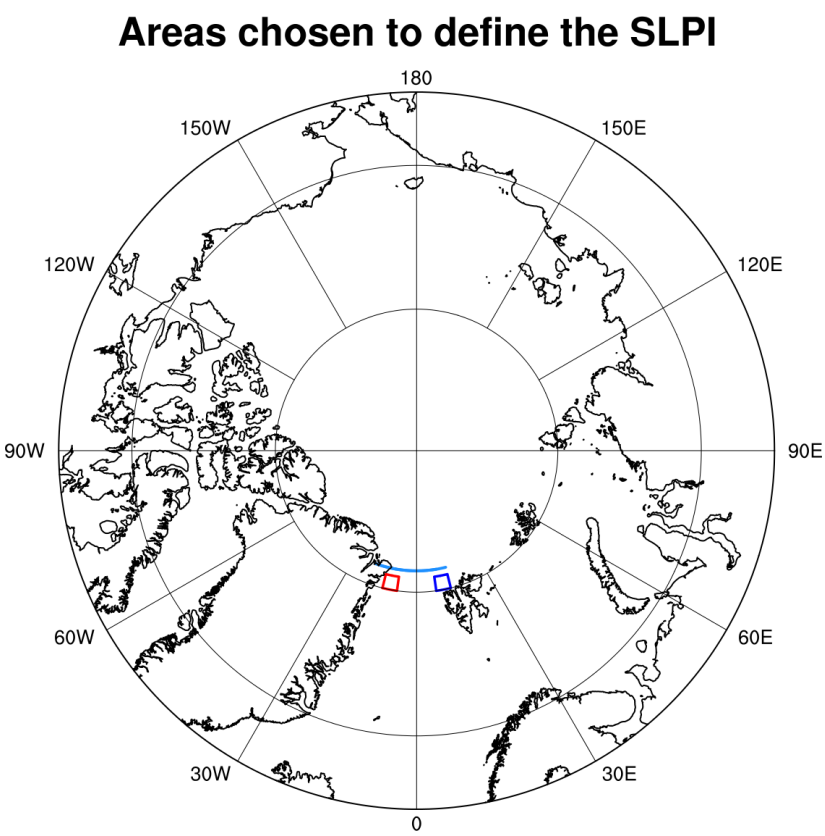

Figure 5.1: Representation of the chosen regions for the calculation of the SLP difference.

We decided to keep the boxes at quite a high latitude to avoid capturing some pressure gradients created by cyclones and anti-cyclones situated too far south that would not impact the flow over the Arctic. Also, as the pressure gradient we observed was at sea level, we avoided any continental regions.

5.1.1 Pressure difference

Using the previously defined regions, we defined the SLP over the two regions:

— P_{Gl}: Average SLP over the blue box near Greenland (hPa)

— P_{Sv}: Average SLP over the red box near Svalbar (hPa)

We then used both pressures, and plotted the P_{Gl} against the P_{Sv} for our top 20 strongest cases at t=-12h and then every 24h until 4 days prior to the CAO.

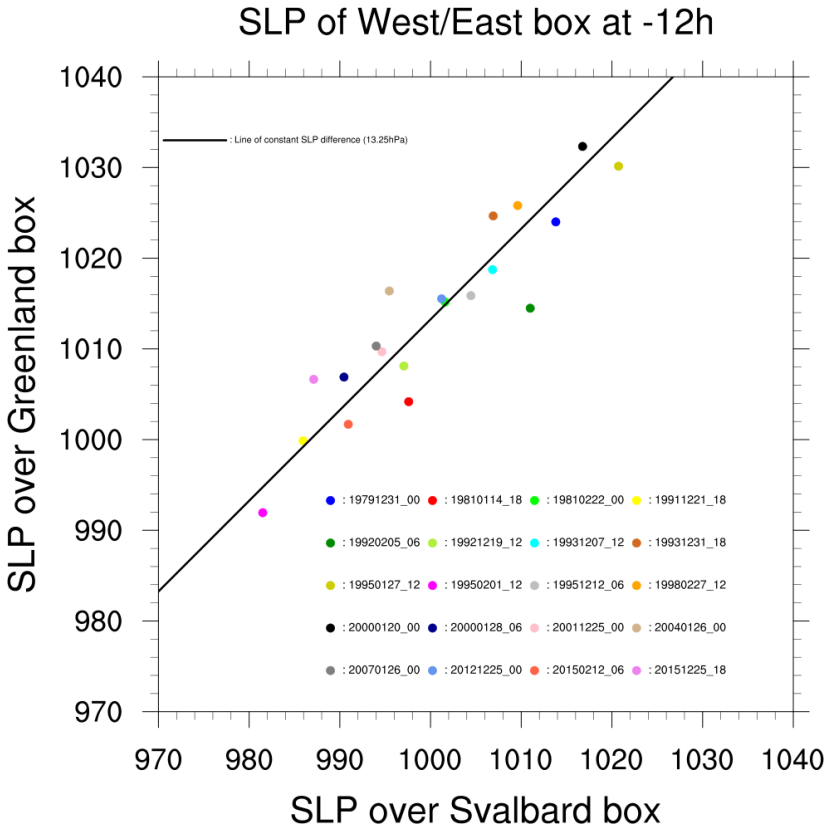

Figure 5.2: Scatter plot of P_{Gl} against P_{Sv} for our top 20 strongest cases at -12h with colors corresponding to each event. The black line represents the mean SLP difference of the 20 cases.

Figure 5.2 shows something very interesting. All 20 points of different cases are located near a straight line representing a SLP difference of 13.25hPa. The mean SLP difference for the region is of 2.6hPa, therefore this pressure difference is high. This shows that all CAOs of this sample have occurred with similar condition of pressure difference.

The positive pressure difference is representative of the configuration seen in section 4. The pressure is always higher over Greenland than Svalbard but in our sample, the absolute SLP over each region can vary from over 1030hPa to near 992hPa for Greenland and from 1022hPa to 982hPa for Svalbard. This would imply that the condition for the occurrence of a CAO is a strong pressure gradient of 13.25hPa but this condition can be achieved with either a strong anti-cyclone and weak cyclone or a weak anti-cyclone with a strong cyclone.
The days before the outbreak of the CAO airmass over the ocean show also all cases with a similar pressure difference.

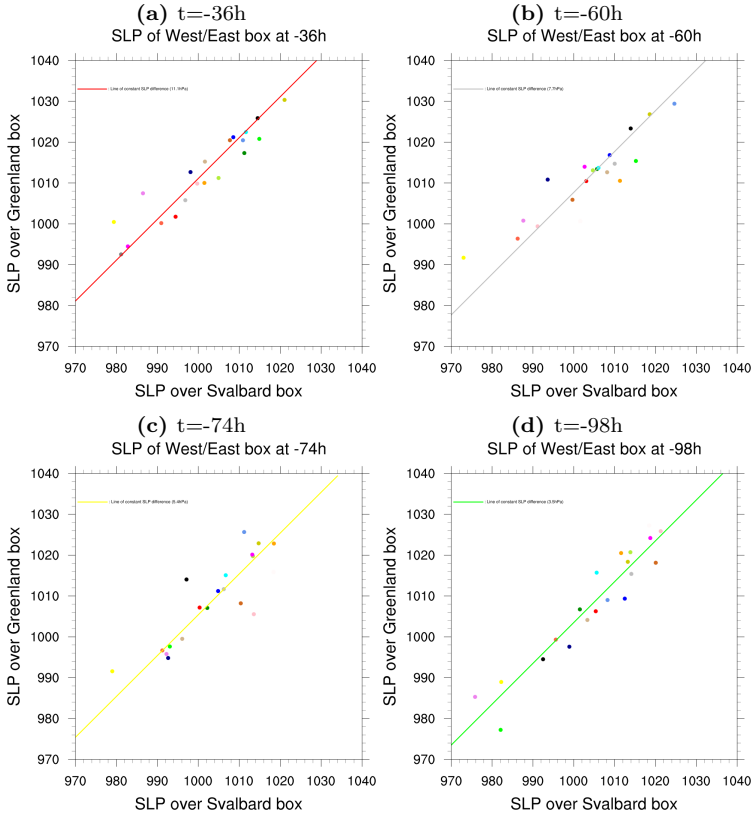

Figure 5.3: Plot of P_{Gl} against P_{Sv} from (a)1 day before, to (b) two days, (c) three days and (d) 4 days before the CAO. The colors are based on the label of Figure 5.2. The lines show the mean SLP difference of all cases.

Going back in time, the mean SLP difference between both regions decreases from 13.25hPa at 12h before to only 3.5hPa at -98h. Figure 5.3 reveals that we have a gradual increase in pressure difference from 4 days before to the date of the event, very similar between cases.

Looking at the different panels, we also realise that the line of constant pressure difference that we drew moves to the left (smaller SLP over Svalbard) with time suggesting that the anti-cyclone over Greenland is more of a stationary feature in time and that the arrival of the cyclone in the vicinity of Svalbard is increasing the pressure difference until it is strong enough to lead to a CAO.

In summary, the pressure difference leading to a CAO is very similar between CAOs and increases in a very similar manner for different cases from day 4 onwards. This pressure difference is mostly created by a stationary high pressure system over Greenland and a low pressure system east of Svalbard.

In the next section we will continue our investigation for the entire ERA-interim period.

5.1.2 Greenland-Svalbard SLP index (GSI)

To further investigate this on a climatological scale, we defined a SLP Index using the average SLP over the region near Greenland and Svalbard.

$$GSI = \frac{\Delta P - \Delta P_{mean}}{\sigma_{\Delta P}} \tag{5.1}$$

GSI: Greenland-Svalbard SLP index
ΔP ($\Delta P = P_{Gr} - P_{Sv}$): SLP difference between Greenland and Svalbard at each time-step (hPa)
ΔP_{mean}: Mean SLP difference between Greenland and Svalbard over entire ERA-interim period (hPa)
$\sigma_{\Delta P}$: Standard deviation of SLP difference between Greenland and Svalbard (hPa)
P_{Sv}: SLP averaged over the Svalbard box for each time-step (hPa)
P_{Gr}: SLP averaged over the Greenland box for each time-step (hPa)

The index defined in equation 5.1 is standardized to allow an accurate and appropriate analysis of the pressure difference over Fram Strait. Based on this definition, a positive GSI is indicative for a positive pressure gradient across Fram Strait: higher pressure over Greenland and lower over Svalbard.

We will first see how this index behaves for our three cases during the 10 days prior to the occurrence of a CAO.

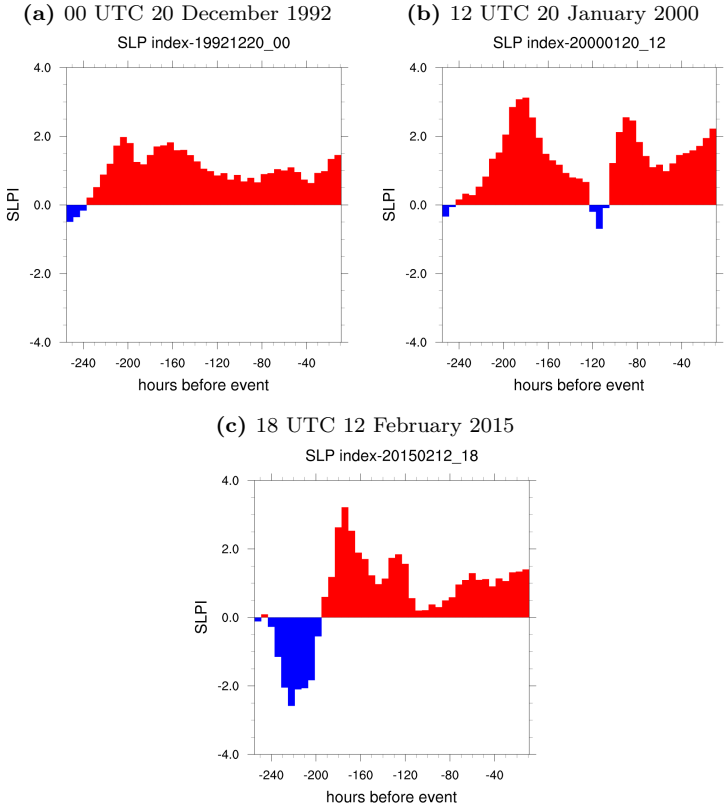

Figure 5.4: GSI for our three cases from 10 days prior until advection over the Ocean.(a) Typical case, (b) atypical case with splitting of CAO air masses and (c) atypical case with warming period. In red values are positive and negative values are blue.

It is striking to see in Figure 5.4 that the index is most of the time positive for the entire 10 day prior to the outbreak of the CAO airmass over the ocean. Although variations can be quite strong during the 10 day period leading to a few maxima, the GSI increases in all three cases from a certain time onwards. This shows how the pressure gradient is being build up few hours before the CAO, similarly to the way we observed it both during the analysis of our cases but also in the previous section. The gradual increase in pressure difference is associated with an increase in GSI.

This pattern becomes even clearer if we plot the GSI for the three winters 1992/1993, 1999/2000 and 2014/2015.

(a) Winter 1992/1993 **(b)** Winter 1999/2000

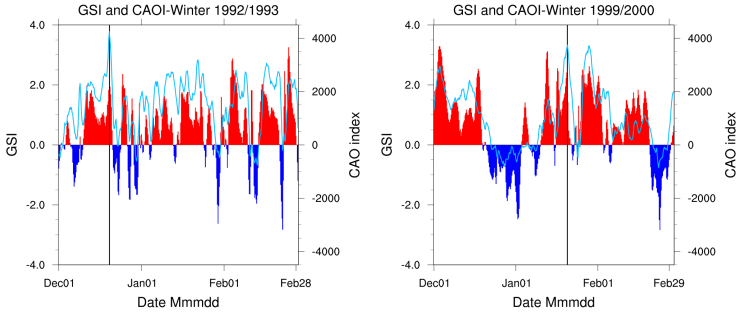

(c) Winter 2014/2015

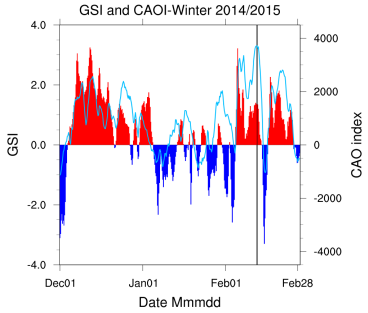

Figure 5.5: GSI for the three winters together with the CAOI as a blue curve. (a) Winter 1992/1993, (b) winter 1999/2000 and (c) winter 2014/2015. The black vertical line is here to locate the exact time of each of the chosen CAOs.

The pattern is even more striking in Figure 5.5 where all maxima of the CAOI, corresponding to a CAO, are correlated to maxima in GSI. We observe most of the time a strong increase in the GSI correlated with an increase in the CAOI. However, the value of the maxima of the GSI do not seem to be correlated with the relative strength of CAOI. Strong CAOs can happen with both weak and strong maxima of GSI.

GSI is at first strongly correlated to the occurrence of a CAO but not with the strength of CAOs. Based on these observations we expect a rather

high correlation between the GSI and the CAOI. We therefore computed the correlation between both indices for the entire ERA-interim period.

Index	Pearson correlation	Spearman Rank correlation
GSI-CAOI	0.582	0.587

Table 5.1: Correlation factors between GSI and CAOI.

We have computed both the Pearson and the Spearman Rank correlation to test for both possible linear and non-linear relations. The Spearman Rank correlation being more robust than the Pearson correlation in the case of not normally distributed data.

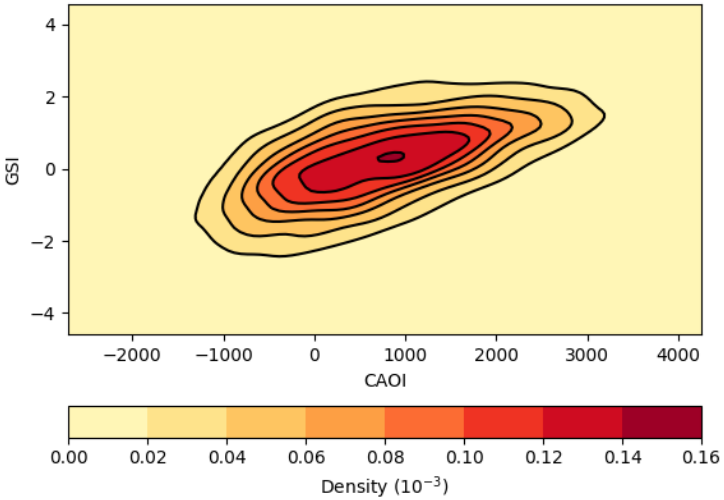

Figure 5.6: Scatter plot: GSI against CAOI with color-shading representing the density of points in an area of specific GSI and CAOI.

The results in Table 5.1 show definitely a strong correlation by both indices. This confirms that the pressure gradient with southward flow is a key component responsible for the formation and occurrence of CAOs even on a climatological scale.

Before we move on, we will take a look at the scatter plots between the GSI and the CAOI. This scatter plot in Figure 5.6 gives us some further informations. Most CAOs have a cumulative CAOI of around 1000 with a GSI near to 1. The highest concentration of CAOs is around the weaker ones. In section 3.1, we determined that the CAOI has a slight decreasing trend. As we confirmed the key role of the GSI in the occurrence of CAOs it is not unlikely that a change in the GSI with time could be partly responsible for this decrease.

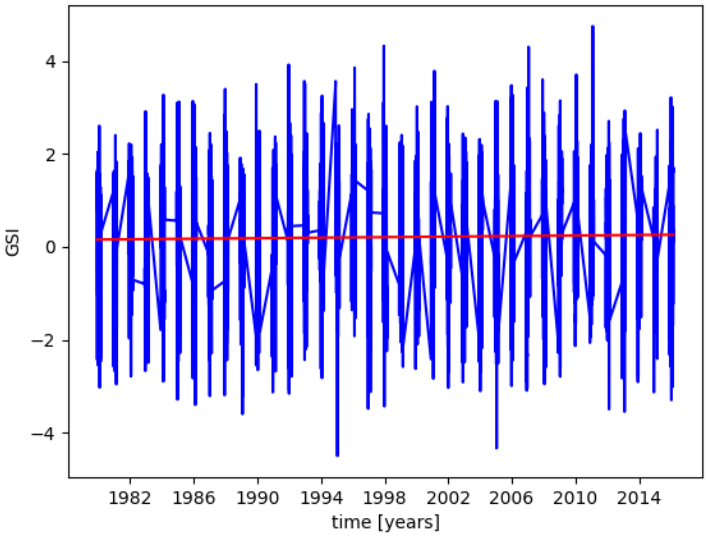

Figure 5.7: Trend of the winter (December/January/February) GSI during the ERA-interim period

Figure 5.7 shows a small trend towards higher values. This is consistent with a northward shift of the storm track diagnosed with climate change [Shaw et al., 2016]. The increase is of about $8{\cdot}10^{-6}$ per time-step which results in a total increase of 0.1 in 37 years.

Besides being a very small trend, an increase would not explain a decrease in the CAOI but rather an increase. Indeed, an increase should lead to more positive values of GSI and therefore more frequent occurrence of higher pressure over Greenland and lower over Svalbard that is linked to CAOs. In short, the trend of the GSI cannot explain a decrease in CAO frequency.

We have now confirmed the key role of the pressure gradient across Fram Strait for the formation of CAOs both looking at case studies and the climatological scale. Continuing with SLP pattern we will shortly look again at the Iceland-Lofoten pressure difference (ILD).

5.1.3 Iceland-Lofoten Pressure difference (ILD)

We saw in section 3.2 how the ILD correlated with the CAOI but without identifying the cause for this correlation. Based on the detailed analysis we have done until now, we should be able to find the explanation for this link. We now follow the same procedure as for the GSI, and look at the ILD and our three case studies. As opposed to the GSI, the ILD (see Figure 5.8) is mostly negative prior to a CAO. A negative ILD being indicative of a cyclonic situation over Scandinavia, this is an expected result. This negative value should correspond to the cyclone that creates the pressure gradient over Fram Strait.

In Figure 5.9 we can see that at the exact time (0h) when the ILD is lowest we have a strong cyclone over the Lofoten region. The minima of ILD are therefore due to cyclones moving over the Lofoten region.

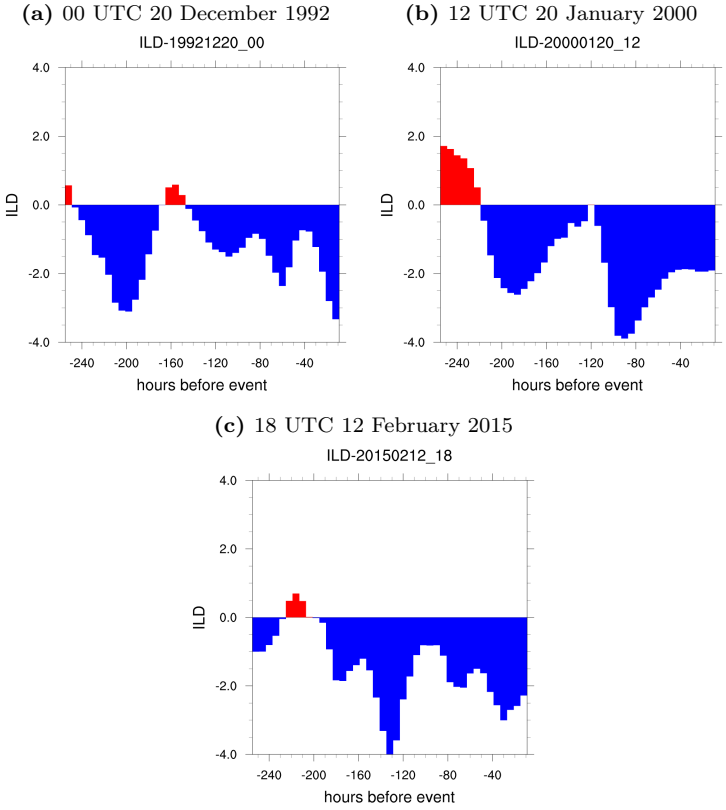

Figure 5.8: ILD for our three cases from 10 days prior until advection over the Ocean.(a) Typical case, (b) atypical case with splitting of CAO air masses and (c) atypical case with warming period. In red values are positive and negative values are blue.

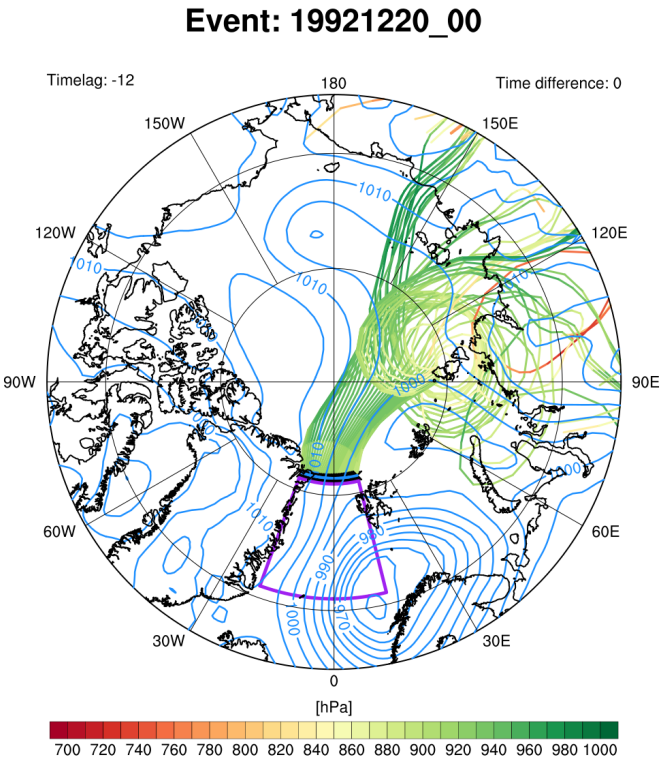

Figure 5.9: SLP of 19921220_00 at 0h

We observe that, the minima in the ILD are not always at the exact time when the CAO is happening. For the GSI we saw that we have an increase of the index which reaches a maximum as the CAO happens, but for the ILD the minimum happens a few hours before in case 20150212_18 and 20000120_12.

Figure 5.10 shows clearly that this lag is very common. Most of the time, a CAO is occurring slightly after the ILD reaches a minimum. This might be explained by the geographical position of the Lofoten region/box defined in section 3.2.

(a) Winter 1992/1993

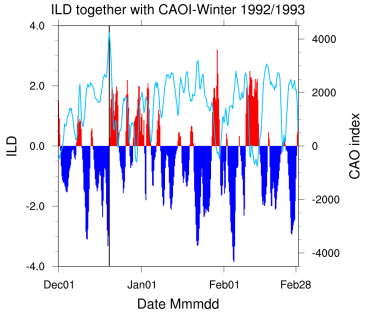

(b) Winter 1999/2000

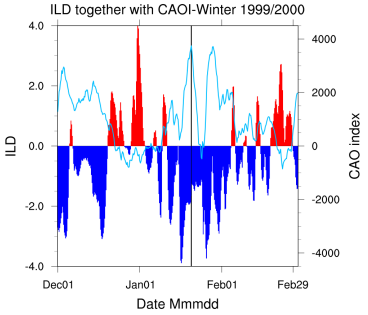

(c) Winter 2014/2015

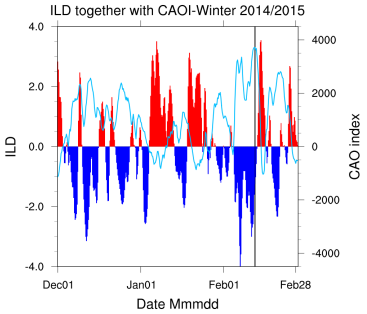

Figure 5.10: ILD for the three winters together with the CAOI as a blue curve. (a) Winter 1992/1993, (b) winter 1999/2000 and (c) winter 2014/2015. The black vertical line is here to locate the exact time of each of the chosen CAOs.

The cyclone moves across the Lofoten region creating a minimum in ILD, it then moves away from the region increasing the ILD but maintaining or reinforcing the pressure gradient leading to the CAO. This seems to be happening in the case studies and explaining the time-lag between ILD minima and CAOI maxima.

The ILD shows when cyclones move over the Lofoten region, the same cyclones are partly responsible for the advection of cold air masses out of the Arctic. In Figure 5.10 we observed, despite the time-lag, a strong anti-correlation between ILD and CAOI.

However, if we look at GSI and ILD together we see strong similarities.

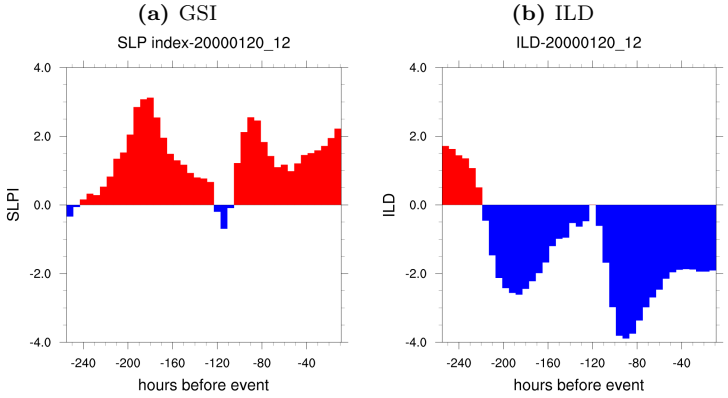

Figure 5.11: (a) ILD and (b) GSI for 20000120_12.

Figure 5.11 shows how the ILD is almost mirroring the GSI only with opposite signs.

Index	Pearson correlation	Spearman Rank correlation
ILD - GSI	-0.577	-0.578

Table 5.2: Correlation factors between ILD and GSI.

Both indices are strongly correlated with each others as can be seen in Table 5.2. This correlation has an explanation.

We saw previously that the pressure gradient is formed through the combined work of a stationary anti-cyclone over Greenland and a moving cyclone near Svalbard. The ILD allows to identify when a cyclone moves across the Lofoten region and creates a favourable pressure gradient for the outbreak of a CAO together with a stationary anti-cyclone. The ILD gives therefore very similar information as GSI but also complementary informations.

GSI is probably a sufficient indicator for the likeliness of a CAO but the ILD might help in identifying cyclones moving over the Lofoten region and that could induce a southward advection. The ILD could be a good predictor combined with the GSI.
Pressure patterns at sea level play a key role for the occurrence of CAOs but are unlikely the only decisive factors, in particular if we consider the strength of a CAO.

5.2 Thermodynamic patterns

In section 4, we determined that the θ at 900hPa over the Arctic region is mostly anomalously cold before the event and more specifically at the location of the pre-CAO air masses. This observation make us suggest that for a CAO to happen, it is a key component that the Arctic should be anomalously cold.
We investigated this hypothesis on a climatological scale, to verify if this applies to most cases or not. This is very important since the cases we have studied until now were among the strongest. The $\theta_{anomaly}$ could therefore be a trait of strong CAOs. As the $\theta_{anomaly}$ is directly linked to θ, we will therefore also investigate θ.

To identify the $\theta_{anomaly}$, we used the $\theta_{anomaly}$ defined in section 2.2.3. Then we defined the Arctic region as being North of 75°N and computed the surface mean of the $\theta_{anomaly}$ at each time-step for the entire region. This surface mean uses the values per grid-cell with a weight corresponding to the surface area of each grid-cell. This provides an accurate representation of the mean $\theta_{anomaly}$ over the Arctic.
This procedure has also been used in a similar manner for θ as we will see later on.

5.2.1 $\theta_{anomaly}$

We will analyse the $\theta_{anomaly}$ in a similar fashion as the GSI and start by looking at our three cases.

Figure 5.12 confirms our first hypothesis that the Arctic has a mean negative $\theta_{anomaly}$ before the CAO. This mean negative $\theta_{anomaly}$ is quite important for the three cases, even for 20150212_18, which had a strong warming period.

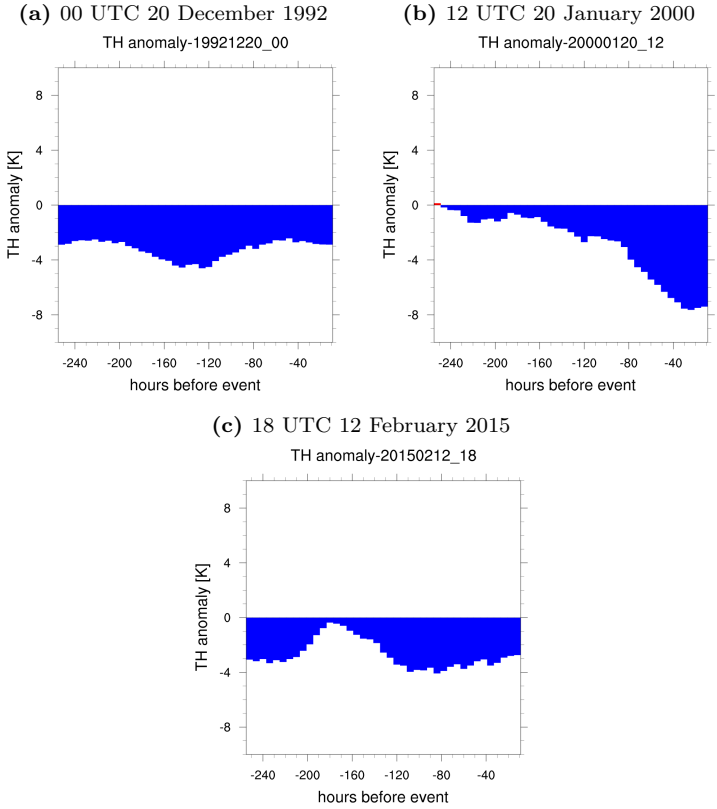

Figure 5.12: $\theta_{anomaly}$ for our three cases from 10 days prior until advection over the Ocean.(a) Typical case, (b) atypical case with splitting of CAO air masses and (c) atypical case with warming period. In red values are positive and negative values are blue.

During the 10 day period, their is no distinct pattern for all three cases in the mean $\theta_{anomaly}$. However we can observe that the mean $\theta_{anomaly}$ is more negative just before the CAO in the first two cases. Continuing with the case studies, we will analyse the mean $\theta_{anomaly}$ during the three winters of our corresponding CAO together with the CAOI.

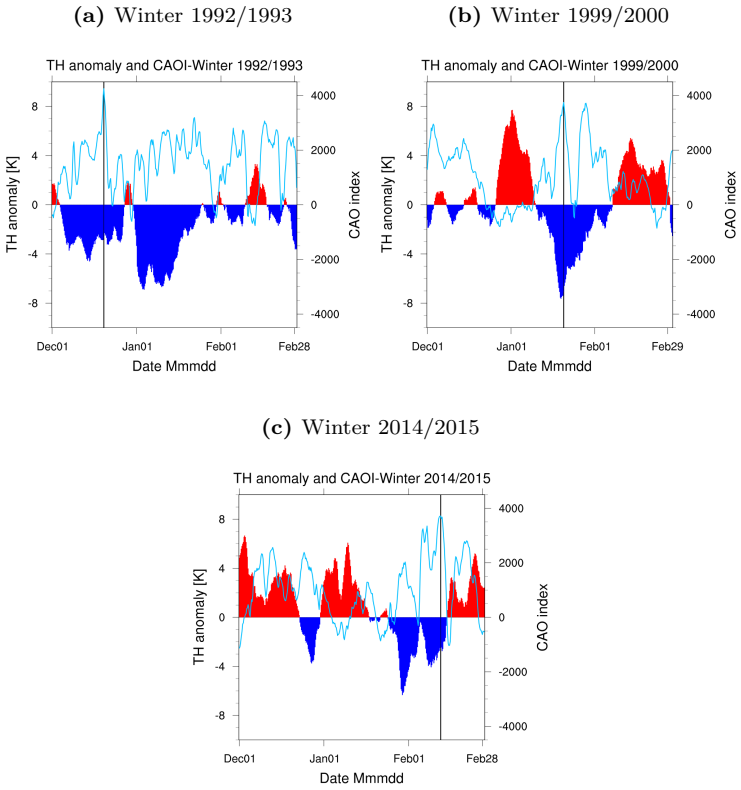

Figure 5.13: $\theta_{anomaly}$ for the three winters together with the CAOI as a blue curve. (a) Winter 1992/1993, (b) winter 1999/2000 and (c) winter 2014/2015. The black vertical line is here to locate the exact time of each of the chosen CAOs.

In Figure 5.13 the pattern we saw in the first two cases appears to be very common. Indeed, a maximum in the CAOI is generally associated with a minimum in mean $\theta_{anomaly}$. This minimum in $\theta_{anomaly}$ is not always negative. For example during December 2014 we have a few CAOs during a period of positive mean $\theta_{anomaly}$ but they still happen during local minima.

Even though the $\theta_{anomaly}$ minima are not necessarily negative, we still observe more CAOs during period of negative mean $\theta_{anomaly}$. Based on these observations, CAOs occur more during periods of mean negative $\theta_{anomaly}$ but the decisive point is that CAOs occur always at a local minimum in

mean $\theta_{anomaly}$. Furthermore, we see that after a CAO the mean $\theta_{anomaly}$ is increasing.
Together with the previous observation we can suggest that CAOs happen when the mean $\theta_{anomaly}$ is decreasing and reach a minimum, but afterwards the mean $\theta_{anomaly}$ increases. This means that the Arctic is building up a mean cold anomaly before this cold air is being advected south emptying the Arctic of its cold air and simultaneously refilling it with warm air from the South.

Concerning the occurrence of CAOs during periods of positive mean $\theta_{anomaly}$, we have to keep in mind that the Arctic region we defined is very large and that some parts do not interact directly with the region of Fram Strait. The minima could be showing a localised negative $\theta_{anomaly}$ is forming but that is not strong enough to get the mean $\theta_{anomaly}$ over the entire Arctic to be negative. This can explain CAOs during warm periods.
We further extend our analysis to the entire ERA-interim period and compute the correlation between $\theta_{anomaly}$ during the winter months and the CAOI. Table 5.3 shows an negative correlation between the mean $\theta_{anomaly}$ and the

Index	Pearson correlation	Spearman Rank correlation
Mean $\theta_{anomaly}$-CAOI	-0.375	-0.367

Table 5.3: Correlation factors between $\theta_{anomaly}$ and CAOI.

CAOI. This correlation is, as expected, less strong than between GSI and CAOI.

A scatter plot between the CAOI and $\theta_{anomaly}$ will give further informations on the nature of the relation between the CAOs and the mean $\theta_{anomaly}$.

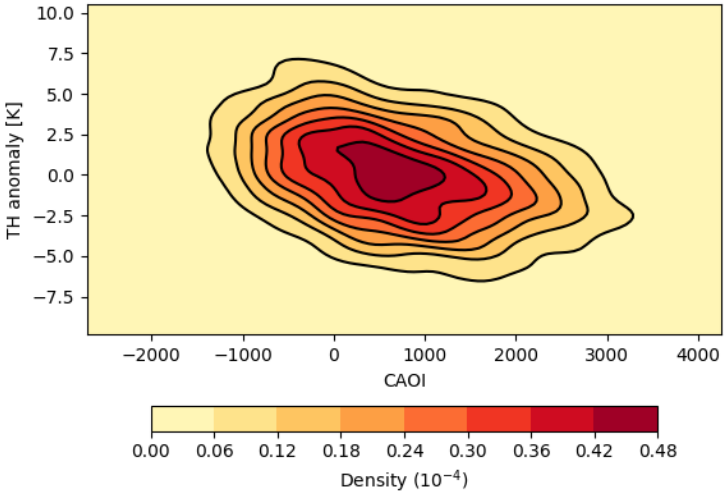

Figure 5.14: Scatter plot between CAOI and mean $\theta_{anomaly}$

In fact, Figure 5.14 shows that most CAOs are, as already mentioned, weak CAOs with a small mean negative $\theta_{anomaly}$. In the next scatter plot, we plot CAOI and GSI with $\theta_{anomaly}$ as color-shading.

The scatter plot in Figure 5.15 shows something very interesting in combining both indices. We saw in the previous section that GSI could not explain the strength of CAOs. In this figure however, we can clearly see the strongest CAOs happening with the strongest negative anomalies. The combination of both indices can help to determine if a CAO can occur (through the GSI) and how strong the CAO can be (through the $\theta_{anomaly}$).

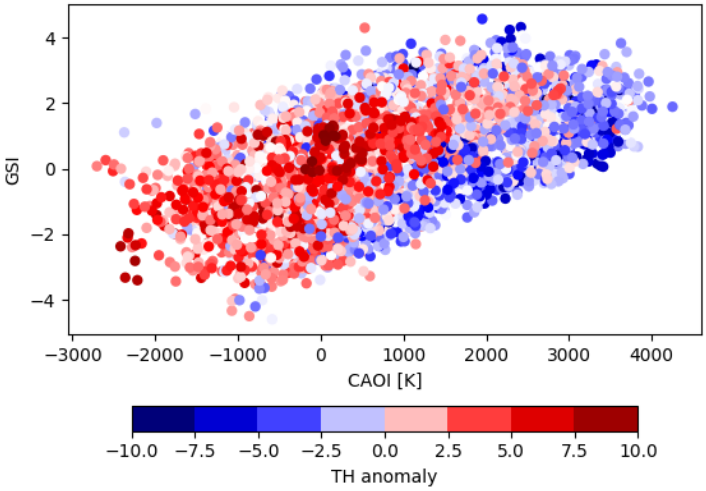

Figure 5.15: Scatter plot between CAOI and GSI with mean $\theta_{anomaly}$ as color-shading.

We need to keep in mind that the mean $\theta_{anomaly}$ is a simple metric that has the flaw not to account well enough for local variations. For example, if we restrict the calculation of the mean $\theta_{anomaly}$ over only half of the Arctic (from 90°West to 90°East) we obtain a much stronger correlation.

Index	Pearson correlation	Spearman Rank correlation
Mean $\theta_{anomaly}$ (half of Arctic)-CAOI	-0.58	-0.59

Table 5.4: Correlation factors between $\theta_{anomaly}$ over half of the Arctic and CAOI.

The stronger correlation is an expected result but using only half of the region excludes regions where the CAO air masses travel and interact radiatively with their environment. Also, the stronger correlation can be biased because we are looking at a region where CAOs can account for a large amount of cold air.

This is only to point out some flaws of this metric but more importantly that negative mean $\theta_{anomaly}$ and in general minima of $\theta_{anomaly}$ are strongly

correlated with CAOs. The strength of CAOs is correlated with the amplitude of the mean negative $\theta_{anomaly}$.

We also computed the correlation between the mean $\theta_{anomaly}$ and the CAO frequency established in section 3.1. As we only have monthly and yearly values for the CAO frequency, we calculated the average of the mean $\theta_{anomaly}$ for each year and winter.

(a) Yearly values **(b)** Winter values

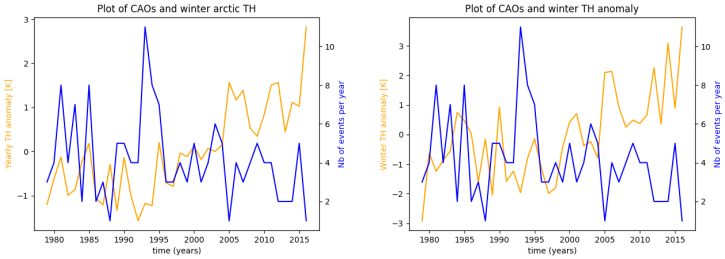

Figure 5.16: Mean $\theta_{anomaly}$ with number of CAOs for each (a) year and (b) winter.

Both figures show a correlation between years and winters with stronger negative anomalies, and a higher CAO frequency.

Index	Pearson correlation	Spearman Rank correlation
Mean $\theta_{anomaly}$-CAOI per year	-0.34	-0.21
Mean $\theta_{anomaly}$-CAOI per winter	-0.39	-0.31

Table 5.5: Correlations between mean $\theta_{anomaly}$ per winter and year and CAOI.

The yearly mean $\theta_{anomaly}$ has a low Spearman Rank correlation that is explained due to the fact that the anomaly during months outside of the winter is likely to have a negligible impact on CAO frequency. However, the winter mean $\theta_{anomaly}$ shows a relatively strong correlation, showing that winters with more negative anomalies co-occur with winters with more CAOs.

We have now identified the key role of the mean $\theta_{anomaly}$ for CAO formation. We now test if the negative trend of CAOs can be explained by the

mean $\theta_{anomaly}$. If we look at the trend of $\theta_{anomaly}$, we see a clear tendency towards more positive anomalies.

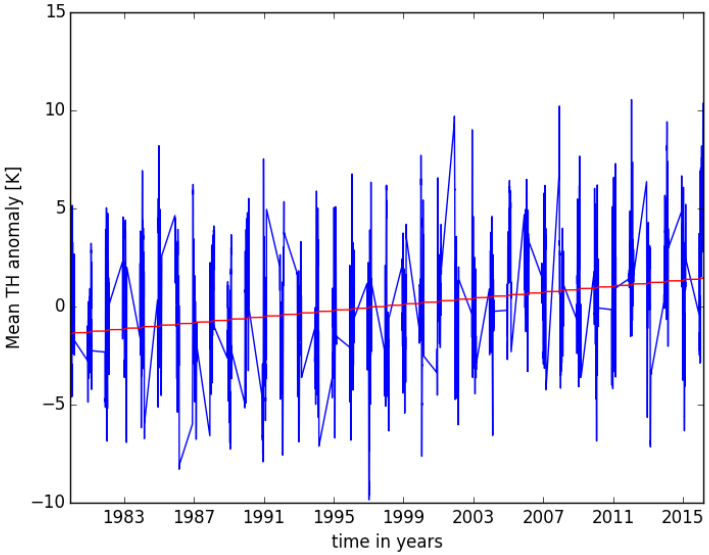

Figure 5.17: Mean $\theta_{anomaly}$ winter trend for the ERA-interim period.

The increase in Figure 5.17 is of $4.89{\cdot}10^{-5}$K per time-step which adds up to an increase of 2.8K for the entire period. Contrary to GSI, this increase is significant. We have to remember that the key component for a CAO to occur in addition to a favourable pressure gradient over fram strait are the cold air masses that are advected over a warmer ocean. If we increase the $\theta_{anomaly}$, we decrease the likelihood of sufficiently cold air to be transported southward. However, if the ocean warms up at a similar rate, the temperature difference that defines a CAO, could be maintained.

It is known however, that the ocean has a higher inertia and does not warm up as fast as the atmosphere. If we compute the mean sea surface temperature (SST) over the violet box and the trend during this period, we should be able to compare the SST and $\theta_{anomaly}$ trend.

We computed the skin temperature (SKT: same as SST but also defined over ice and land surfaces) over the region and took care of removing parts of the ocean covered by sea ice. Removing this, avoids a biased increase due to the retreat of sea ice in the region.

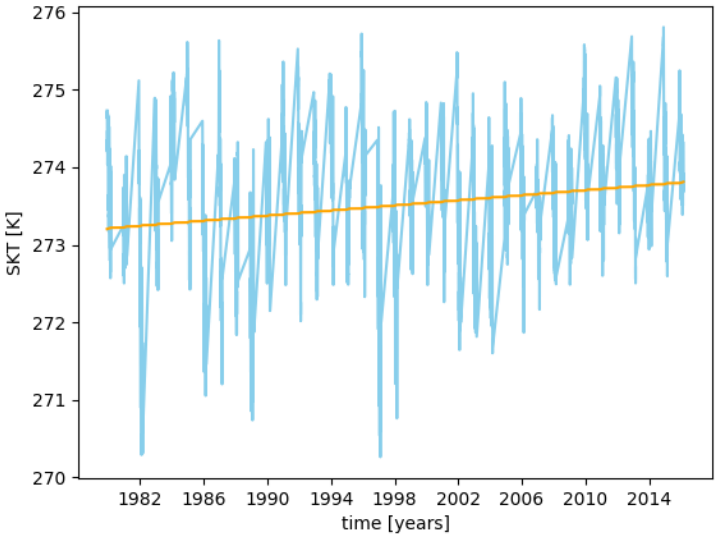

Figure 5.18: Mean SKT winter trend for the ERA-interim period.

Figure 5.18 shows the increasing trend of SKT. This trend is distinctly smaller than $\theta_{anomaly}$ with an increase of only 0.6K. This differential increase is likely to be responsible for at least at temporary reduction of CAO frequency. Global warming and especially its strong effect over polar regions could be responsible for this reduction.

The mean $\theta_{anomaly}$ is definitely a key driver of CAO formation and an indication how strong a CAO can become in the case of a favourable large-scale flow. It is likely that the positive trend in $\theta_{anomaly}$ together with the smaller increase in SKT explain the negative trend in CAO frequency. To continue and investigate the relationship between θ and CAO formation, we will also analyse θ in the Arctic and globally.

5.2.2 Arctic and global temperature

The mean $\theta_{anomaly}$ trend has shown interesting results but it only reveals deviation from the climatological mean. Looking at the absolute values of mean θ over the Arctic (north of 75°N) might reflect a more direct link between temperature trends and CAOs frequencies.

The mean Arctic θ is very similar to the $\theta_{anomaly}$ with the only difference that we did not substract the climatological mean.

Index	Pearson correlation	Spearman Rank correlation
Mean θ over the Arctic-CAOI	-0.36	-0.35

Table 5.6: Correlation factors between mean θ over the Arctic region and CAOI.

Note that the correlation between the Arctic mean theta and the CAOI is of similar strength as the correlation between the Arctic mean theta anomaly and the CAOI. Furthermore, the increase in θ is almost the same as for $\theta_{anomaly}$ with 2.81K compared to the trend in the $\theta_{anomaly}$ of 2.8K.

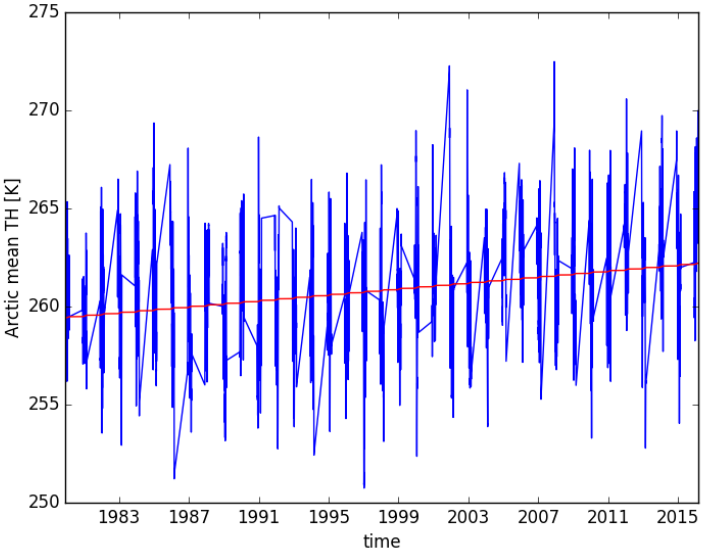

Figure 5.19: Mean θ over the Arctic and trend for the ERA-interim period

The trend in Figure 5.19 very much alike the trend for $\theta_{anomaly}$.

We continued our analysis by also looking at the mean θ over the entire Earth to investigate the link between global warming and the CAO frequency over Fram Strait.

Index	Pearson correlation	Spearman Rank correlation
Mean θ over the Earth-CAOI	-0.023	-0.024

Table 5.7: Correlation factors between global mean θ and CAOI over Fram Strait.

As expected, in Table 5.7 the correlation is very low as the physical link between the thermodynamic state of the entire Earth and CAOs is unlikely to be significant.

We also looked at the relationship between θ over the Arctic and the Earth, and the CAO frequency.

(a) Arctic **(b)** Global

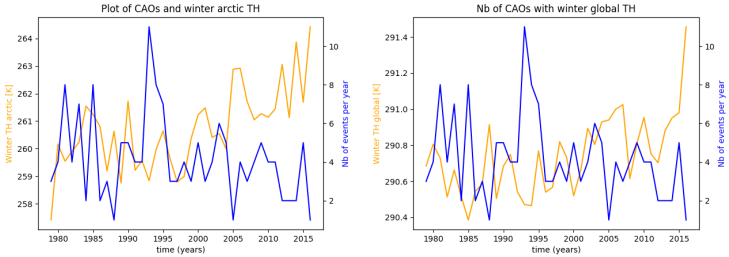

Figure 5.20: Mean θ with the number of CAOs (a) over Arctic region and the (b) Globe for each winter.

Looking at Figure 5.20, we already see that the relationship between the Arctic region and CAO frequency is much stronger.

Index	Pearson correlation	Spearman Rank correlation
Mean yearly θ over the Earth-CAOI	-0.41	-0.30
Mean yearly θ over the Arctic-CAOI	-0.39	-0.31

Table 5.8: Correlation factors between mean yearly θ over the Earth and the Arctic over the winter, and CAOI.

This is not clearly reflected when looking at correlation factors. In Table 5.8, we obtain quite high correlation factors for both mean θ but also a great difference between Pearson and Spearman correlation. Note that for this analysis we only have one data-point per year, which is not enough. The correlation with the Arctic can be explained in the same way as for the mean $\theta_{anomaly}$.
Regarding the mean yearly global θ, we can assume a relatively strong correlation with the mean yearly Arctic θ that would explain the strong correlation with the CAO frequency.

The extended analysis of the θ, shows us a clear link between the mean Arctic θ in winter that corroborates the previous analysis on the mean $\theta_{anomaly}$. Also, the increase in mean Arctic θ suggests that the negative trend in CAO frequency and CAOI could be induced by the warming of the Arctic region.

6

Conclusion

In the last years, studies on CAOs have become an integral part of the research on Arctic meteorology. More and more is known about their evolution, which can lead to important impacts on the weather in lower latitudes. However, the formation processes leading to CAOs has not been in the focus of the recent literature. Our study reached the goal to fill parts of the gap by understanding the driving mechanisms and precursors of CAOs in the Fram Strait region, using a Lagrangian perspective.

We first identified, the variation in CAO frequency from a climatological perspective across the ERA-interim period. This showed both a decrease of frequencies of CAOs and a clear seasonality. The month of December has compared to January and February clearly more CAOs during the 37 year period.
Before going into more detail, we also determined that CAOs do not seem to be affected by the NAO but are strongly correlated with the Iceland-Lofoten Pressure Difference.

As the core of our analysis we studied the history of a sample of CAOs. Our first sample of 20 strongest cases revealed that the origin of most air masses is spread between the interior Arctic and Russia. This sample also revealed a clear diabatic cooling of the air masses during their evolution and the presence in 70% of them of a vortex feature.

Based on this first identification of the main characteristics of CAOs, we reduced our sample and used three case studies (one typical and two atypical) to continue our analysis. In those case studies we saw that the vortex feature is formed by a stationary and barotropic cyclone that extends throughout the troposphere. The advection of the CAO air masses is due to the pressure gradient at sea level created by a low pressure near Svalbard and a high

pressure zone over Greenland.

Concerning the thermodynamic evolution of the pre-CAO air masses, the cooling is primarily due to outgoing longwave radiation in very dry regions. A very striking feature is the distinct negative θ anomaly in most of the Arctic and specifically in the region of CAO air masses. This feature is coupled to tropopause level disturbances creating a positive PV anomaly which stretches down to the mid level troposphere above a negative θ anomaly.

In the last section, we had the objective to verify that the findings from our case studies were applicable also on a climatological level. The first step was to determine the importance of the pressure gradient between Svalbard and Greenland. We not only confirmed its undeniable importance but also showed that the pressure gradient must be strong. We also established that this pressure gradient is formed from a stationary anti-cyclone and a more transient cyclone. Using the GSI we found a strong correlation with the CAOI, similar to the ILD which is complementary to the GSI.
The second and last step demonstrated the key role of Arctic temperatures. The Arctic has necessarily a negative mean θ anomaly prior to the event. More precisely, the Arctic is building up a mean negative θ anomaly prior to a CAO and is warming afterwards. The correlation with the CAOI is strong already looking at the mean θ anomaly over the Arctic but even more if we focus more on the region near Fram Strait. Furthermore, the mean θ anomaly is a good predictor of the potential strength of a CAO.
Both the mean θ anomaly and mean θ also revealed a clear correlation with the CAO frequency and probably with the decreasing frequency in CAOs.

The combination of these results, especially the GSI index and the mean θ anomaly, enables to better understand and predict earlier on the occurrence and the strength of a CAO.

In the previous section we already pointed out some aspects that we should look into more deeply. Here, we underline some interesting outlooks. In section 4.5 we already identified the possible correlation between TPVs and the cold "pools" that are a key component of CAO formation. Studying TPVs in relation with CAO formation could reveal the dynamical processes leading to these cold pools. Further, we identified that within our 20 samples, in 70% of cases, the air masses gather within a possible TPV prior to the CAOs advection over the open ocean. The relationship has not been shown yet on a climatological scale and therefore it should be one of the next steps to determine the importance of these weather features.
In section 3.1 we identified a negative trend in both the CAO frequency and the CAOI. We already pointed out that a linear trend is an approximation that does not take into account yearly and decadal variability. To verify the significance of this trend, we should extend the period of analysis by either

using data sets starting earlier or by waiting if this trend continues. Obviously, this goes together with assessing the importance of global warming in decreasing the probability of CAO formation.

Bibliography

Barnston, A. G., Livezey, R. E., 1987. Classification, seasonality and persistence of low-frequency atmospheric circulation patterns. Monthly Weather Review, 115 (6), 1083–1126, doi: 10.1175/1520-0493(1987)115<1083:CSAPOL>2.0.CO;2, url: https://doi.org/10.1175/1520-0493(1987)115<1083:CSAPOL>2.0.CO;2.

Bracegirdle, T. J., Gray, S. L., 2008. An objective climatology of the dynamical forcing of polar lows in the Nordic seas. International Journal of Climatology, 28 (14), 1903–1919, doi: 10.1002/joc.1686, url: http:https://doi.org/10.1002/joc.1686.

Cavallo, S. M., Hakim, G. J., 2010. Composite structure of tropopause polar cyclones. Monthly Weather Review, 138 (10), 3840–3857, doi: 10.1175/2010MWR3371.1, url: http://dx.doi.org/10.1175/2010MWR3371.1.

Dee, D. P., Uppala, S. M., Simmons, A. J., Berrisford, P., Poli, P., Kobayashi, S., Andrae, U., Balmaseda, M. A., Balsamo, G., Bauer, P., Bechtold, P., Beljaars, A. C. M., van de Berg, L., Bidlot, J., Bormann, N., Delsol, C., Dragani, R., Fuentes, M., Geer, A. J., Haimberger, L., Healy, S. B., Hersbach, H., Hólm, E. V., Isaksen, L., Kållberg, P., Köhler, M., Matricardi, M., McNally, A. P., Monge-Sanz, B. M., Morcrette, J.-J., Park, B.-K., Peubey, C., de Rosnay, P., Tavolato, C., Thépaut, J.-N., Vitart, F., apr 2011. The ERA-Interim reanalysis: configuration and performance of the data assimilation system. Quarterly Journal of the Royal Meteorological Society, 137 (656), 553–597, doi: 10.1002/qj.828, url: http://doi.wiley.com/10.1002/qj.828.

Dickson, R., Lazier, J., Meincke, J., Rhines, P., Swift, J., 1996. Long-term coordinated changes in the convective activity of the North Atlantic. Progress in Oceanography, 38 (3), 241–295.

Holton, J. R., 2004. An introduction to dynamic meteorology. Vol. 88. Elsevier Academic Press.

Hoskins, B., 2015. Potential vorticity and the PV perspective. Advances in Atmospheric Sciences, 32 (1), 2–9, doi: 10.1007/s00376-014-0007-8.

Iwasaki, T., Shoji, T., Kanno, Y., Sawada, M., Ujiie, M., Takaya, K., 2014. Isentropic Analysis of Polar Cold Airmass Streams in the Northern Hemispheric Winter. Journal of the Atmospheric Sciences, 71 (6), 2230–2243, doi: 10.1175/JAS-D-13-058.1, url: http://journals.ametsoc.org/doi/abs/10.1175/JAS-D-13-058.1.

Jahnke-Bornemann, A., Brümmer, B., 2009. The Iceland-Lofotes pressure difference: Different states of the North Atlantic low-pressure zone. Tellus, Series A: Dynamic Meteorology and Oceanography, 61 (4), 466–475, doi: 10.1111/j.1600-0870.2009.00401.x.

Kolstad, E. W., oct 2011. A global climatology of favourable conditions for polar lows. Quarterly Journal of the Royal Meteorological Society, 137 (660), 1749–1761, doi: 10.1002/qj.888, url: http://doi.wiley.com/10.1002/qj.888.

Papritz, L., Spengler, T., 2017. A Lagrangian climatology of wintertime cold air outbreaks in the Irminger and Nordic Seas and their role in shaping air-sea heat fluxes. Journal of Climate, 30 (8), 2717–2737, doi: 10.1175/JCLI-D-16-0605.1.

Shaw, T. A., Baldwin, M., Barnes, E. A., Caballero, R., Garfinkel, C. I., Hwang, Y. T., Li, C., O'Gorman, P. A., Rivière, G., Simpson, I. R., Voigt, A., 2016. Storm track processes and the opposing influences of climate change. Nature Geoscience, 9 (9), 656–664, doi: 10.1038/ngeo2783.

Sprenger, M., Wernli, H., 2015. The LAGRANTO Lagrangian analysis tool – version 2.0. Geoscientific Model Development, 8 (8), 2569–2586, doi: 10.5194/gmd-8-2569-2015.

Wacker, U., Potty, K. V. J., Lüpkes, C., Hartmann, J., Raschendorfer, M., Nov 2005. 'A case study on a polar cold air outbreak over Fram Strait using a Mesoscale Weather Prediction model'. Boundary-Layer Meteorology, 117 (2), 301–336, doi: 10.1007/s10546-005-2189-1, url: https://doi.org/10.1007/s10546-005-2189-1.

Wernli, H., Davies, H. C., 1997. A Lagrangian-based analysis of extratropical cyclones .1. The method and some applications. Quarterly Journal of the Royal Meteorological Society, 123 (538), 467–489, doi: 10.1256/smsqj.53810.

Eidgenössische Technische Hochschule Zürich
Swiss Federal Institute of Technology Zurich

Declaration of originality

The signed declaration of originality is a component of every semester paper, Bachelor's thesis, Master's thesis and any other degree paper undertaken during the course of studies, including the respective electronic versions.

Lecturers may also require a declaration of originality for other written papers compiled for their courses.

I hereby confirm that I am the sole author of the written work here enclosed and that I have compiled it in my own words. Parts excepted are corrections of form and content by the supervisor.

Title of work (in block letters):

Authored by (in block letters):
For papers written by groups the names of all authors are required.

Name(s):	**First name(s):**

With my signature I confirm that

- I have committed none of the forms of plagiarism described in the 'Citation etiquette' information sheet.
- I have documented all methods, data and processes truthfully.
- I have not manipulated any data.
- I have mentioned all persons who were significant facilitators of the work.

I am aware that the work may be screened electronically for plagiarism.

Place, date	**Signature(s)**

For papers written by groups the names of all authors are required. Their signatures collectively guarantee the entire content of the written paper.